Space Programs Summary No. 37-26, Volume VI

for the period January 1, 1964 to February 29, 1964

Space Exploration Programs and Space Sciences

jpl

JET PROPULSION LABORATORY

CALIFORNIA INSTITUTE OF TECHNOLOGY

PASADENA. CALIFORNIA

March 31, 1964

ink caps

Space Programs Summary No. 37-26, Volume VI

for the period January 1 1964 to February 29 1964

Title all caps | *Space Exploration Programs and Space Sciences,*

Preface

The *Space Programs Summary* is a six volume, bimonthly publication designed to report on JPL space exploration programs, and related supporting research and advanced development projects. The subtitles of all volumes of the *Space Programs Summary* are:

Vol. I.   The Lunar Program (Confidential)

Vol. II.   The Planetary–Interplanetary Program (Confidential)

Vol. III. The Deep Space Instrumentation Facility (Unclassified)

Vol. IV.   Supporting Research and Advanced Development (Unclassified)

Vol. V.   Supporting Research and Advanced Development (Confidential)

Vol. VI.   Space Exploration Programs and Space Sciences (Unclassified)

The *Space Programs Summary*, Volume VI consists of: an unclassified digest of appropriate material from Volumes I, II, and III; original presentation of the JPL Space Flight Operations Facility development progress; and a reprint of the space science instrumentation studies of Volumes I and II. This instrumentation work is conducted by the JPL Space Sciences Division and also by individuals of various colleges, universities, and other organizations. All such projects are supported by the Laboratory and are concerned with the development of instruments for use in the NASA space flight programs.

W. H. Pickering, *Director*
Jet Propulsion Laboratory

Space Programs Summary No. 37-26, Volume VI

Contents

LUNAR PROGRAM

THE PLANETARY–INTERPLANETARY PROGRAM

THE DEEP SPACE INSTRUMENTATION FACILITY

OPERATIONAL AND TEST FACILITIES

Contents (Cont'd)

LUNAR PROGRAM

I. *Ranger* Project

A. Introduction

The *Ranger* Project was established to develop a space flight technology for transporting engineering and scientific instruments to the Moon and planets. This technology is then to be utilized for deriving information regarding the nature and history of the Moon. Nine *Ranger* launchings, using *Atlas D–Agena B* rockets, are now planned, six of these flights have been made.

Rangers 1 and *2* (Block I) were not lunar-oriented, but were engineering evaluation flights to test the basic systems to be employed in later lunar and planetary missions. Several scientific experiments were carried on a noninterference basis. The *Ranger 3, 4*, and *5* (Block II) spacecraft carried a gamma-ray instrument, a TV camera, and a rough-landing seismometer capsule. All three of these flights experienced failures.

The objective of the *Ranger* Block III (*Rangers 6* through *9*) flights is to obtain TV pictures of the lunar surface which will be of benefit to both the scientific

program and the U.S. manned lunar flight program. The *Ranger 6* spacecraft, which was launched from Cape Kennedy on January 30, 1964, and impacted the Moon on target on February 2, 1964, did not accomplish the primary flight objective due to a failure of the TV subsystem to transmit pictures. An investigation of the failure is being conducted. The *Ranger 7* spacecraft was shipped to Cape Kennedy on January 29; however, the launch has been postponed, pending results of the *Ranger 6* TV failure investigation. Assembly of the *Ranger 8* spacecraft is complete and system tests are being performed. The *Ranger 9* spacecraft is being assembled.

Ranger Block IV, planned as a series of three flights, and *Ranger* Block V, planned as a six-flight series, were cancelled by the Office of Space Sciences, NASA, due to budgetary constraints.

1. Ranger 6 Flight Performance

Ranger 6 was launched from Pad 12 at Cape Kennedy, Florida, on January 30, 1964, at 15:49:09.092 GMT. The

Atlas and *Agena* stages performed within tolerance and injected the spacecraft on a lunar flyby trajectory with a miss distance of approximately 600 miles. The Sea of Tranquility had been selected as the general area of impact since it was the most favorable location for the prevailing lunar surface lighting conditions. The center of the target area was the intersection of the coordinates 8.5 deg north latitude and 21.0 deg east longitude. *Ranger 6* impacted the Moon at 09:24:33.145 GMT February 2, 1964. The impact point was 9.3 deg north latitude and 21.5 deg east longitude, approximately 20 miles from the chosen target area center.

The *Ranger 6* mission performance was nearly normal from launch countdown until 15 min before lunar impact. (Abnormal events were: TV cruise telemetry came on for 69 sec at launch plus 140 sec, and seven temperature measurements began to indicate unrealistic values during the midcourse maneuver.) During the last 15 min of flight, the primary mission objective was not fulfilled because of failure of the TV subsystem to transmit the expected TV pictures of the lunar surface.

Initial Sun and Earth acquisition occurred well within the nominal times. Earth reacquisition after midcourse required only 1 sec. The accuracy with which the midcourse maneuver was accomplished was the outstanding event of the mission.

Because of the geometry of the trajectory, no terminal maneuver was required. The final phase of the flight was planned to occur during the Goldstone Tracking Station view period. At 06:10:55 GMT on February 2, 1964, the Echo Station at Goldstone acquired the spacecraft signal at a level of −118 db and contact was continuously maintained at this level through impact. At approximately 08:00 GMT on February 2, the spacecraft, then 5280 miles from the Moon, was traveling toward it with a relative velocity of 3450 mph. The 64-hr TV clock pulse was received at Goldstone at 08:20:41 GMT, indicating that the TV clock was working and would automatically turn on the F-channel of the TV subsystem for warmup at the programmed time. The P-channel warmup was initiated by a real-time command sent and verified by Goldstone. Both channels were to go to full power automatically 5 min after warmup initiation. Telemetry indications were that both channels went into some sort of warmup mode at the proper time, but that full power operation was not achieved.

When there were no indications that the TV subsystem had switched to full power, two additional real-time commands were sent and each was verified. The first command was sent to switch the emergency telemetry and the second to return to video. There was no indication that either TV channel transmitted any RF from the spacecraft.

2. Ranger 6 TV Subsystem Failure Investigation

An investigation of the *Ranger 6* TV subsystem failure was instituted by the *Ranger* Project Office. The complexity of the problems involved in resolving the video failure caused a delay for the remainder (*Rangers 7–9*) of the Block III missions.

The following committees were established to investigate the *Ranger 6* mission failure; a summary of their respective objectives is included.

a. Investigation Committee. The primary objectives of this committee were:

(1) To analyze all operational and functional data to determine the cause(s) of the malfunction(s).

(2) To determine the possible modifications which could be made to eliminate the probability of a similar failure in future missions.

The committee, headed by the JPL TV subsystem cognizant engineer, included JPL and RCA personnel. The initial phase of activity has been completed, and the committee is presently engaged in examining appropriate modifications for *Ranger 7*.

Three senior RCA engineers were assigned to evaluate the detailed activities of the RCA effort within the Investigation Committee. The group participated in meetings of the Investigation Committee, as well as those of the Section Chiefs Committee. The committee's formal activities have been completed.

b. JPL Section Chiefs Committee. A group composed of JPL Section Chiefs was established by the *Ranger* Project Office to accomplish the following:

(1) Examine the broader aspects of the *Ranger* program for any phenomena relating to the *Ranger 6* TV failure.

(2) Review the results of the Investigation Committee.

(3) Suggest areas for further investigation.

(4) Assess the proposed corrective actions in light of the most probable cause or causes of failure.

(5) Present its findings and recommendations to the *Ranger* Project Office.

This group is continuing the effort to determine the cause of the failure of *Ranger 6*.

3. Launch Vehicles

The launch vehicle for the *Ranger 6* underwent successful composite testing. Both the *Atlas* and *Agena* stages performed satisfactorily during the *Ranger 6* mission. The *Ranger 7* stages were delivered to the Atlantic Missile Range and underwent successful composite testing. Following the decision to postpone the *Ranger 7* launch, both stages were removed from the pad and placed in storage at Cape Kennedy. The *Ranger 8* stages completed final assembly and are presently undergoing checkout procedures.

4. Space Flight Operations System

The Space Flight Operations System completed integration and operational readiness testing with the Deep Space Instrumentation Facility stations and demonstrated its readiness to support the *Ranger 6* mission. During the mission all elements of the System operated in a nominal fashion. The Spacecraft Data Analysis Team and the Flight Path Analysis Team are continuing the analysis of the data from the flight.

5. Deep Space Instrumentation Facility

All stations were operational at the time of the *Ranger 6* launch, and nearly all operations were nominal during the mission.

The Johannesburg Station acquired two-way lock earlier than planned so that a TV turn-off command could be issued if required. The tracking data provided by the Deep Space Instrumentation Facility were of such quality that a very accurate lunar transfer orbit was obtainable.

The conversion from L-band to S-band is being planned, pending establishment of launch schedules for *Rangers 7–9*.

B. *Ranger 6* Mission

1. Preflight Operations

a. Space Flight Operations System. The Space Flight Operations (SFO) System is made up of the equipment, computer programs, and groups of technical and operational personnel required for support of the mission. The SFO Complex which supported the *Ranger 6* mission consisted of the Atlantic Missile Range (AMR), the Deep Space Instrumentation Facility (DSIF), and the Flight Operations Facility (FOF) at JPL.

The SFO Complex preparations for mission readiness were conducted in accordance with the SFO Test Plan. This plan provides for the following preflight tests: (1) spacecraft-DSIF/SAF[1]/FOF compatibility, (2) FOF operational and technical personnel training, (3) DSIF/ FOF compatibility, (4) operational command procedures, (5) operational FOF/DSIF integration, and (6) operational readiness. A fast-reaction failure analysis system was employed to ensure that all equipment malfunctions, procedural deficiencies, and operational problems disclosed by the tests were recorded in a series of failure reports. These reports were individually processed during critiques held immediately following every test, and the remedial actions were initiated. The reports were used as a follow-up control to verify that appropriate corrective actions were accomplished.

b. Spacecraft assembly and checkout at AMR. The *Ranger 6* spacecraft and the operational support equipment (OSE) arrived at the Atlantic Missile Range on December 23, 1963. By December 31, the following operations had been performed: (1) the OSE was installed and checked out; (2) the spacecraft hand-carried items were reassembled; (3) the TV subsystem was checked out; (4) an attitude-control subsystem test was performed, and (5) the spacecraft was given an initial system test.

On January 3, a backup-functions system test was performed, the solar panels were checked with the new solar panel illumination OSE, and the secondary Sun sensors were checked. The spacecraft was then transported to the explosive safe area for an attitude-control system leak test and preparations for the initial on-pad operations.

---

[1] SAF designates the *Ranger 6* spacecraft and its associated operational support equipment located at the JPL Spacecraft Assembly Facility.

Operations from January 6 to 9 included the following:

(1) Installation of midcourse propulsion subsystem and electrical checkout.

(2) Installation of TV subsystem.

(3) Weight determination and center-of-gravity adjustments.

(4) Match-mate with *Agena* adapter.

(5) Attitude-control gas system pressurization to flight pressure.

(6) Installation of shroud.

(7) Operational checkout of spacecraft in the explosive safe area.

On January 9, spacecraft operations started at Launch Complex 12. An umbilical safe check was performed. A dummy precountdown was run. Spacecraft operations were normal, except when the TV RF power came on. This was a noise and lock-up problem which was corrected by installing a 20-db attenuator in the omni-transmitter link.

A combined RFI test, a dummy run countdown, and the spacecraft joint flight acceptance composite test were performed. An anomaly with the dc power supply in the launch shelter, an open fuse in the vehicle command destruct package, and an improper roll gyro sync indication occurred during these tests. As a result, the RFI test was rerun. All spacecraft operations were normal during the rerun.

Mechanical preparation for the final system test was made in Hanger AM. The TV subsystem was demated and the shroud removed. The batteries were then removed and inspected. The spacecraft was installed on the system test stand.

The flight TV subsystem cameras were calibrated. During a test performed prior to installing the TV shrouds, it was found that diodes of the temperature sensors assembly were defective. A spare temperature sensor assembly was installed; it performed correctly. The TV shrouds were installed and final button-up for flight was completed.

The solar panel and battery continuity wiring test was performed satisfactorily. To obtain more information about the gyro sync problem discovered during the joint flight acceptance composite test, the spacecraft was turned on three additional times, and the voltages and gyro outputs were recorded. Proper gyro sync was obtained on each spacecraft turn-on with no abnormal indications.

The final system test was performed on January 18, utilizing full-time computer support. Some difficulty was experienced with the communications system. A damaged cable at the communications OSE was removed, redressed, and reinstalled. No other problems were noted during this test, and the spacecraft was committed to flight.

The TV subsystem was exercised in cruise mode with the battery jumper plugs installed. Battery temperature measurements were correctly obtained. A special test was performed on the TV subsystem to verify proper backup operation and correct timing of the TV-clock-pulse watch. A solar panel exciter test was successfully accomplished. The high-gain antenna was installed, and the antenna deflection test was completed.

After final explosive-safe-area operations, the spacecraft was moved to the launch pad on January 25, and the electrical checkout was completed. Then a special test was conducted to verify proper gyro operation and more accurately determine midcourse-motor leak rate. The leak rate on the midcourse motor was not considered to be excessive. Spacecraft operation was normal.

A simulated launch was performed. Spacecraft operations were normal, and the test was considered successful. Another special test was performed to again verify proper gyro operation. Spacecraft power was turned on. No spacecraft problems were noted.

On January 30, 1964, at 10:22 GMT ($T-210$ min), the launch countdown was begun.

2. Mission History

After two scheduled and two unscheduled holds, the *Ranger 6* spacecraft was launched from Cape Kennedy, Florida, at 15:49:09 GMT, on January 30, 1964. Major events are listed in Table 1. At the time of the first *Agena* cutoff, the *Agena B–Ranger 6* spacecraft was in a circular parking orbit which was terminated by second *Agena* ignition. Second *Agena* cutoff marked the time of injection into the lunar transfer orbit.

Table 1. Major events of the *Ranger 6* mission

Prelaunch holds[a], 1-30-64

T—time, min	Start, GMT	End, GMT	Reason
T—155	11:25	11:50	*Atlas* fuel tanking operation problem
T—60	13:22	14:03	Scheduled hold
T—15	14:47	15:27	General Electric Company guidance ground station power supply problem
T—7	15:35	15:42	Scheduled hold

Spacecraft events and postlaunch events

Event (sec after liftoff, nominal/actual)	Time, GMT	Date
Launch Plan 30E (Plan E, dated 1-30-64)	—	—
Launch azimuth, 95 deg	—	—
RTC-2 transmitted, antenna preset angle	12:21	1-30-64
Spacecraft to internal power central computer and sequencer (CC&S)	15:43:50	1-30-64
CC&S start counting	15:47:02	1-30-64
Liftoff	15:49:09.092	1-30-64
Booster cutoff		
Booster jettison		
Sustainer cutoff		
Vernier cutoff		
Shroud ejection (307.6/306.038)	15:54:15.130	1-30-64
Atlas-Agena separation (310.6/309.628)	15:54:18.720	1-30-64
First *Agena* ignition (357.0/351.878)	15:55:00.970	1-30-64
First *Agena* cutoff		
Second *Agena* ignition (1574.0/1638.378)	16:16:27.470	1-30-64
Second *Agena* cutoff		
Firing of payload interface connectors (1813.0/1808.108)	16:19:18.200	1-30-64
Spacecraft separation from *Agena* (1818.0/1814.108)	16:19:23.200	1-30-64
Agena retro ignition (2208.0/2220.208)	16:26:09.300	1-30-64
Spacecraft transmitter power up, predicted time	16:12:01.8	1-30-64

Spacecraft events and postlaunch events (cont'd)

Event (sec after liftoff, nominal/actual)	Time, GMT	Date
TV cruise telemetry on	16:36:34	1-30-64
Begin solar panel extension	16:49:01.8	1-30-64
Begin Sun acquisition	16:52:01.3	1-30-64
Complete Sun acquisition	16:55:30	1-30-64
Begin Earth acquisition	19:20:02	1-30-64
Complete Earth acquisition	19:45:00	1-30-64
RTC-3 initiated, switch to high-gain antenna	21:12:00	1-30-64
RTC-3 verified, switch to high-gain antenna	21:12:39	1-30-64
RTC-3 initiated, switch to low-gain antenna	08:20:00	1-31-64
RTC-3 verified, switch to low-gain antenna	08:20:39	1-31-64
RTC-4 initiated, initiate midcourse maneuver	08:30:00	1-31-64
RTC-4 verified, initiate midcourse maneuver	08:30:39	1-31-64
SC-1, roll turn initiated (—54 sec nominal)	08:30:45	1-31-64
SC-1, roll turn complete	08:31:39	1-31-64
SC-2, pitch turn initiated (—328 sec nominal)	08:40:09	1-31-64
SC-2, pitch turn complete	08:45:38	1-31-64
SC-3, motor burn initiated (67 sec nominal)	08:57:08	1-31-64
SC-3, motor burn complete	08:58:17	1-31-64
Sun reacquisition initiated	09:00:39	1-31-64
Sun reacquisition complete	09:05:20	1-31-64
Earth reacquisition initiated	09:28:39	1-31-64
Earth reacquisition complete	09:29:42	1-31-64
RTC-3 initiated, switch to high-gain antenna	09:44:00	1-31-64
RTC-3 verified, switch to high-gain antenna	09:44:39	1-31-64
TV subsystem backup clock pulses		
16-hr	08:15:50	1-31-64
32-hr	00:20:11	2-1-64
48-hr	16:20:32	2-1-64
64-hr	08:20:41	2-2-64
Backup TV F-channel initiation	09:05:42	2-2-64
RTC-7 initiated, TV channels on command	09:08:00	2-2-64
RTC-7 verified	09:08:39	2-2-64
RTC-7 initiated, command P-channel to emergency mode	09:15:29	2-2-64
RTC-7 verified	09:16:08	2-2-64
RTC-7 initiated, command P-channel back to TV	09:19:21	2-2-64
RTC-7 verified	09:20:00	2-2-64
Impact	09:24:33.145	2-2-64

[a]No holds were called because of the *Ranger 6* spacecraft.

Agena–spacecraft separation occurred and *Ranger 6* continued on a lunar impact trajectory. Event blips observed by Woomera Tracking Station at 16:50:06 and 16:52:01.3 GMT, respectively, indicated solar panel extension and initiation of the Sun acquisition sequence. Earth acquisition was indicated by observance of an event blip at 19:20:02 GMT by Woomera.

The first ground commands were sent to the spacecraft by the Johannesburg Tracking Station on January 30. Two "clear commands" were sent at 21:08:00 and 21:10:00 GMT. These were followed by the spacecraft antenna changeover command sent at 21:12:00 GMT. This last command switched the spacecraft transmitter from the omni-antenna to the high-gain antenna. A rise in received signal strength and the observance of an event blip at 21:12:40 GMT confirmed the antenna switchover.

Preliminary spacecraft orbit computations indicated that a trajectory correction was required to achieve lunar impact in the preselected target area. The corrective maneuver commands were sent to the spacecraft by the

Echo Station starting at 07:20:00 GMT on January 31. All guidance commands were correctly received by the spacecraft, changeover was made from the high-gain antenna to the omni-antenna, and the midcourse-maneuver execute command was initiated at 08:30:00 GMT.

Midcourse-maneuver motor ignition occurred at 08:57:08 and terminated at 08:58:17 GMT. The two-way doppler shift during the maneuver and the time duration of the shift indicated that the midcourse maneuver had been executed as planned. After the maneuver the spacecraft, responding to on-board commands, reacquired first the Sun and then the Earth. The Echo Station then sent the command that switched the spacecraft transmitter from the omni-antenna to the high-gain antenna.

Ranger 6 was again in a cruise mode, proceeding on a lunar impact trajectory. Based on subsequent orbital computations using postmidcourse tracking data, it was decided that a terminal maneuver would not be required. At 09:08:00 GMT on February 2, Echo Station sent the backup command for activating the TV subsystem warmup. Two additional commands were sent to the spacecraft in what proved to be a futile attempt to obtain some video or engineering telemetry data. *Ranger 6* impacted in the lighted area of the lunar surface at the Sea of Tranquility at 09:24:33.145 GMT[2] on February 2. The Moon-referenced impact velocity was about 5950 mph, and the altitude from the Earth was 238,930 miles. Total flight time was $65^h35^m24^s053$.

3. Space Flight Operations System Performance

The space flight operations (SFO) for *Ranger 6* began at approximately 10:00:00 GMT on January 30, 1964, when communications were established between the JPL Flight Operations Facility (FOF) and AMR.

The Central Computing Facility and the DSIF completed the mission with no critical failures. The communications, although not causing any critical mission problems, were not satisfactory to the overseas DSIF stations because of propagation difficulties along the voice and teletype paths. The communications problem was the greatest SFO System difficulty encountered during the flight. The facilities within the FOF also operated satisfactorily. No backup mode of equipment operation was required during the entire mission.

---

[2] Impact time recorded at Echo station; this does not include the time correction for signal transit.

The Spacecraft Data Analysis Team continuously monitored the spacecraft data as received and provided the SFO director with status and capability information relative to the spacecraft during the entire mission. All real-time recommendations for commands to the spacecraft were correct.

The Space Science Analysis and Command group provided information relative to the midcourse and terminal maneuvers since these maneuvers affected the quality of the expected video pictures. The principal investigator and the co-investigators were important operational additions to the mission team; their contributions to the mission proved to be highly effective.

The primary Flight Path Analysis and Command function, to provide orbit information of satisfactory quality as required within the flight sequence, was accomplished without exception.

The premidcourse orbit computations indicated that *Ranger 6* would miss the lunar surface on the leading side and that closest approach would occur on the non-visible side approximately 2550 km from the Moon's center.

Midcourse maneuver parameters were computed which would change the spacecraft trajectory such that *Ranger 6* would impact a point chosen by the investigators on the visible side of the Moon. The aiming point chosen was near the light/shadow terminator so that desirable lighting conditions would prevail for the TV pictures.

Postmidcourse maneuver orbit computations indicated that *Ranger 6* would impact the Moon in the desired target area. Flight path analysis parameters for premidcourse and postmidcourse orbit computations and the midcourse maneuver are given in Table 2.

The *Ranger 6* flight was characterized by normal performance of all spacecraft subsystems, with the following exceptions:

(1) The spacecraft Channel 8 TV cruise mode telemetry turned on inadvertently at approximately *Atlas* booster jettison and remained on for 69 sec. The turn-off did not coincide with any other known flight event. This telemetry turned on again at the normal time and indicated normal TV subsystem performance through 65 hr of cruise operation. This inadvertent turn-on was not considered to be the result of a possible failure until the time that the TV subsystem failed to perform at the end of the mission.

**Table 2. Flight path analysis parameters for premidcourse and postmidcourse orbit computations
and the midcourse maneuver**

Premidcourse maneuver trajectory		Postmidcourse maneuver trajectory	
Target conditions (selenographic)		**Actual target conditions (selenographic)**	
Radius of closest approach to center of Moon	2550 km	Latitude at impact[a]	9.39 ± 0.5 deg north
Altitude at closest approach to surface of Moon[a]	812 ± 80 km	Longitude at impact[a]	21.51 ± 0.5 deg east
Latitude at closest approach	10.01 deg south	Epoch at impact[a]	09:24:32.18 GMT
Longitude at closest approach	190.66 deg east		± 1.7 sec, 2-2-64
Epoch at closest approach	08:54:25.327 GMT	Velocity at impact	2.655 km/sec
	± 66 sec, 2-2-64	Path angle	−42.47 deg
Velocity at closest approach	2.319 km/sec	Azimuth angle	13.08 deg
Path angle	0 deg	**Orbit conditions (based on fifth postmidcourse**	
Azimuth angle	290.86 deg	**orbit computation on 2-2-64)**	
Orbit conditions (based on data consistency orbit		Semimajor axis	317,695 km
computation on 1-31-64)		Eccentricity	0.97943
Semimajor axis	376,041 km	Inclination (from equator)	30.681 deg
Eccentricity	0.982545	Right ascension of ascending node	187.089 deg
Inclination (from equator)	28.510 deg	Argument of perigee	192.311 deg
Right ascension of ascending node	187.761 deg	**Earth-fixed spherical coordinates at midcourse**	
Argument of perigee	192.100 deg	**maneuver**	
Midcourse maneuver information		Epoch	08:58:21.0 GMT,
Commanded spacecraft maneuver			1-31-64
Spacecraft roll turn	−11.86 deg	Range	170,130 km
Spacecraft pitch turn	−71.09 deg	Latitude	−3.597 deg
Maneuver velocity magnitude[b]	41.273 m/sec	Longitude	276.785 deg
Nominal maneuver aiming information		Velocity	12.154 km/sec
Impact time	09:24:24 GMT, 2-2-64	Path angle	8.534 deg
Impact selenographic latitude	8.50 deg	Azimuth angle	271.021 deg
Impact selenographic longitude	21.0 deg		
Commanded midcourse maneuver velocity vectors			
with probe-Earth vector	21.89 deg		
with probe-Sun vector	71.06 deg		

[a] All uncertainties are 1 σ.
[b] This magnitude results in 1351 spacecraft accelerometer pulses.

(2) The midcourse motor chamber temperature transducer appears to have shorted during motor burn, which resulted in the loss of the motor temperature measurements and seven cruise mode temperature measurements for the last 2 days of the mission. This component failure had no deleterious effect on the mission.

(3) The TV subsystem was commanded into warmup about 16 min before impact, following a presumed turn-on of the F-channel by the backup clock at 18 min before impact. There is evidence of both the F- and P-channels having initiated warmup, but no conclusive evidence that either channel achieved full power. The failure to achieve full power in either of the camera/transmitter systems resulted in no pictures being recovered.

4. DSIF Tracking Performance

The DSIF stations tracked the *Ranger 6* spacecraft from shortly after injection into the lunar transfer orbit at 16:16:48.40 GMT on January 30, 1964, until lunar impact at 09:24:33.145 GMT[3] on February 2, 1964. In general, the quality of the tracking data received from the DSIF stations was excellent.

Preliminary analysis of the angular data indicates that the correction polynomials used to describe the systematic angular pointing error are not adequate. This is evidenced by an approximate bias of 0.04 deg which remained after the corrections had been applied to the inflight data. The reason for this discrepancy is that the

---

[3] For further information regarding the DSIF participation in the *Ranger 6* mission, see SPS 37-26, Vol. III.

correction polynomials are based on a series of optical star tracks which will describe the optical error. But, since the optical axis and the RF axis do not necessarily coincide, the remaining angular error may be attributed to RF error. A new method of determining correction polynominals based on celestial radio source tracks is required.

Angular residuals (orbit determination program computed values minus observed values) are, with exception of the Johannesburg hour angle, comparable with those observed on previous missions. There appears to be a general degradation in the Johannesburg hour angle residuals. This was first noted in the recent *Atlas–Centaur* (*AC-2*) mission and is still being investigated.

Preliminary evaluation of the two-way doppler data indicated very good agreement between the residuals observed on this mission and those of previous missions.

Fig. 1. Illumination test of a solar panel electrical section on *Ranger 6*

C. *Ranger 6* Power Subsystem

1. Solar Panels

Testing. The *Ranger 6* flight solar panels, Serial Nos. 8 and 14, underwent the following tests while mounted on the *Ranger 6* spacecraft at JPL: weight and center-of-gravity test, spacecraft simulated environmental vibration, and secondary Sun sensor and temperature transducer loop test. After these tests were completed, the solar panels were again checked for electrical performance.

One of the first spacecraft tests conducted at the Atlantic Missile Range employed solar panels for furnishing system power. With the exception of a performance demonstration with the *Ranger* proof test model, this test marked the first time such an operation was possible. The test involved the electrical cabling of the solar panels to the spacecraft and the illumination of the panels with the newly designed solar panel "exciter" (Fig. 1). The exciter consists of a bank of twenty 500-w sealed-beam tungsten lamps and their associated power control units. After final spacecraft system testing, this test was repeated with the solar panels assembled to the spacecraft and electrically connected for flight. The 100% continuity of the electrical interconnections between the solar panels and the spacecraft ring harness, including redundant paths, was verified in the final checkout.
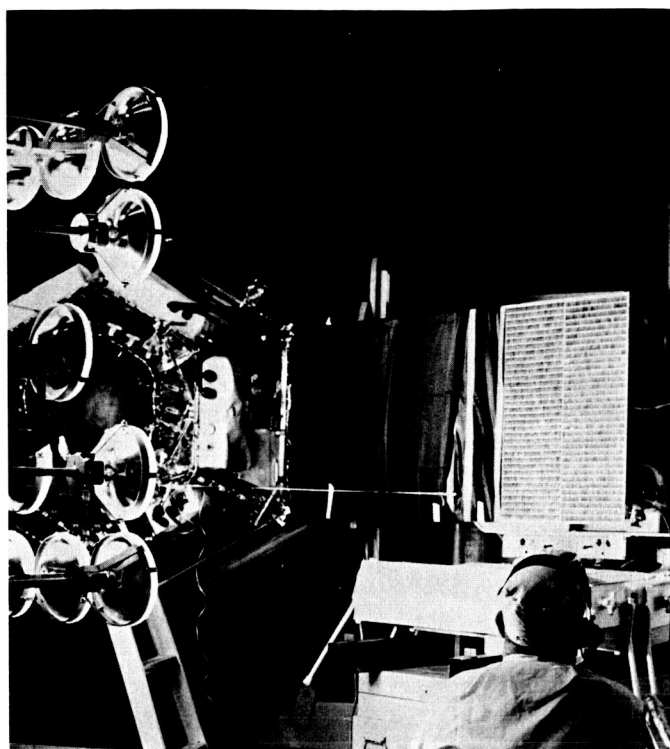
Flight performance. On January 30, 1964, at 16:55:30 GMT the *Ranger 6* spacecraft was completely Sun-oriented, and the solar panels were supplying the total spacecraft electrical power load. During the cruise mode from Sun acquisition to the beginning of the midcourse maneuver, the panels supplied approximately 120 w at 29 v to the booster regulator, or about 125 w at 30 v to the input of the power switch and logic. At the start of the midcourse maneuver at 08:30:00 GMT on January 31, 1964, the raw power requirement of the booster regulator increased to approximately 140 w. The spacecraft pitch turn was initiated at 08:40:09 GMT. At approximately 220 sec into the pitch turn, at a pitch angle of about −48 deg, the solar panels were no longer able to supply the complete bus load. Therefore, the power subsystem switched from the solar panel mode to the battery–solar panel sharing mode. At this time the input voltage to the booster regulator dropped from approximately 28 to 23 v.

After the midcourse motor burn was completed (08:58:17 GMT), the spacecraft began to reacquire the Sun at 09:00:39 GMT. At approximately 09:01:40 GMT, the voltage input to the booster regulator increased from 22 to 28 v, indicating that the panels were supplying all of

the required power. By 09:29:42 GMT, the spacecraft had reacquired the Earth and the midcourse maneuver had been completed. During the latter part of the midcourse maneuver, the power required by the booster regulator gradually dropped from 140 w back to about 120 w. During the cruise mode from the end of the midcourse maneuver to lunar impact at 09:24:33.145 GMT, February 2, 1964, the solar panels continued to supply 120 w at 29 v to the booster regulator.

2. Batteries

Testing. Both spacecraft batteries underwent testing similar in concept to that of the solar panels. This included a bench checkout and approximately 50 min of operation under spacecraft load, during which the simulated squib tests were performed. Additional battery testing included a 100% continuity test and cell voltage checks under load, throughout the explosive-safe-area operation, just prior to launch operations.

Flight performance. The flight of *Ranger 6* was the first time that two batteries were flown, for redundancy, in a diode-isolated parallel configuration on a *Ranger* spacecraft. It was also the first time that the battery terminal voltages were telemetered. During the *Ranger 6* flight, battery usage was much less than the capability. The prelaunch use was about 2.5 amp-hr per battery, which is one-half the maximum allowable use before flight, and the launch loading was as predicted.

Although 30 min is allowed for Sun acquisition, it took less than 2 min on *Ranger 6*. Since the midcourse maneuver was such that the panels were not fully disoriented from the Sun, the batteries and panels were in a "share" mode. The total time of the share mode was less than 18 min, during which the panels supplied about 2 amp and the batteries about 4.5 amp. There was no further loading of the batteries because no terminal maneuver was performed and no emergency situation arose. The battery use was 5 amp-hr prelaunch and 9 amp-hr during flight, or a total usage of only 14 amp-hr.

The voltages under load were between 21.5 and 22.0 v, exclusive of squib loading, and the open-circuit voltage was between 23 and 26 v. The temperatures of the two batteries were approximately the same throughout the flight, starting at 70°F, rising to about 85°F before the midcourse maneuver and about 92°F during the maneuver, decreasing to about 90°F shortly afterward, and staying at that level for the remainder of the flight.

The battery use was not great enough to evaluate the total capabilities of the design in an actual flight, but the data available indicate that there was no degradation in performance or capability from that observed during laboratory testing.

3. Electrical Conversion

Testing. The electrical conversion equipment operated properly throughout the preflight testing. Some concern was expressed about a possible low output voltage from the 4A14 three-phase 400-cps unit during one of the on-pad checks. Past test data on this and similar units were reviewed and failed to indicate any problems with any converters that could result in a condition of this nature. The 4A14 unit was judged to be completely flightworthy, and it remained in the spacecraft for the *Ranger 6* launch.

Flight performance. During all phases of the *Ranger 6* flight, the power conversion equipment performed satisfactorily. The conversion equipment supplied the individual subsystems with the required voltage without any abnormalities occurring. All power telemetery measurements on voltage, current, and temperature were as predicted.

D. Ranger 6 Midcourse Propulsion Subsystem

Testing. The *Ranger 6* propulsion subsystem was fueled and pressurized on January 19 and 20, 1964, and installed in the spacecraft on January 21. Telemetry readings showed a very gradual increase in GN_2 reservoir pressure, indicating a slight leak in the high-pressure circuit. The tank pressure decayed from 3225 psia on January 21 to 3140 psia on January 30, a loss of about 9 psia per day. There is some question regarding the possibility of telemetry drift. The propulsion subsystem had not exhibited any detectable leaks prior to delivery to the spacecraft assembly area. The final leak checks will henceforth be performed with helium instead of nitrogen in order to increase confidence in the leak-tightness of the propulsion subsystem.

Flight performance. The propulsion subsystem performed normally during the *Ranger 6* mission. A velocity

increment of 41.27 m/sec was required, corresponding to a predicted motor burn-time of 67 sec. Actual burn-time was 68 sec due to a slightly lower-than-estimated regulated tank pressure. Predicted propellant tank regulated pressure was 301 psia, and the actual pressure was approximately 297 psia. The high-pressure nitrogen reservoir pressure decayed from 3312 psia to 1640 psia. Both of these pressure readings are believed to be slightly high as a result of a measurement error, but the differential is near that expected. A positive shutoff was obtained at the end of motor burn; the tank pressures remained stable until impact.

E. Systems Testing

1. Proof Test Model

The following tests were performed on the *Ranger* proof test model (PTM): (1) the acoustical verification test in the JPL acoustic test facility, (2) firing of the midcourse-motor propulsion valves with live pyrotechnics in the Spacecraft Assembly Facility (Fig. 2), and (3) the final PTM system test.

The PTM was operated simultaneously with the Atlantic Missile Range (AMR) countdown and the flight of *Ranger 6*. After the *Ranger 6* flight, the PTM was prepared for special TV tests in an attempt to duplicate the failure which occurred on *Ranger 6*. After extensive testing, the problem is still under investigation.

2. Ranger 7

The *Ranger 7* vibration test (Fig. 3) and the post-vibration system test were completed. The TV subsystem was removed from the spacecraft. TV camera

Fig. 2. Test setup for firing of the *Ranger* PTM midcourse-motor propulsion valve
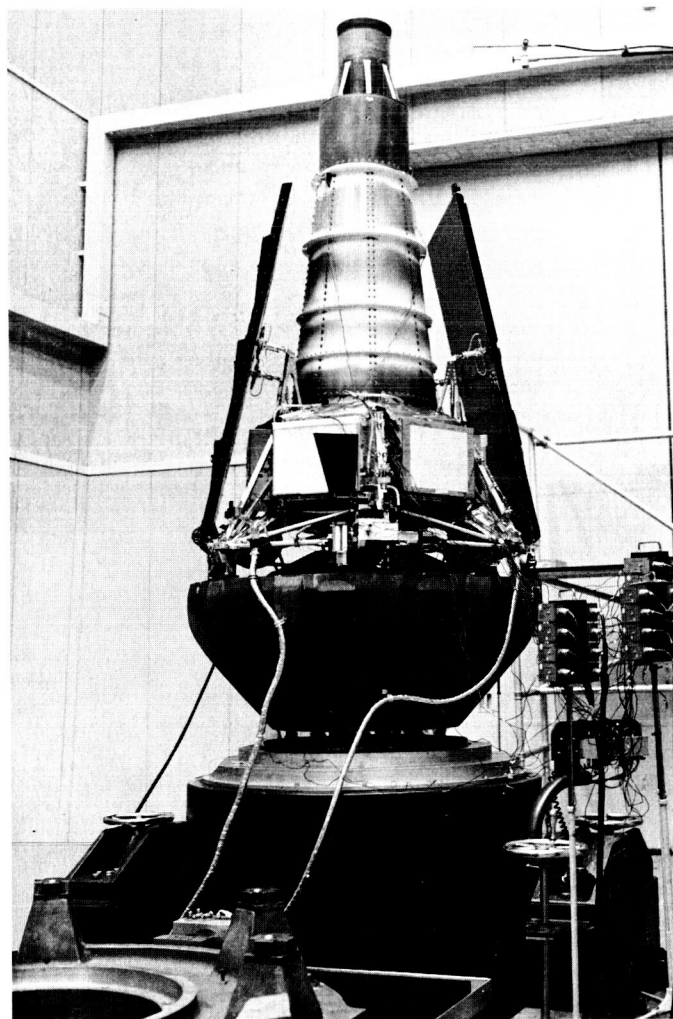
Fig. 3. *Ranger 7* vibration test setup

calibrations and a focus check were performed. Problems occurred with two of the cameras, a transmitter power supply, and the telemetry commutator. While the TV units were being repaired, the spacecraft was cabled to the OSE. The repaired TV subsystem was then mated with the spacecraft.

Mission Test 1 was started on January 3 (Fig. 4). Problems occurred in the TV subsystem during the high-temperature mission test. Camera P2 and associated electronics and the complete transmitter system of Channel P were replaced with the same equipment from *Ranger 8*. The launch, midcourse, and terminal phases of the test were then completed with no problems encountered.

The launch, midcourse, and terminal portions of the low-temperature mission test were also completed with no spacecraft problems. The spacecraft portion of the Flight Operations Facility compatibility test and a pre-shipment system test were performed; no problems were encountered. The spacecraft and OSE were shipped on January 29, arriving at the AMR on February 1. The postshipment backup-functions system test was performed and all spacecraft functions were normal.

After the rescheduling of *Ranger 7*, the TV subsystem was shipped to Astro-Electronics Division of RCA in New Jersey on February 12.

3. Ranger 8

The *Ranger 8* initial power application and subsystem power tests were conducted. All voltage checks were normal. The subsystems were powered and operated satisfactorily, except that the roll gyro did not come up to proper speed or sync. The gyro package was replaced with a spare unit.

The TV subsystem was checked out, mated with the spacecraft, and the following tests were performed: System Tests 1, 2, and 3; backup command timer checkout; re-acceptance tests; backup-functions system test; thermal-control power survey; and attitude-control rate motion checks. No major problems were encountered.

A physical inspection and electrical continuity check were performed on the adapter and shroud. The spacecraft was mated to the adapter for spring-constant checks, which indicated a spring-constant in either the bus or adapter that was too soft. The magnitude of this problem is being determined.
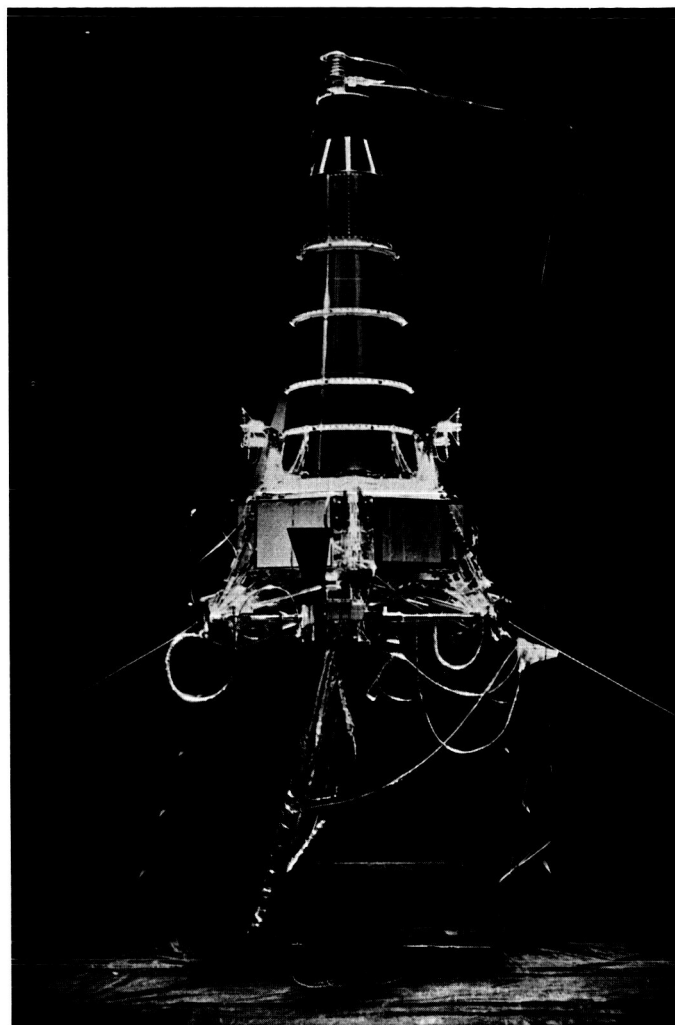

Fig. 4. *Ranger 7* mission test setup

RF tests, a dummy run precountdown, and the extension system verification test, which included a full power TV turn-on with no OSE attached, were performed. After the tests, the TV subsystem was removed and investigation was started into the premature turn-on of Channel P into full power.

F. Attitude-Control Modules

The *Ranger* attitude-control system requires angular rate and angle information about each of the three major axes: pitch, yaw, and roll. Angular rate information

is used during the acquisition and cruise periods for stabilization of the system. During the maneuver period for midcourse correction, the angle information is also required.

The gyro subassembly derives this information by a unique application of three, single-degree-of-freedom, floated integrating gyros. This gyro is filled with a low-viscosity, high-density fluid which provides full flotation at 115°F. A low-viscosity fluid has been selected which permits operation of the gyro without the use of heaters. Damping and precession axis restraint are accomplished by a torque feedback loop. The restraint provided by this electronic loop remains relatively constant, independent of changes of fluid viscosity due to temperature.

Included in the gyro subassembly are: (1) the *gyro module* containing (a) three gyros, (b) switching relays, and (c) a bank of capacitors, which contains the passive integrators for the derivation of the angle information required by the system, and (2) an *electronic control module*, which contains the three servo amplifiers and command current regulators. The *accelerometer module* is contained in a separate subassembly.

The magnitude of the velocity increment added during the midcourse maneuver for midcourse correction is measured by means of the accelerometer. This accelerometer is a pendulous, force-balance, flexure-suspended, proof-mass design. A pulse torque rebalance loop is provided by the associated electronics. The pulse is directly proportional to the applied acceleration.

The digital computer in the central computer and sequencer stores the velocity increment correction, which is transmitted from an Earth command. Upon activation of the midcourse motor, the constant acceleration of the spacecraft is measured by the accelerometer, and the digital pulse output is matched with the stored digital information to derive the motor cutoff command.

G. Telecommunications

1. Telemetry Subsystem

The *Ranger* Block III telemetry subsystem was, of necessity, an offshoot of the Block II subsystem. The experience gained in preparing for the earlier missions

resulted in the following: (1) a new auxiliary clock was designed, (2) all decommutators, which had been experiencing a rapidly increasing failure rate, were replaced with a second-generation design, (3) a design improvement program was initiated on the airborne voltage-controlled oscillators, and (4) significant improvement was made in the screening methods used to select component parts for the airborne subsystem.

The new auxiliary clock module (Fig. 5) was manufactured in the standard form factor used for the *Ranger* data encoder and is $6 \times 6 \times 1$. The circuitry is mounted on two terminal boards on opposite sides of the module. The auxiliary clock module provides both 400- and 25-cps clock signals, thus ensuring a commutation clock and a synchronized decommutation signal. The module will provide an alternate clock source in the event of failure or excessive degradation of either of the two central computer and sequencer input pulses. The auxiliary clock frequency is 398 cps instead of 400 cps; consequently, the operation of this clock in the system will be evident in the telemetry signal.

Improvements were made in the synchronization circuit of the second-generation digital decommutators (Fig. 6), and the capacity of the decommutator to transmit near-real-time data from the Deep Space Instrumentation
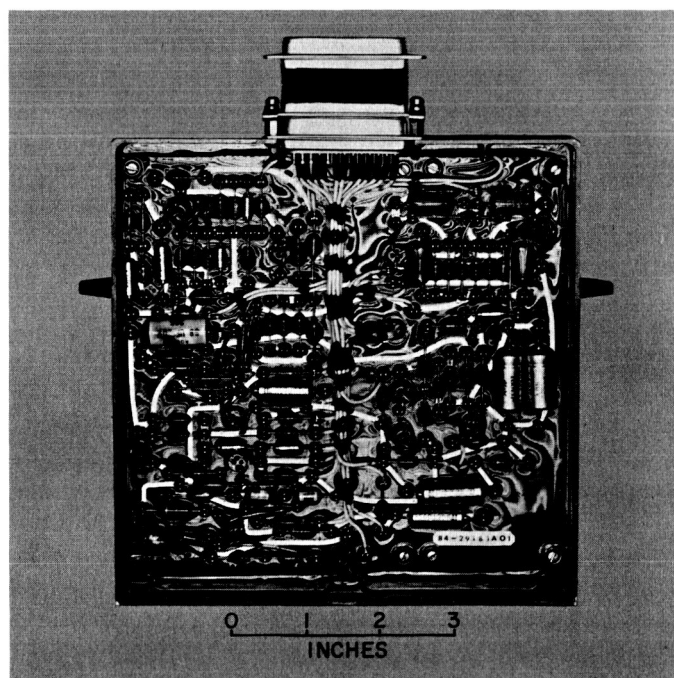

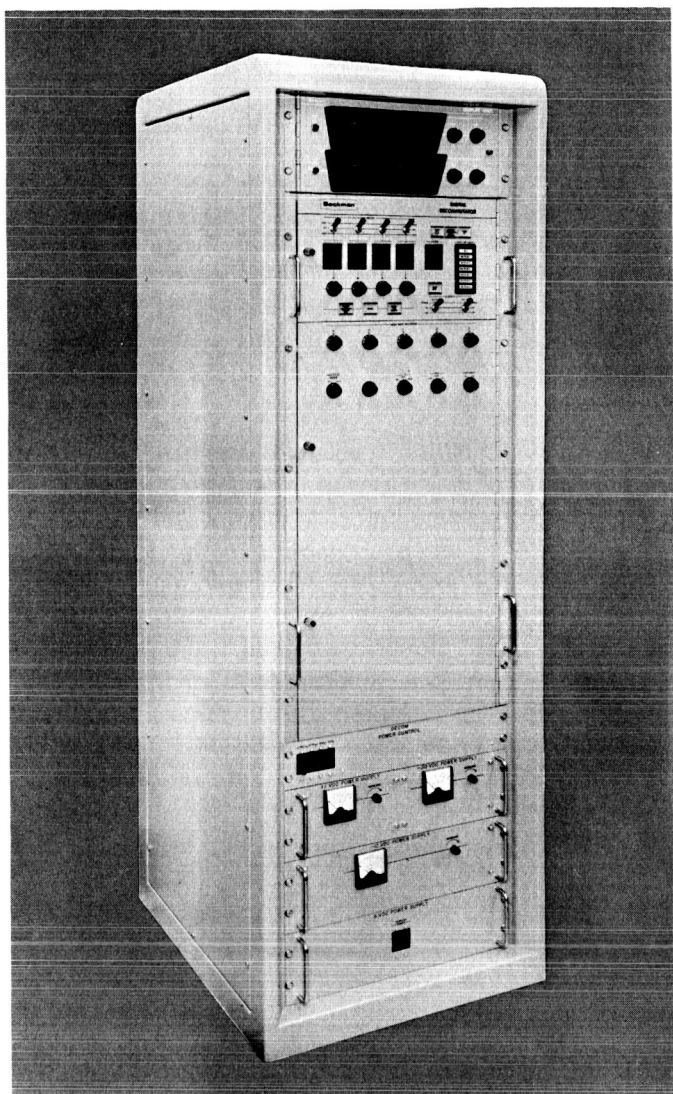**Fig. 5. Auxiliary clock module**

Fig. 6. DSIF digital decommutator

Facility was improved to allow transmission of 94% (versus approximately 30% for the previous design) of the available data.

Performance tests of the synchronization capabilities were made to determine the effectiveness of the "sync-locked loop" scheme utilized by this decommutator. The equipment used included the *Ranger* design-evaluation-vehicle spacecraft, ground receiver, data encoder, and data display (with a Beckman digital decommutator and three period counters) and a precision noise mixer. The primary objective was to determine the deviations in sync recognition by the decommutator. It was concluded that the sync-locked loop is capable of maintaining sync up to and beyond the capability of the subcarrier discriminators (essentially 0-db signal-to-noise).

2. L-Band Transponder

Revised Mark II L-band transponders were built for the *Ranger* Block III project because of the Block III design constraints specified (no sterilization and minimum design change to achieve greatest reliability consistent with rescheduling; sterilization had seriously impaired the reliability of the L-band transponder). Diplexers, directional couplers, circulators, antenna transfer switches, and quad-cavity amplifiers (which, along with the transponder, make up the total RF communications package) were also fabricated to meet the specifications.

3. Ground Command Subsystem

The Block II ground command subsystem (read, write, and verify) was redesigned for the Block III project. The same broad design concepts used in Block II were used in Block III units, but significant improvements in reliability and operational flexibility were made. The Block III ground command subsystem is shown in Fig. 7.
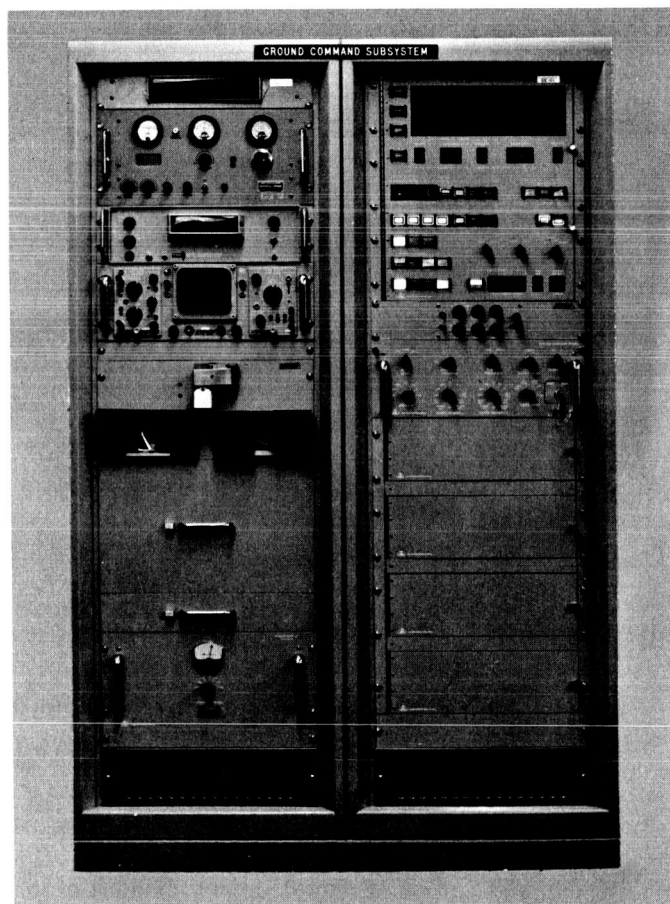

Fig. 7. Ground command subsystem

One major improvement enables the subsystem to accept, process, and transmit either *Ranger* or *Mariner* data by setting a single switch and the interchange of RF receivers.

Considerable thought was given to human engineering of the subsystem. Rotary switches are used for changing from one scheme of operation to another. Pushbutton switches are used to initiate all functions of the subsystem in any one operational mode. An operator must push two buttons in order to initiate a command. Also, the "command initiate" is removed from all other switch functions; thus, the probability of accidental operation is almost eliminated. Indicators are either white, red, green, or yellow. An indicator is lit to signify an *on* state or dark to signify an *off* state. System monitor outputs are available for computer and/or printer monitor functions. A time-of-day display is provided.

Mechanization has been incorporated which will inhibit the RF transmitter in case a transmission error is detected. This function is optional and can be eliminated by setting a switch. Three switches and indicators are always powered by an emergency power supply, which gives a continuous indication as to emergency supply readiness.

4. Flight Command Subsystem

Minor design changes were made in the Block II flight command subsystem for the Block III project. New command subsystems were fabricated because of the requirement that no equipment which had been subjected to heat sterilization would be used on any Block III spacecraft.

Subassemblies of the spacecraft command subsystem are shown in Fig. 8. Command information is sent to the spacecraft over a radio link. The information is delivered to the spacecraft command subsystem in the form of a binary, frequency-shift-keyed subcarrier tone. The subcarrier tone is demodulated in the command detector subassembly, and the binary command information is then applied to the command decoder subassembly. The command decoder interprets the command word and issues the appropriate signals to the designated spacecraft subsystems.
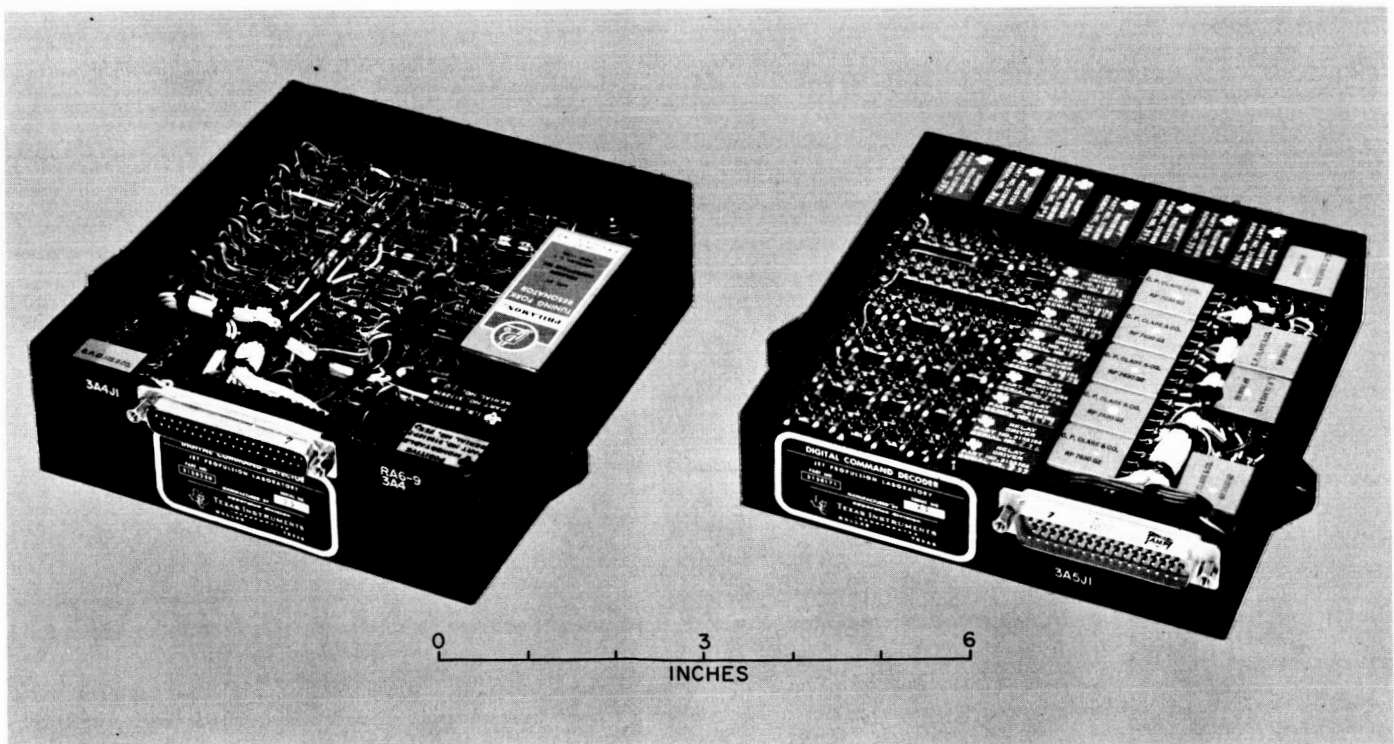

Fig. 8. Subassemblies of the spacecraft command subsystem

II. *Surveyor* Project

A. Introduction

The *Surveyor* Project will take the next step in advancing lunar technology by making soft landings on the Moon, beginning in 1965 with a group of four test missions whose objective is to demonstrate successful soft landing by post-landing spacecraft operation. An engineering payload including elements of redundancy, increased diagnostic telemetry, touchdown instrumentation, and survey TV will be used.

The general objective after 1965 is to perform operations on the Moon contributing new scientific knowledge and basic data in support of manned lunar landings. A group of four flights planned for 1966 will carry a scientific payload selected from the following experiments: two-camera TV, micrometeorite ejecta, single-axis seismometer, alpha-particle scattering, soil properties (surface sampler), and touchdown dynamics.

In 1965 and 1966, the 2150-lb (separated weight) spacecraft will be injected into the lunar trajectory by direct ascent, using single-burn *Atlas–Centaur* vehicles.

Hughes Aircraft Company is under contract to develop and manufacture the first seven spacecraft. Studies are under way at the Bendix Corporation, Systems Division, and the General Motors Defense Research Laboratories on the feasibility and design of lightweight lunar roving vehicles as possible later payloads for *Surveyor*.

B. Space Flight Operations

During this reporting period, *Surveyor* space flight operation (SFO) planning efforts have included specification and placement of requirements for support of the *Surveyor* P-42 mission upon the operational facilities and technical groups comprising the *Surveyor* SFO system.

Computer programs for data analysis, spacecraft command generation, and test data simulation are being developed. Design of on-site data processors to be used

in *Surveyor* operations is in progress. In conjunction with personnel of the Atlantic Missile Range (AMR), the following has been accomplished: (1) presentation of *Surveyor* requirements for telemetry data handling at AMR, (2) definition of detailed electrical interfaces between JPL and AMR, and (3) discussion of hardware commitments.

Functional design specifications of the technical groups and associated computer programs have been requested from the technical area directors. The groups are formulating standard and nonstandard engineering operational procedures, particularly those required for control of spacecraft performance.

C. Spacecraft System Development

The following material relating to the *Surveyor* spacecraft system development was prepared by the Hughes Aircraft Company. The principal model designations and vehicles discussed are defined in Table 1.

Table 1. Model and vehicle designations

Designation	Description
SC-1—4	Flight spacecraft with engineering payload
SC-5—7	Flight spacecraft with scientific payload
A-21	Model designation for spacecraft with engineering payload (SC-1—4)
A-21A	Model designation for spacecraft with scientific payload (SC-5—7)
T-21	Model A-21 prototype system test spacecraft
T-21A	Model A-21A prototype system test spacecraft
T-2	Simplified spacecraft for evaluation of terminal descent propulsion and flight control
S-2	Test spaceframe for vibration, shock, and static structural tests
S-6, -7	Test spaceframe for vernier propulsion system tests
S-8	Test spacecraft for flight control buzz tests

System engineering. A preliminary draft of a technical description of the A-21 spacecraft has been issued; a similar document for the A-21A is being prepared. The A-21 functional diagrams have been updated. A transponder system composed primarily of spacecraft components is being designed for the SD-1 and SD-2 spacecraft dynamic models for use in *Centaur* test flights.

Scientific payload. Integration study and preliminary design are being carried out on proposed scientific instrument changes. Equipment design and fabrication for the Payload Systems Laboratory have continued. In this laboratory, a test verified the TV viewability of surface sampler operations. Hardware fabrication, except for motors, is nearly completed for the type approval surface sampler. The survey television camera has been installed on the T-21 system test spacecraft, although several modifications will be required to overcome problems encountered in flight acceptance testing. Assembly of the approach camera is nearly completed.

System analysis. As a part of an analysis of spacecraft acquisition in a direct ascent trajectory by the Deep Space Instrumentation Facility, the tradeoffs involved in delayed separation of the spacecraft from the *Centaur* have been studied. Another study was made on the capability of the vernier propulsion system in supplying spacecraft moment for attitude control. A method for achieving maximum TV frame rate by synchronizing received video signals with ground commands was determined, and a review of approach camera capability indicates that shutter time can be increased considerably without picture smear.

Flight control. Circuit changes are being made in the flight control electronics unit to improve landing capability in nonvertical descents on sloped surfaces. The primary Sun sensor completed type approval tests, and the first inertia switch and telemetering accelerometer completed flight acceptance tests.

Electronics. A vibration isolation mount developed for the frequency control crystals in the receivers and transmitters has reduced phase jitter to acceptable limits. The type approval test specification for the compartment thermal control and heater assembly has been completed. A radar altimeter and doppler velocity sensor system that had received the electrical checkout and thermal–vacuum portions of acceptance testing has been installed on the T-21 spacecraft.

Electrical power supply. The solar panel for type approval testing has completed all environmental phases successfully and is receiving final performance tests at Table Mountain. An updated estimate of solar panel performance has been made based on solar cell module test results and higher estimates for transit and lunar temperatures. Damage to two prototype main batteries in vibration tests is under investigation; two batteries

have completed about 90% of flight acceptance testing. Type approval testing of the auxiliary battery is under way.

Thermal control. Several modifications of the thermally controlled compartments are being considered as a result of vibration tests on the S-2 vehicle. A thermal design modification for the vernier propulsion system to reduce fuel inlet temperature at the thrust chambers has been studied in conjunction with a fuel boiling problem. The thermal design of the transponder package for the dynamic models to be used in the *Centaur* test program was completed. The Thermal Model MT-1 Sector 1 was tested in a simulated transit environment at JPL.

Engineering mechanics. Landing gear shock absorbers for T-21 have been delivered. Clearances between adjacent thermal switch radiator mirrors and between the switches and compartment thermal trays under static and vibration loads have been studied. In lateral vibration testing of the S-2 vehicle, the Compartment B upper supports failed and the planar antenna support arm broke in a weld; redesign on both problems is under way.

Propulsion. Three flight type retro-engines gave satisfactory performance in simulated altitude firings. One engine was fired with a thermal gradient simulating the post-transit condition. Quality assurance testing of the safe and arm assembly is starting. Initial test results indicate that the fuel jacket cooling problem in the RMD vernier thrust chamber can be solved by reducing fuel inlet temperature and oxidizer-to-fuel ratio at low thrust levels.

Spacecraft vehicle and mechanism for basic bus. The T-21A spaceframe is being used to build a vehicle designated S-8 that will replace S-6 in spacecraft buzz tests. Type approval vibration tests of the SD-4 dynamic model indicated a need for increased strength in the antenna/solar panel mast. Separation of the altitude marking radar dish from the retro-engine was evaluated in two firings; separation of both the dish and the wiring harness was satisfactory.

Reliability, quality assurance, and system test. Comprehensive testing of pyrotechnic devices has disclosed

several areas for reliability improvement. In the T-2 descent test program, acoustic coupling of the radar system to noise from the vernier system was confirmed; T-2 was mounted horizontally in a static test stand so that the radar beams were unobstructed. Foam coverings for the radar dishes have reduced coupling effects to an acceptable level. System testing of the T-21 prototype spacecraft is continuing on a two-shift basis.

Mission operations. A preliminary compatibility test was made on the command and data handling console and associated spacecraft and Deep Space Instrumentation Facility elements. Procedures and requirements are being determined for support equipment used in preparing the spacecraft for launch; two major items are the mobile temperature control unit and the safety console.

D. Alternate Thrust Chamber Assembly

Development of the flightweight design of the alternate thrust chamber assembly (TCA) by Space Technology Laboratories is proceeding. The alternate TCA was designed for use on a plug-in basis in the vernier propulsion system currently under development by the Thiokol Chemical Corporation and the Hughes Aircraft Company. The alternate TCA is made up of a throttling mechanism, propellant *on, off* valves, and an ablative thrust chamber. The throttling mechanism consists of two variable-area cavitating venturis to control the propellant flow rates and a single coaxial variable-area injector element to maintain appropriate propellant injection velocities for high combustion efficiencies. The throttle valves and injector are linked together and positioned by a single electrohydraulic servoactuator which uses the fuel (monomethylhydrazine) as the power fluid.

THE PLANETARY - INTERPLANETARY PROGRAM

III. *Mariner* Project

A. Introduction

The early objective of the Planetary-Interplanetary Program is the initial probing of the planets Mars and Venus by unmanned spacecraft. The initial probing of Venus was successfully accomplished by *Mariner 2*. The next step toward this objective is the initial probing of Mars by a *Mariner C* spacecraft planned for the 1964–1965 opportunity.

The primary objective of the *Mariner C* mission (*Mariner* Mars 1964 Project) is to conduct closeup (flyby) scientific observations of the planet Mars during the 1964–1965 opportunity and to transmit the results of these observations back to Earth. The planetary observations should, to the greatest practical extent, provide maximum information about Mars. A TV system and a reasonable complement of field and particle experiments will be carried.

A secondary objective is to provide experience and knowledge about the performance of the basic engineering equipment of an attitude-stabilized flyby spacecraft during a long duration flight in space farther away from the Sun than the Earth. Another objective is to perform certain field and/or particle measurements in interplanetary space during the trip and in the vicinity of Mars.

It is planned to conduct two launchings of *Mariner C* missions from two separate pads. In order to exploit the limited launch period to the maximum extent, the spacecraft and launch vehicles will be processed in parallel, so that following the launch of the first space vehicle the second vehicle may be launched without delay, no earlier than two days after the first.

The proof test model (PTM) spacecraft is proceeding through its test cycle. Subsystems tests, system tests, and the engineering changes resulting from these tests have been accomplished.

All of the spacecraft design changes that were required as a result of the change to the over-the-nose shroud have been completed and qualified. The guiderails and springs that have been added to the panels will increase the spacecraft weight by 4 lb.

B. Flight Analysis Program

The *Mariner C* spacecraft during their flights to Mars will transmit approximately 10^7 words of engineering telemetry data. During normal cruise-phase operation, most of this data is repetitive and contains only a small amount of information. Nevertheless, all data must be analyzed daily by cognizant engineers in order to correctly assess the flight performance of the spacecraft, a tedious and time-consuming job if done by visual and manual methods. In order to reduce the time and effort necessary, a digital computer program, called here the guidance and control flight analysis program (GCFAP), is being developed to analyze automatically the telemetry data. The program objectives are: (1) to identify areas of abnormal performance for the attention of the cognizant engineers, and (2) to compute the routine performance quantities that are published in daily status reports.

The GCFAP program will use as its input the data obtained from two other programs. The basic data reduction program provides decommutated telemetry data converted into engineering units with occurrence times (time tags) assigned. The attitude reference program supplies spacecraft-Earth and spacecraft-Sun ranges as a function of time.

Experience with previous analysis programs has demonstrated that telemetry data must be edited to remove perturbations caused by random noise in the spacecraft-to-Space Flight Operations Facility communications link before certain computations are performed upon it, otherwise the results may be of little or no use. Four types of tests are applied to the data; failure to pass any of the four causes the data under test to be rejected for computational use, but to be listed under an appropriate heading in the program printout. The first type of test rejects any data having parity errors identified by the data reduction program. The second discards data having discrepancies in their time tags. The third rejects data outside the adjustable limits assigned to each data channel. The fourth applies several rate-of-change tests to the data. To be acceptable, the data points must pass the rate tests in specific sequences. In the event of exceptionally poor data quality and consequent high rejection rate, a comment is made in the program output to inform the engineers that a closer human inspection of the data is necessary.

The GCFAP program consists of four parts: (1) the data editing routine which is used by the other three parts, (2) an attitude control analysis subprogram, (3) a central computer and sequencer (CC&S) analysis subprogram, and (4) a power analysis subprogram. Except for their mutual dependence upon the data editing part, the latter three parts are independent of each other.

C. Systems Testing

All interfaces between subsystems of the proof test model were open-circuit and closed-circuit checked, using extensive instrumentation. Most of the interfaces checked out normally and compared favorably with the circuit data sheets. The telemetry interface checkout was successful and showed only minor problems. The science and video tape recorder checkout resulted in some problems associated with the start and end of tape recorder signals in various modes; this subsystems interface test included playback of two lines of TV data to the ground telemetry station and gave preliminary confidence that the total TV data link was operable.

The prelaunch-to-postencounter system test was performed. General results of the test were encouraging and indicate that the spacecraft performs to specification.

The simulated planet encounter sequence of the system test appeared to be normal. The postencounter portion checked out the backup modes at encounter and played back one picture from the video tape recorder. The TPS was "on line" during the recording phase, monitoring the 10.7-kc data automation system output to the tape recorder; however, difficulties were encountered in the playback mode. These difficulties are being investigated.

During the system testing, severe transients on the main 2.4-kc voltage line resulted from load changes. In particular, addition of cruise and encounter science loads resulted in a 20- to 25-v dip in the voltage that lasted 100 to 200 sec. After analysis, the problem was found to stem from three items: (1) a relatively slow response time for the booster regulator, (2) an input choke in the main 2400-cps inverter, and (3) an input filter capacitor and choke in the 400-cps single-phase inverter. Engineering changes were made that will greatly improve the load response of the booster. The input choke in the main inverter and the input L-C filter in the 400-cps single-phase inverter have been electrically removed.

Command circuit compatibility between subsystems issuing power turn-on and turn-off commands and the power subsystem were verified. The power consumed by all subsystems was measured. Results of a thermal control power survey compared closely with the power dissipation data used in the design.

The Spacecraft Assembly Facility (SAF) computer data system was "on line" for the system test. The event and telemetry programs were considered operational at the start of the test, although the event program did present some problems that were cleared up. The telemetry portion of the system was "on line" during the entire test and information was printed out from both the line and character printers.

Computer monitoring of *Mariner C* operations has been demonstrated to be feasible; effort will now be made to make the system completely operational and more useful by the time that the flight spacecraft are available for systems testing.

Fig. 1. STM on vibration fixture showing panel tip deflection test setup

D. Spacecraft Development and Testing

1. Structural Test Model Testing

Following the developmental vibration tests, modifications were made in the structural test model (STM) to strengthen the design. More realistic flight-type hardware changes were incorporated into two solar panels, the propulsion system propellant tank and bladder, and the thermal shields and blankets. The STM was then successfully subjected to the qualification vibration test program. Motion pictures of the solar panel tip deflections taken during critical tests indicated no dynamic deflection problems (Fig. 1). After these tests, successful component qualification testing was completed on the following structural assemblies: (1) the solar panel-damper structural system (Fig. 2), (2) the midcourse propulsion unit (Fig. 3), and (3) the high-gain antenna (Fig. 4).

2. Solar Panels

The solar pressure vanes must not reflect light into the Canopus sensor and must withstand large temperature extremes during boost and maneuvers. Difficulties have been encountered in finding a suitable solar pressure vane material.

Tests have indicated that severe degradation of the one-mil black-pigmented Mylar occurred when the vane was folded to the back side of the solar panel and exposed directly to solar simulation. The black pigmenting reduced the capability of the Mylar to withstand thermal degradation.

This troublesome heating environment occurs only on the Bay III panel during the parking orbit, when one vane faces the Sun. Since the Canopus sensor faces the opposite direction (Bay VIII), the vane on the Bay III panel which faces the Sun does not have to have a black back, although it is desirable that all of the vanes be the same. The present solution is to use three of the aluminized black Mylar vanes and one aluminized Teflon vane for Bay III. However, black Teflon has been ordered and will be evaluated for the Bay III application. If it is acceptable, all four vanes will be changed to this material to gain the added allowable temperature range.

Protective skid rails have been added to the solar panels to prevent their damage in the event of a non-standard shroud ejection. A series of tests were conducted
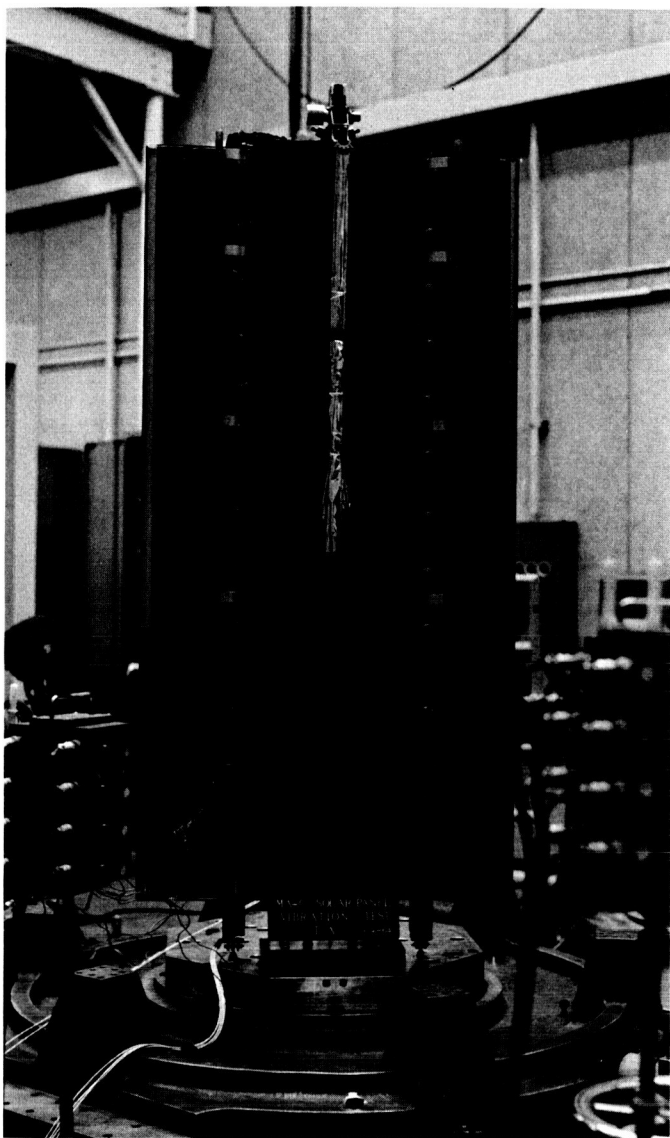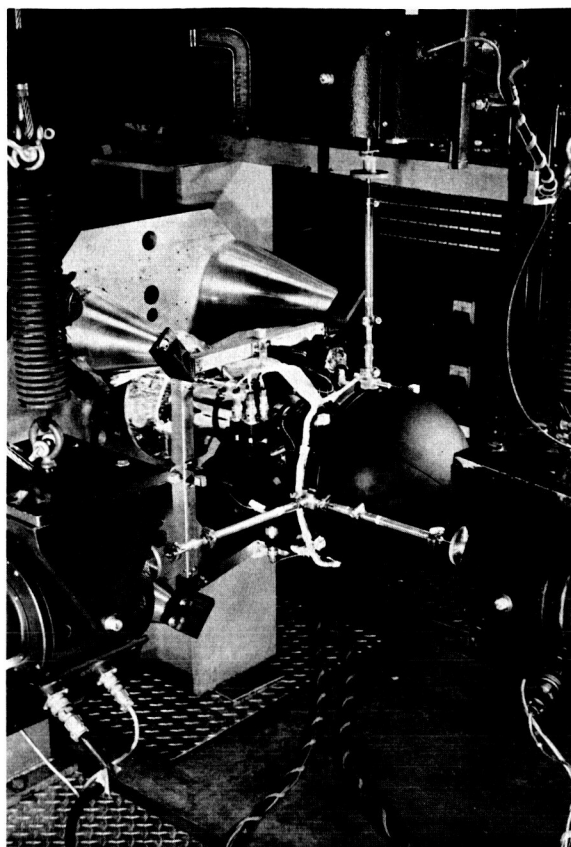
Fig. 2. Solar panel structure—damper qualification test

Fig. 3. Post injection propulsion system modal vibration test setup

Fig. 4. High-gain antenna structure on vibration exciter

to study the dynamic behavior of the solar panel damper system when exposed to a simulated shroud impact. Preliminary results indicate that no damage will be incurred by the solar panel system from shroud impact velocity of 14 in./sec. The largest impact velocity estimate is 8.4 in./sec.

3. Electrical Conversion

Several problems concerning electronics Case VIII have been resolved. The high magnetic field associated with the power switch has been reduced by changing the switch case material to Mumetal. Removal of a lag

circuit in the boost regulator reduced the overshoot experienced during power turn-on. Another change in the booster regulator reduced the low frequency "jitter" in its output and greatly improved its transient response. Minor circuit modifications in the 400-cps single-phase inverter increased the range of input voltage during synchronization from ±6% to approximately ±15%. Battery charger switch voltages for turn-on and shut-off were changed from 35 and 41 v to 33 and 38 v in order to eliminate the possibility of the battery being drained under extreme conditions.

4. Batteries

Three batteries have been subjected to the type approval test program. The flight-type test vibration levels were to 16 g for over 10 min in each of three orthogonal axes. Thermal vacuum tests were at 32°F for 4 hr and 140°F for 12 days. All three batteries successfully completed the tests. Two of these batteries have been placed on life tests, one at 59°F, and one at 100°F. Both are being charged at a constant potential of 34.2 v.

5. Postinjection Propulsion Subsystem

Two postinjection propulsion subsystems designated TA-1 and TA-2 were subjected to type approval testing.

No structural damage was noted during the vibration tests on the TA-1 subsystem. Boost-phase vibration testing revealed that the dynamic response of the propulsion subsystem was affected markedly by changes in pressure in the propellant tank. The amplification factor went up with pressure and down with increasing input acceleration. The TA-1 subsystem was also subjected to thermal tests. The first thermal test consisted of a 2-hr soak at 40°F followed by an additional 2-hr soak at 167°F. The subsystem was then fired while at 167°F for 60 sec duration. Nominal subsystem performance was obtained during the test. The subsystem was then soaked at 40°F for 2-hr and was again successfully fired for 30 sec duration.

The TA-2 propulsion subsystem was subjected to 60- and 30-sec thrust calibration tests at a high altitude facility at the Edwards Test Station. Total impulse was measured. The subsystem was then reassembled, filled with propellants, and pressurized. A life test was started at 125°F ambient temperature. The subsystem will be fired in the high altitude test facility at the end of the first and fourth months. The thrust calibration test data will be used to determine any change or degradation in subsystem performance during the firings.

Thrust calibration data were also obtained for the first flight propulsion subsystem. These data will serve as bases for determining the engine burntime required to produce a given velocity increment during the *Mariner C* flight.

THE DEEP SPACE INSTRUMENTATION FACILITY

IV. Introduction

The DSIF is a precision tracking and data acquisition network which is designed to track, command, and receive data from deep space probes. It utilizes large antennas, low-noise, phase-lock receiving systems, and high-power transmitters at stations positioned approximately 120 deg around the Earth. Its policy is to continuously conduct research and development of new components and systems and to engineer them into the DSIF so as to continually maintain a state-of-the-art capability.

The DSIF is comprised of three permanent deep space stations, one mobile station, and one launch station. The three permanent stations are located to provide continuous coverage of a deep space vehicle. Their locations are Goldstone (Pioneer and Echo), California; Woomera, Australia; and Johannesburg, South Africa. The Mobile Tracking Station (MTS) is presently located near the permanent station in South Africa and is used mainly for early acquisition, and tracking and communications with spacecraft from injection into orbit to an altitude of about 10,000 mi. The Launch Station is used to provide real-time telemetry during the spacecraft prelaunch tests and to record spacecraft transmitted telemetry data from launch to the end of the visibility period.

The testing and development engineering of new equipment for the DSIF are performed at the Goldstone Space Communications Stations. In most cases new equipment is installed and tested at Goldstone before it is integrated into the system. An 85- and a 30-ft Az–El antenna are installed at the Goldstone Venus site for primary use in research and development.

Section V of this Report, regarding the DSIF Program, is abstracted from SPS 37-26, Vol. III.

V. Communications Research, Development, and Facilities

A. Tracking Station Operations

1. Ranger 6

a. Goldstone. The Pioneer Station acted as a backup to the Echo Station, and both stations successfully tracked and received telemetry data from *Ranger 6* during all of the Goldstone visibility periods. The 10-kw S-band transmitter, Cassegrainian cone, hyperbolic reflector, acquisition aid antenna, and acquisition aid collimation tower have been installed at the Pioneer Station (Fig. 1). An interim S-band building is under construction.

b. DSIF tracking performance. The tracking data generated by all the DSIF Stations on the *Ranger 6* launch was excellent. The polynomials used in the computer to correct for systematic angular pointing errors need to be corrected to represent RF errors rather than errors obtained optically.

B. Engineering Developments

1. Systems Engineering

a. Project engineering. Specifications, analyses of reports, and plans for tests have been made for all the projects; Technical Memorandum 33-26 is being revised; a preliminary design of the Spacecraft Monitoring Station at Cape Kennedy is in process; and work is being done on various system integration and engineering projects.

b. Suitcase telemetry study. Suitcase telemetry stations have been proposed as an extremely portable, inexpensive means of obtaining telemetry from space probes between launch and DSIF acquisition in those portions of their trajectories which are not covered by existing stations. Using analyses of certain portions of *Mariner 2* nominal trajectories, it has been calculated that the maximum tracking error of an Az–El mounted antenna which is

found to give estimates of the spectrum that are very nearly like more conventional trend-removing schemes.

3. Pointing Errors Due to Quadripod Leg Distortions of New Truss Type Quadripod at Echo Station

The STAIR Computer Program was used to compute the estimated hour angle and declination angle errors due to live loads at the end of the new truss type quadripods which are used on the 85-ft antennas. Maximum hour angle errors of 0.0263 and 0.0195 deg, and maximum declination angle errors of 0.0133 and 0.0098 deg were calculated with loads of 1150 and 450 lb, respectively. This is a 25% increase in accuracy over the old telescoping pipe quadripod based on a load of 650 lb.

4. Mariner C 100-kw Transmitter

A contract for assembling the 100-kw amplifier subsystem, which will be used with *Mariner C*, has been awarded to Energy Systems of Palo Alto, California. Final tests will be made at the Goldstone Venus site.

Fig. 1. S-band Cassegrainian cone and hyperbola

moved in a single plane (tilted azimuth) is less than 5 deg. This means that a 10-deg beamwidth antenna would probably be usable.

2. Tracking Data Monitoring Program

a. Program improvements. The computer program which has been developed to monitor in near real-time the tracking data from a DSIF Station has been found from experience to require a few modifications and corrections. Some input parameters have been made constant; additional output routines have been added to allow different types of typewriter output, and the output doppler has been modified to cps rather than continuous. A doppler prediction program for the SDS 920 has been written.

b. A trajectory-independent method of estimating the noise spectral density of tracking data. A method of monitoring tracking data by means of monitoring the spectral density function of the noise on the data in near real-time has been developed. The method, which is a generalization of analyses of variance to correlated data, has been

C. Research and Development

1. Ground Antennas

a. Precision drive system for 30-ft antenna. The drive system of the 30-ft antenna has been modified to use a system similar to that used on the 85-ft Az–El antenna but with improvements. This system utilizes both high- and low-speed hydraulic motors, each controlled by an electronic second-order servo system with hydraulic pressure and motor rate feedback. A new mechanical counter has been developed which will operate at 6 deg/sec but with some increase in ambiguity.

b. Antenna instrumentation. A second scanner has been added to monitor the wire span temperatures of the extensometers in order to provide temperature correction information. Of six tests outlined in the last *Space Programs Summary*, four were successfully carried out on tests of the 85-ft Az–El antenna after the new surface had been installed.

c. Radio astronomical techniques. The technique of using radio stars for calibrating large antennas was used on January 8 and 9, 1964 to measure the gain of the Echo Station antenna at L-band. This was determined to be 45.6 ±1.5 db. It is hoped to decrease the uncertainty by improving the calibration of the test loads.

d. Radio calibration techniques. Using cryogenic loads and the audio frequency substitution method, measurements have been made on the insertion losses of various portions of the microwave system in the Cassegrainian cone on the 85-ft antenna at the Venus site. These compare favorably with previous measurements and estimates. It was learned that periodic checks and repair of the cryogenic loads are desirable.

e. 85-ft Az–El antenna, reflector resurfacing. The new surface on the Venus 85-ft Az–El antenna meets all of the specifications except that for erection tolerance. The 1-σ value for this error is about three times that specified, and is apparently due to hysteresis in the reflector backup structure. This problem is under study. The new surface material is 0.072-in.-thick aluminum with 0.125-in.-diameter holes providing a porosity of 25%.

2. Planetary Radar Project

a. 100-kw S-band transmitter. During the period between completion of Venus and Jupiter tracking operations and the resumption of planetary radar tracking, several improvements and tests have been made on the 2388-Mc, 100-kw transmitter. The "crowbar" protective circuit electronics (Fig. 2) have been redesigned and improved; transient "crowbar" operations have been recorded; the dc water load has been relocated and partially automated; the 220-v, 400-cps motor generator set and amplidyne units have been relocated; new temperature insensitive attenuators have been installed in the RF power measuring equipment; and measurements have been made of the klystron harmonic power.

b. Nine-channel autocorrelator. The nine-channel autocorrelator automatically extracts from the pseudonoise-coded, biphase-modulated, transmitted, and reflected signal the signal components from nine adjacent range zones. An additional function has been added which makes it possible to subtract the autocorrelation function of pure noise from the autocorrelation function of signal plus noise. The autocorrelator has been tested in the laboratory and has now been installed at the Venus site.
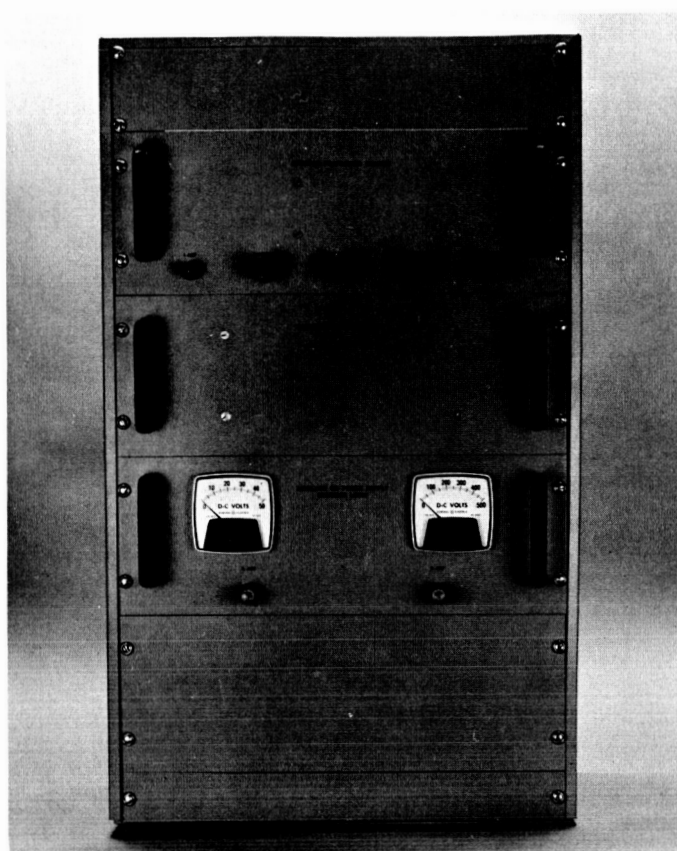

Fig. 2. Crowbar electronics units shown installed

3. Ranging and Tracking System Development

a. Microwave system design performance. The 30-ft antenna at the Venus site will be used at S-band to make lunar and satellite radar measurements with a monostatic system. Detailed calculations of the system losses and gains have been made; these calculations indicate a radiated power of 70.81 dbm, an antenna gain of 42 db, a receiver noise temperature of 516°K for the main channel and 2542°K for the angle error channels, and a receiver threshold of −155.4 dbm.

b. Monostatic satellite and lunar radar synchronous sideband detector. The subsystem designed for odd-order keying sideband lock detection is ineffective on "even" even-order sidebands and requires a predetection bandwidth wider than is optimum for the main-receiver channel. Using a synthesized ramp in time signal four times the keying rate, a 12-db margin of immunity to carrier detection was achieved. Hardware complexity might be reduced by combining reference spectra prior to modulation; this method is being investigated.

c. Monostatic satellite and lunar radar receiver module development. In order to protect the receiver in a monostatic radar operating at a keying rate of several hundred cycles per second, a two-stage, solid-state limiter with a low-level loss of only 0.15 db has been procured. Final approval awaits a resolution of an intermittent condition. A commercial mixer preamplifier has been selected which is smaller than the present JPL standard unit.

d. 10-kw S-band transmitter. The design of the 10-kw S-band transmitter is being improved in four different areas. A beam modulator at rates up to 1000 cps is required; but because of high costs and complexity as proposed by commercial concerns, it may have to be designed by JPL. The diode rectifier which provides cathode heating has been redesigned to withstand peak inverse voltages of 17 kv. The variable attenuators used in the RF forward and back power meter have been replaced with units which are relatively insensitive to temperature changes; in addition, they will be kept in a temperature controlled oven. The beam power supply has been tested with respect to conformity with specification, and its dynamic internal impedance has been measured.

e. Ranging coders. With an assumed maximum target range of 8000 km, the ranging code period is 53300/sec. For this period the optimal number of component codes is 5 and the optimal length is 9. However, because of the clock component and the relative ease by which certain sequences are generated, the component code lengths were selected to be 2, 7, 11, 15, and 23. Four coders will be procured: two for the range gate subsystem and two for target ranging.

f. Register display for Mod III stored program controller. Although it was not thought necessary to include internal register displays of the Mod III stored program controller, it has been found by experience that they are very useful. Consequently, a complete subsystem register display has been designed using primarily standard logic circuits. It has a 14-register capability with a provision for adding 10 additional.

4. Signal Generation and Control

a. Parametric frequency dividers. A parametric $\div 75$ frequency divider has been designed which reduces 35.625 Mc to 475 kc at a bandwidth of 2 Mc. Phase noise measurements indicate that the divider contributes less than 0.002 deg peak-to-peak.

b. PN generator frequency synthesizer. An experimental PN generator frequency synthesizer has been measured to have less than 0.1 deg peak-to-peak phase noise in $2B_L = 5$ cps. The PN generator had a full period of 762 μsec and a digit period of 6 μsec. Some planned improvements are:

(1) Use of better crystals to lower the system noise.

(2) Reduction of the bandwidth in the 10-Mc IF amplifier.

(3) Modification of the PN generator to obtain variable line spacing and finer frequency resolution.

5. S-Band Implementation for DSIF

a. TWM for DSIF. The traveling wave maser was installed in the Cassegrainian cone at the Pioneer Station; test measurements indicated all specifications were met except the gain stability which is still being investigated. A noise temperature of 9 $\pm 1°$K was measured with a gain of 33 db. The prototype closed cycle refrigeration at the Venus site was recently serviced after operating for a total of 7000 hr.

b. Acquisition aid for DSIF. The basic design of the acquisition aid antenna has been completed and three units have been ordered.

6. Mesa Antenna Range

The remote transmitter site, "The East Mesa", of the new ¾-mi antenna range is now complete. This site has a tower with provisions for mounting and positioning two 10-ft-diameter paraboloidal antennas. On the Mesa side of the range, a tower with an azimuth rotator for mounting spacecraft models has been installed. A control room and monitoring antennas have yet to be added.

D. Advanced Antenna System

1. Synopsis

The Advanced Antenna System consists of a 210-ft-diameter parabolic reflector antenna mounted so as to be

positioned in azimuth and elevation. It includes a concrete cylindrical pedestal, a concrete and steel instrument tower, a structural steel alidade and alidade building, an azimuth hydrostatic thrust gearing, an azimuth radial shear bearing, an elevation and azimuth drive assembly, a hydraulic drive system, an electronic servo system, an elevation bearing assembly, a 210-ft reflector, an intermediate reference structure, a feed cone, a quadripod, and a subreflector.

2. Supporting Studies

a. Scale model feed for AAS. RF tests which have been done at X-band frequencies using the 30-ft antenna at the Venus site are now being extended to K_u-band frequencies. The Mesa antenna range will use K_u frequencies for tests of AAS model feeds.

b. Master Equatorial preliminary design analysis. A preliminary calculation of some of the possible errors in the Master Equatorial mounting yoke indicate a total error of about 6 sec of arc in both hour angle and declination. This includes consideration of gravity, bearing runout, thermal gradient, and orthogonality.

c. Wind study program. Final checkout of the wind data recording instrumentation system has been completed; the system has been used since December 20, 1963. It was found necessary to ground the van, guys, and towers and to build a drag sphere calibration box for cali-
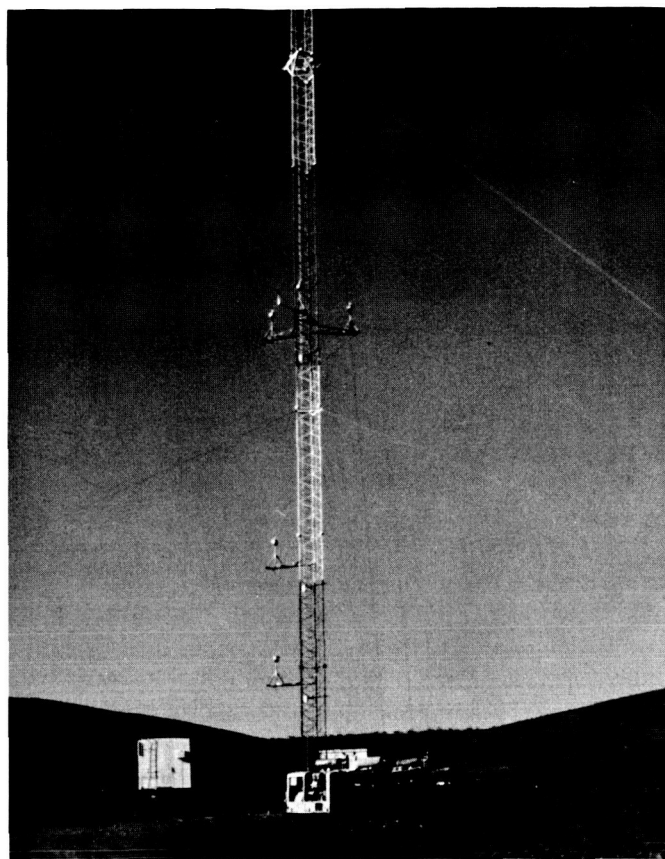
Fig. 3. Main wind tower near Mars Station

brating a sphere in a zero wind environment. The main wind tower near the Mars Station is shown in Fig. 3.

OPERATIONAL AND TEST FACILITIES

VI. Space Flight Operations Facility

A. Facility Description

The general layout of the Space Flight Operations Facility (SFOF) and of the technical areas within the SFOF has been revised from that reported in previous *SPS* issues. The decision to change the layouts was made in July 1963 in order to bring the first operational configuration as close to that of the planned expanded configuration of the SFOF as possible, thus minimizing changes to the facility existing at the time of implementation of the expansion.

The most significant change involved moving the main data processing and the telemetry processing areas from the first to the second floors. The new layout for the second floor is shown in Fig. 1.

The first floor layout (Fig. 2) is predicated upon retaining the former configuration of the operations area and upon the functional placement of the spacecraft performance analysis area between the space science analysis area and the flight path analysis area. The layout of the basement of the SFOF (Fig. 3) remains essentially as it was with the communications control room located between the communications teletype room and the communications terminal room.

The change in the floor layouts resulting from the relocation of the data processing and technical areas on the first and second floors necessarily involved a readjustment of the relocation of equipment, displays, consoles, and desks within the technical areas themselves. The operational capabilities of the technical areas have not changed with the reconfiguration of their layouts.
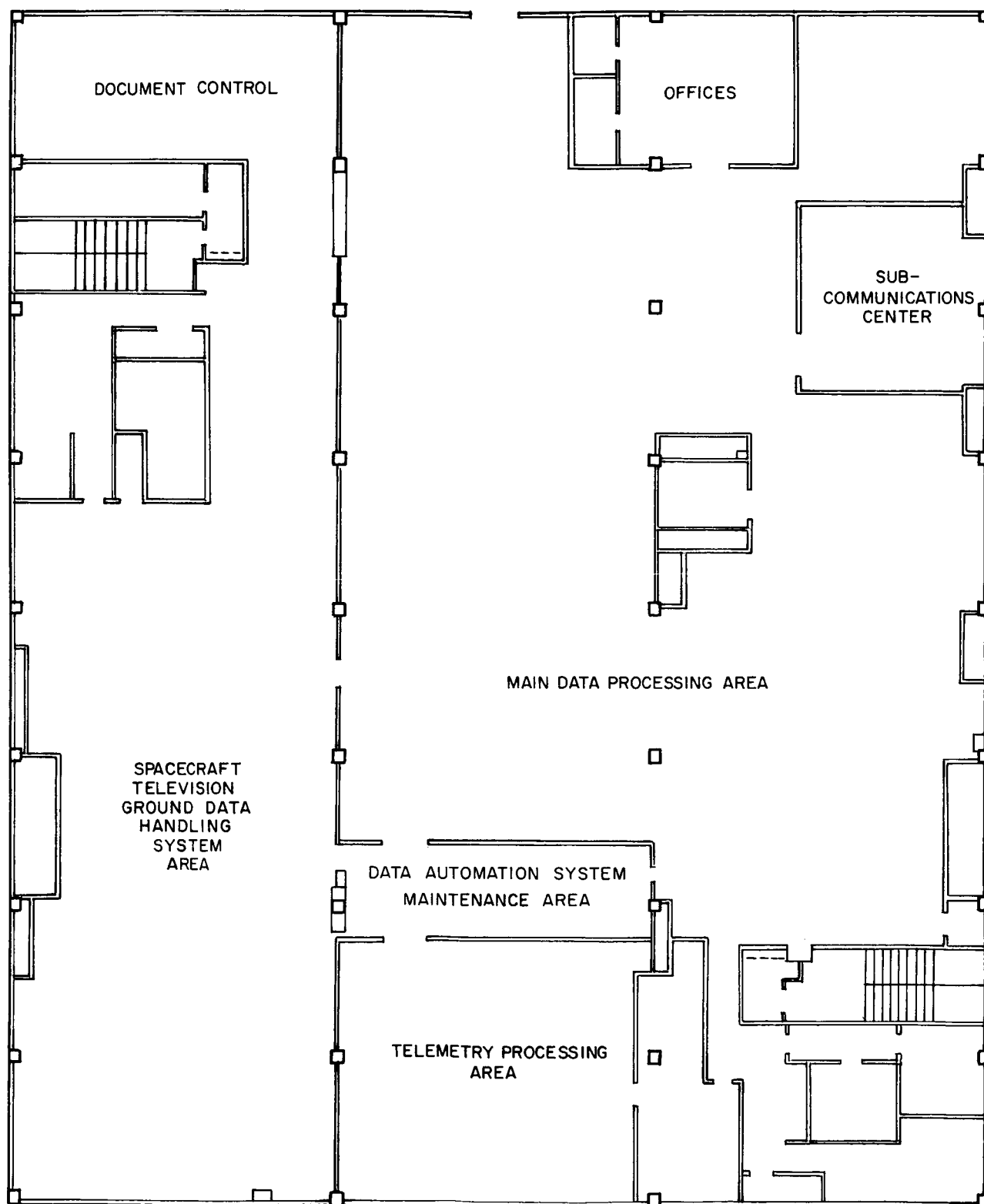
Fig. 1. Plan for second floor, SFOF

DOCUMENT CONTROL

OFFICES

SUB-
COMMUNICATIONS
CENTER

MAIN DATA PROCESSING AREA

SPACECRAFT
TELEVISION
GROUND DATA
HANDLING
SYSTEM
AREA

DATA AUTOMATION SYSTEM
MAINTENANCE AREA

TELEMETRY PROCESSING
AREA
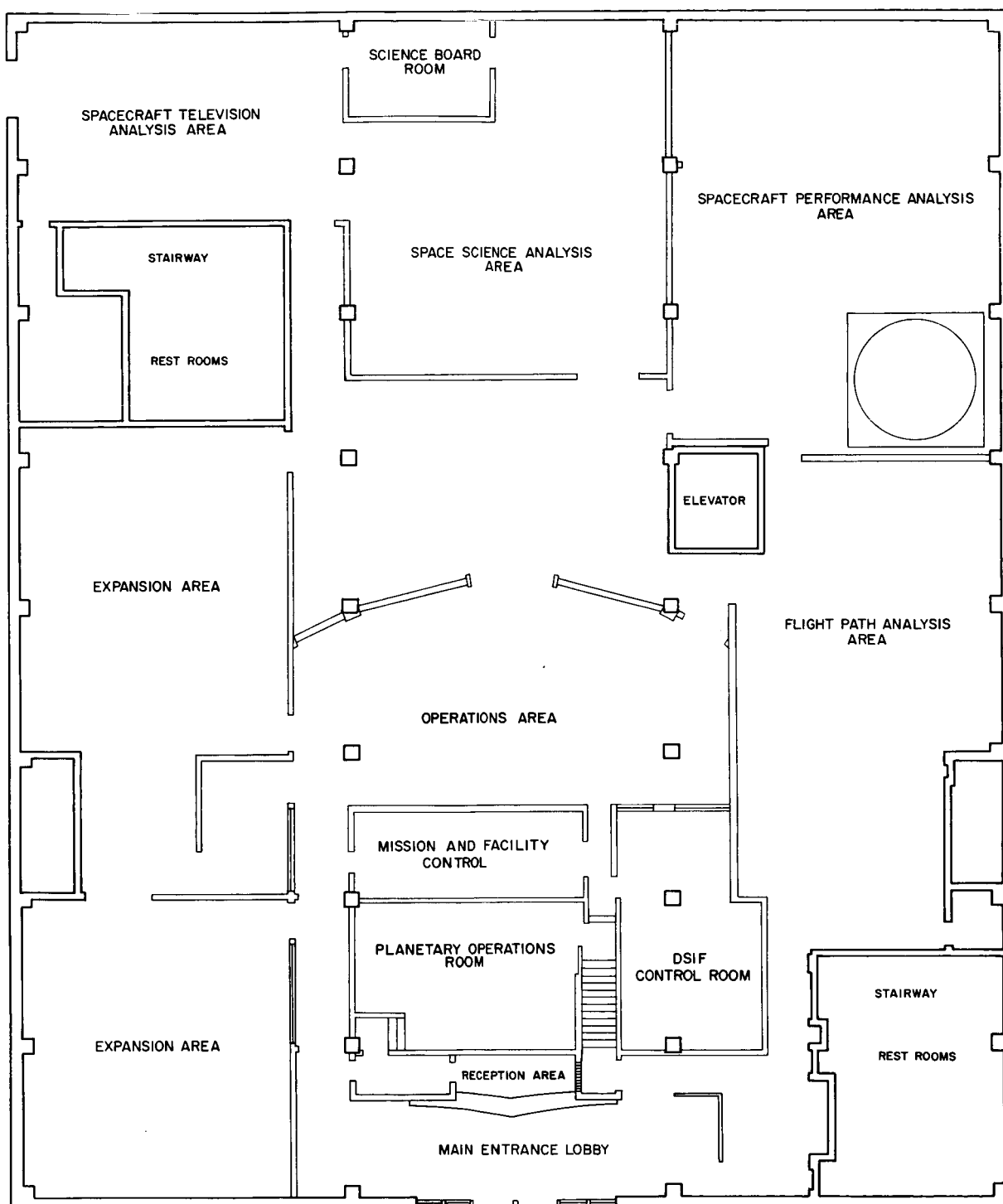
Fig. 2. Plan for first floor, SFOF

The planned configuration of the operations area, mission control rooms, planetary operations room, and Deep Space Instrumentation Facility control room are shown in Fig. 4.

The new configuration of the SFOF gallery is shown in Fig. 5; this represents a change only in the removal of the small observation room and a projection room from that area.
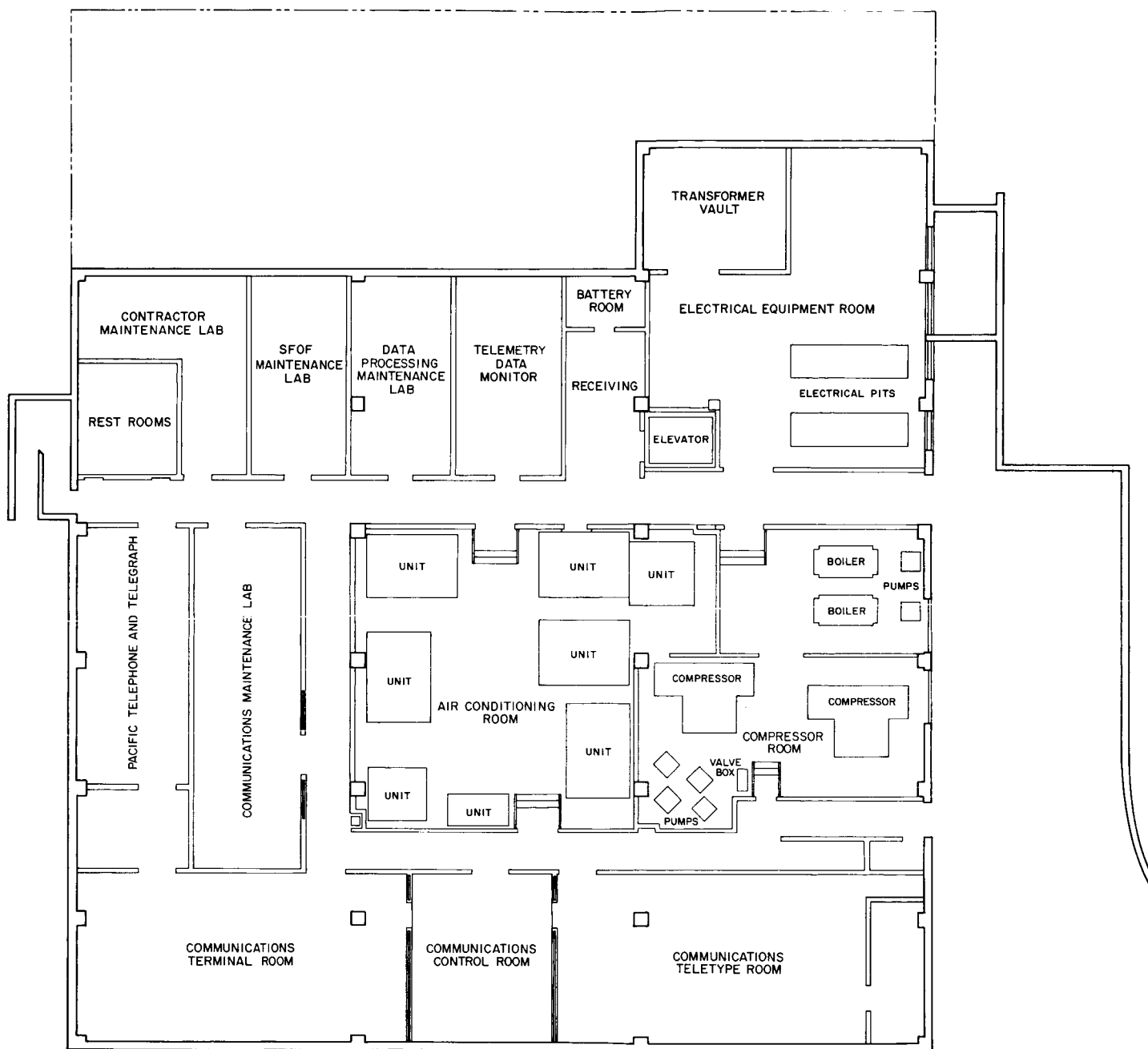
Fig. 3. Basement floor plan, SFOF

Fig. 6 is a progress photograph showing the status of the development of the SFOF operations area as of February 24, 1964. Fig. 7 illustrates the planned configuration of the flight path analysis area while Fig. 8 illustrates the status of development of that area as of February 24, 1964. The planned layout and configuration of the spacecraft performance analysis area is illustrated in Fig. 9 and the February 24, 1964, status of its development is shown in Fig. 10.

The space science analysis area, the science board room and the spacecraft TV analysis area, as they are planned, are all shown in Fig. 11.
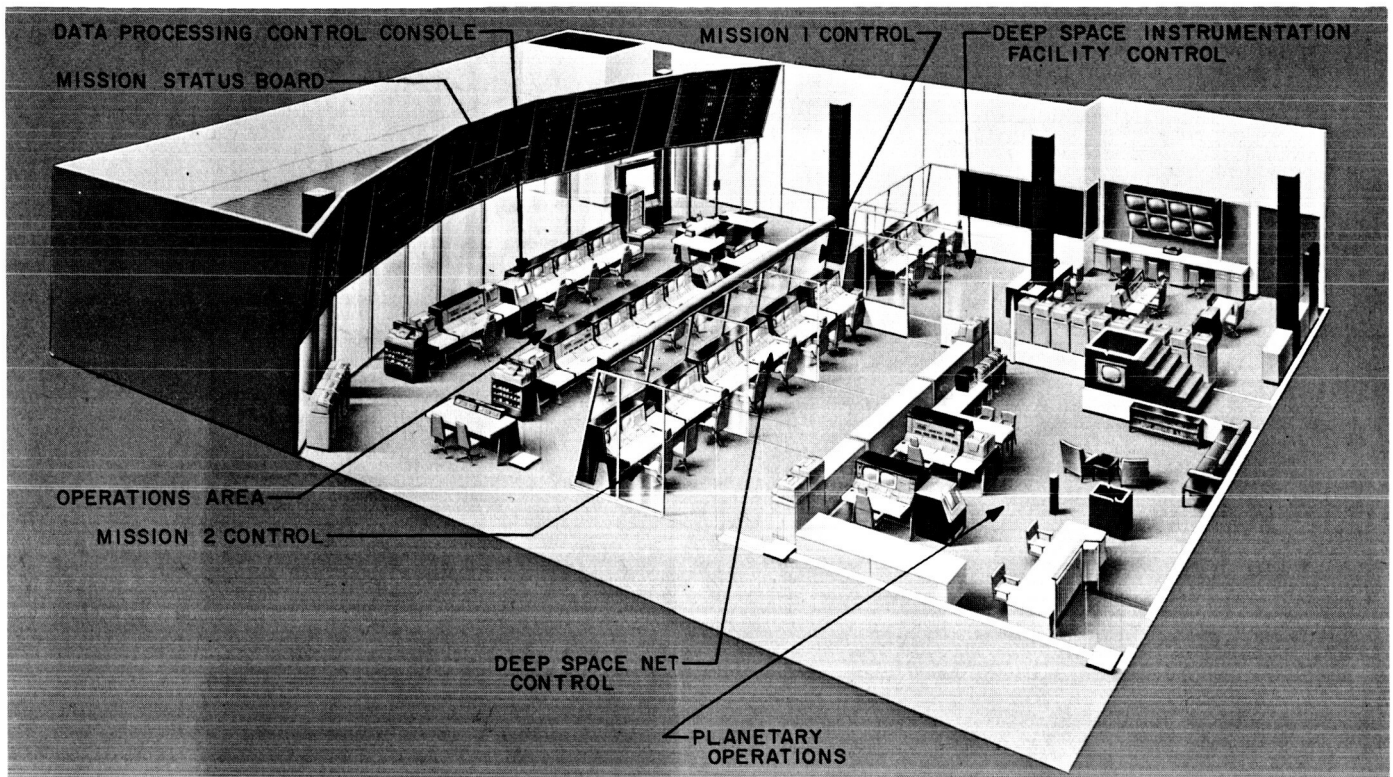
Fig. 4. Planned SFOF operations, mission control, and planetary operations areas
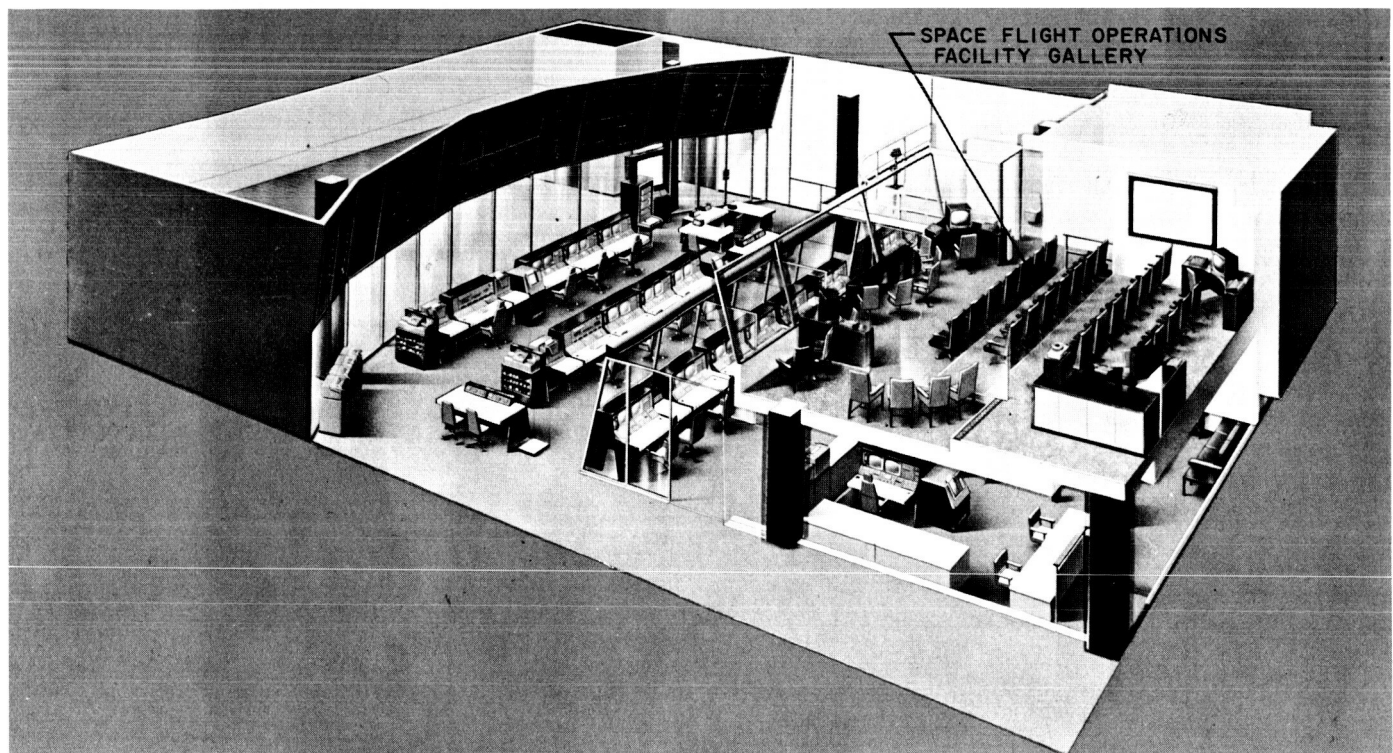
Fig. 5. New configuration for SFOF gallery

Fig. 6. SFOF operations area developmental status

AREA DISPLAYS

REMOTE DISPLAY OF
MISSION STATUS

DATA PROCESSING
SYSTEM OUTPUT
PLOTTERS

TELEVISION
DISPLAY SYSTEM
CAMERAS

AREA DIRECTOR'S
OPERATIONAL
CONSOLE

REMOTE DATA PROCESSING
SYSTEM INPUT/OUTPUT CONSOLE
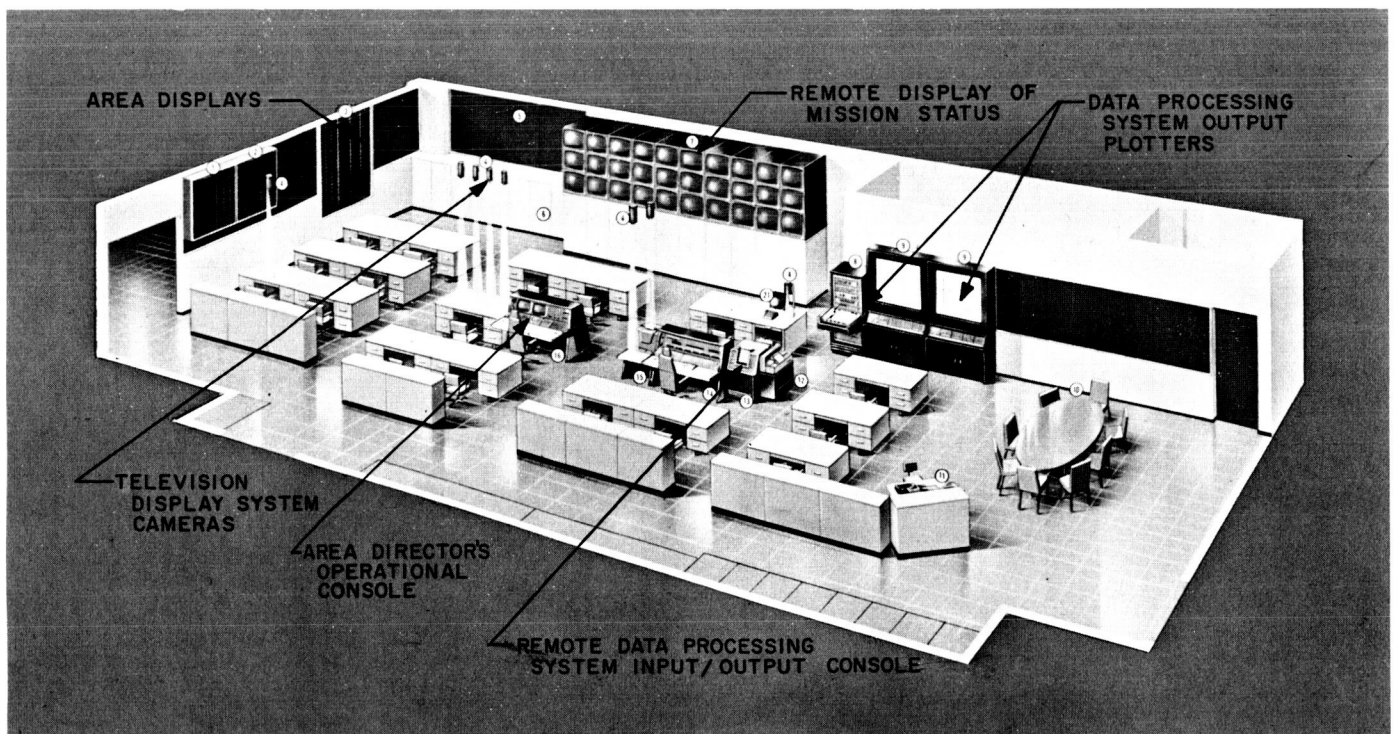
Fig. 7. Planned SFOF flight path analysis area

Fig. 8. SFOF flight path analysis area developmental status
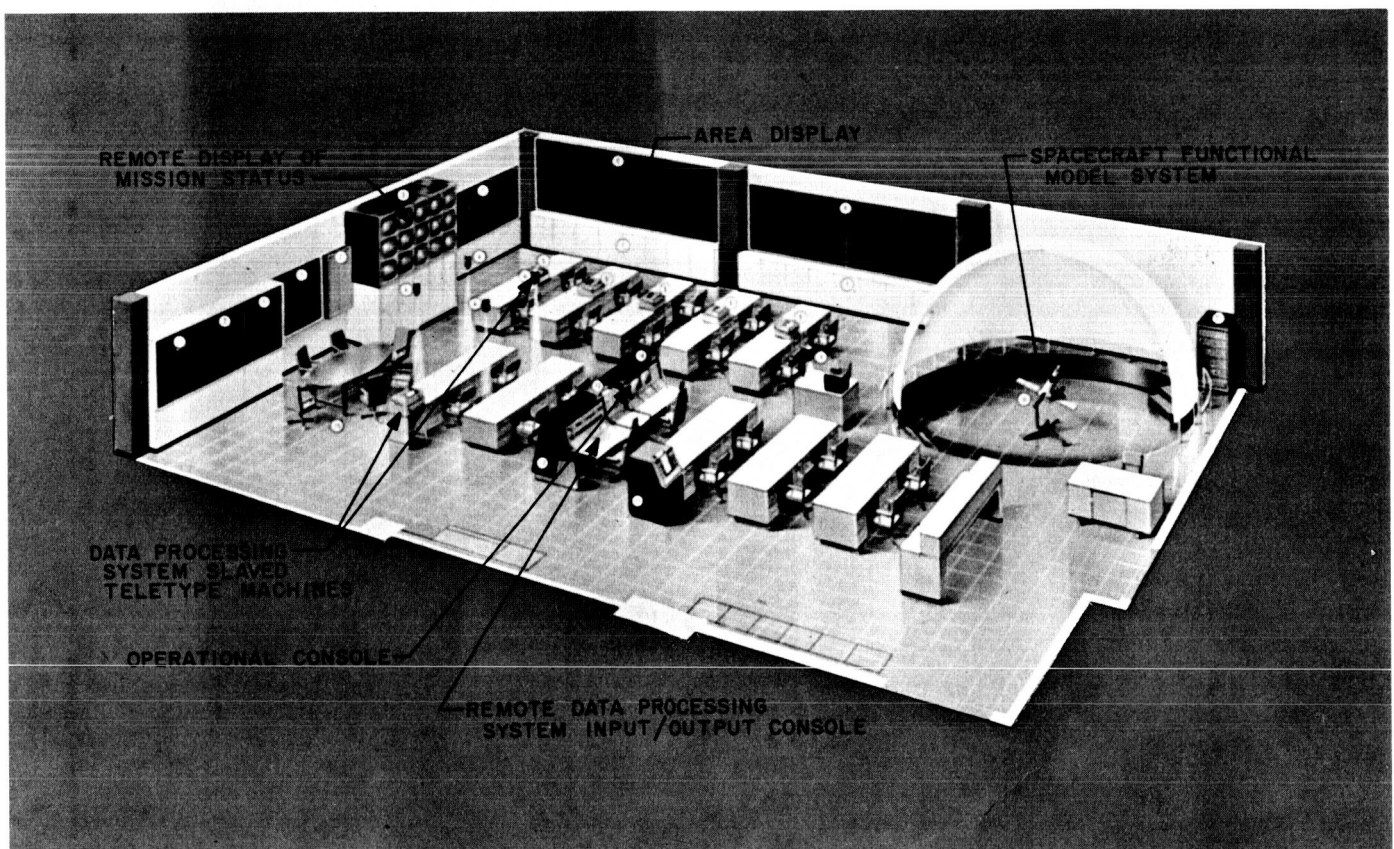
Fig. 9. Planned SFOF spacecraft performance analysis area

Fig. 10. SFOF spacecraft performance analysis area developmental status
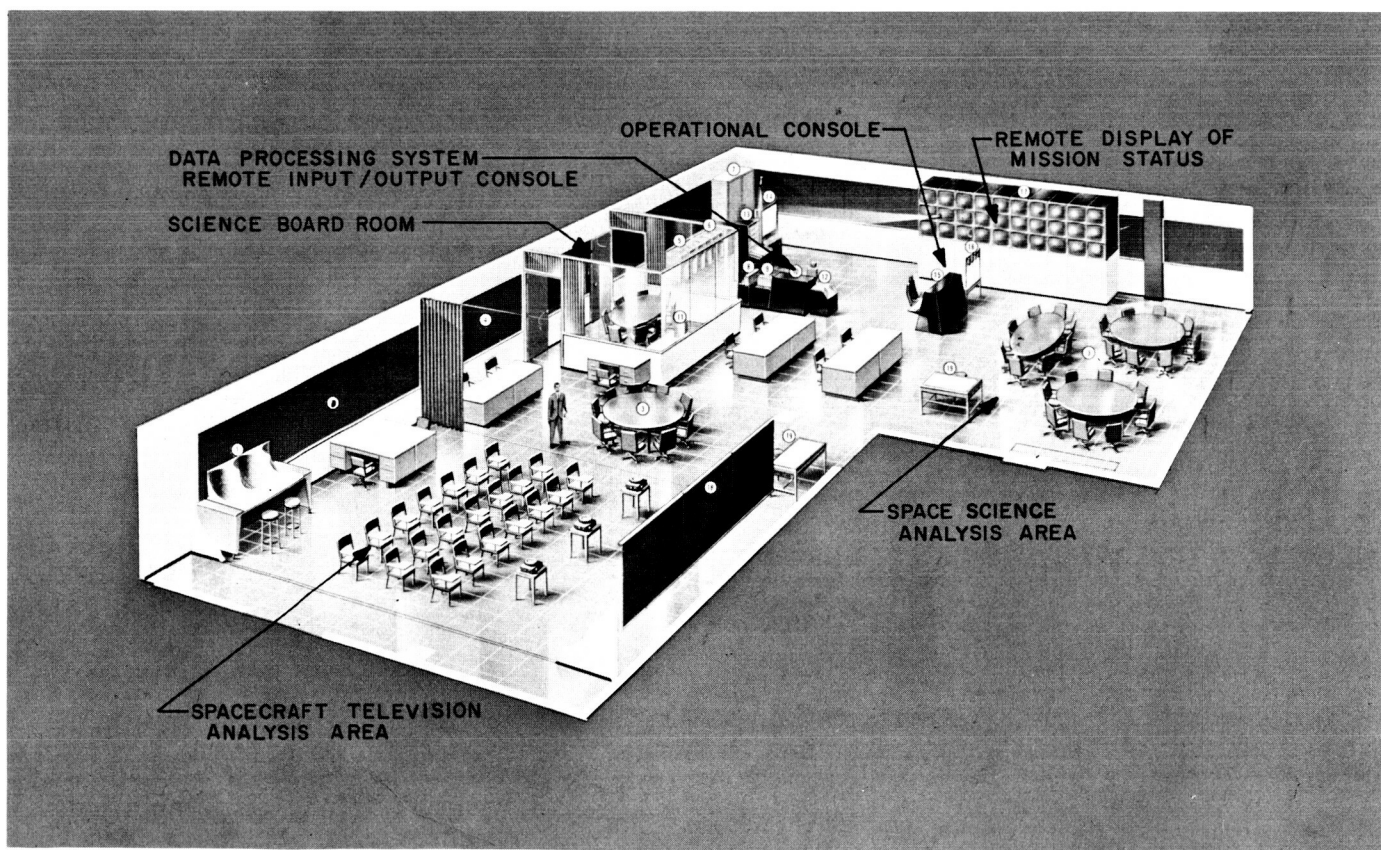
Fig. 11. Planned space science and spacecraft TV analysis areas

B. Communications System

The communications system of the Space Flight Operations Facility (SFOF), as reported in Ref. 1, is composed of a number of subsystems associated with the different media employed in the SFOF. This report describes the functions and composition of the teletype switching subsystem.

1. Teletype Switching Subsystem

a. General description. The teletype switching subsystem (TSS) provides the basic interface between external (36 incoming and 36 outgoing) teletype circuits and the end users or originators of teletype data within the SFOF. The TSS provides for receiving and transmitting capabilities in various teletype modes such as page printers, reperforators, transmitter-distributors, and keyboards at selected SFOF operational and technical areas; and provides direct interchange of data between the teletype circuits and the computers. In addition, the subsystem has the capability of switching incoming external lines and of establishing conference nets on these external lines.

To effect the control of teletype lines and machines, and to facilitate users access to a desired line in a practical manner, four basic control devices are used:

(1) Communications technical coordinator's panel.

(2) Communications data distributor's panel.

(3) Selector boxes.

(4) Television channel selector.

In addition to effecting the control of receiving and transmitting lines and machines, the above devices also provide control signals to activate displays and indicators showing the status of teletype lines on the communications status board (Fig. 12) and other remote areas. Through various control interconnections between the switching equipment, the control consoles, and the communications status display boards, visual indications of line assignment, traffic indications, distortion, and miscellaneous control functions are readily available to control personnel.

b. Communications technical coordinator's panel. The communications technical coordinator's panel is used to control and orient all incoming and outgoing lines and to provide stat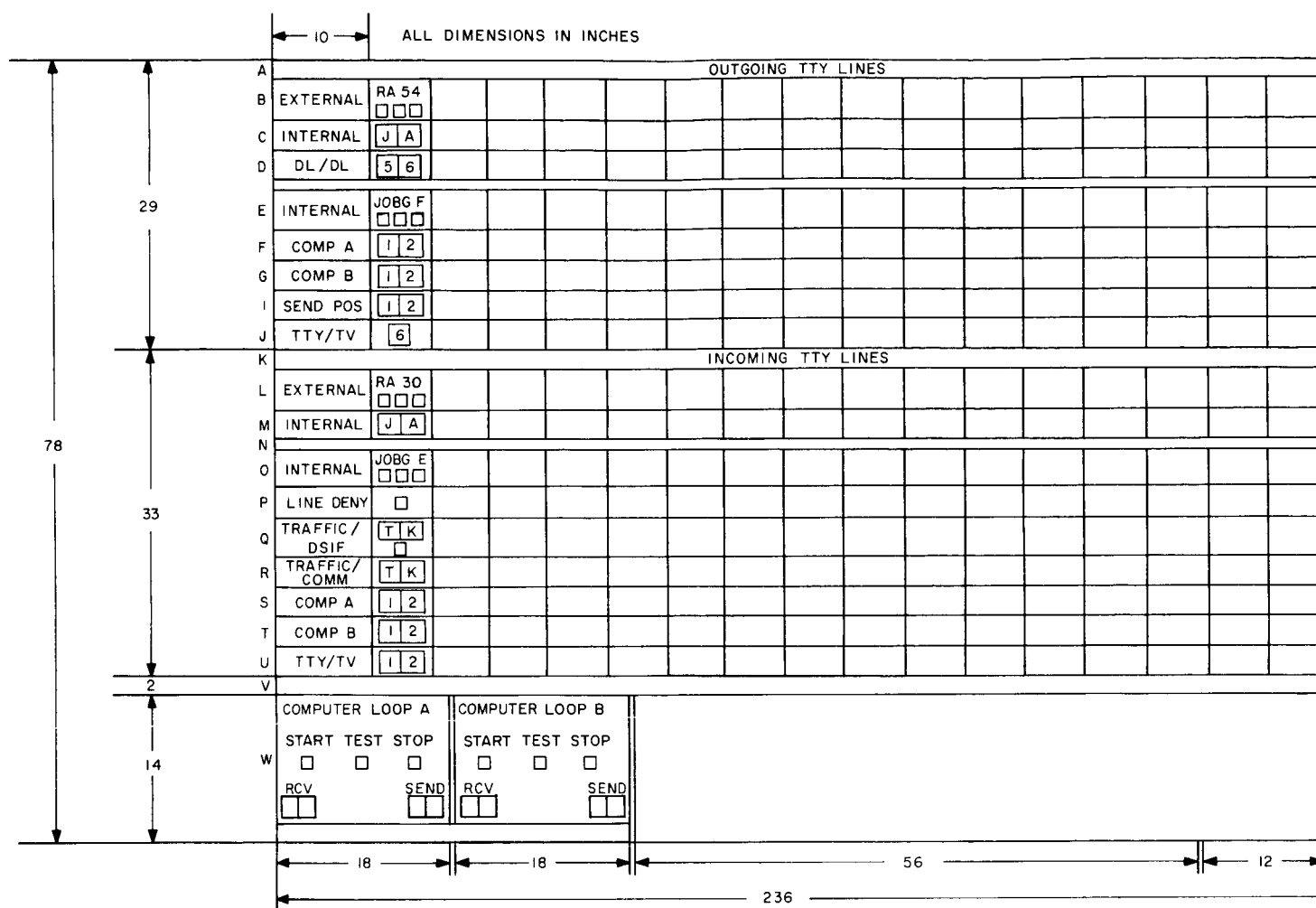us control signals to remote users. The panel layout, shown in Fig. 13, consists of 12 rows of indicator pushbuttons, four rows of indicator lights, and a number of special purpose switches. All switches are of the momentary pushbutton type; each contains an indicator lamp which is illuminated whenever a circuit is selected or is in use. Except for the *good/bad/marginal* rows all selector pushbuttons require a command from either an *enter* or *release* button to initiate the change. Depressing any of the 36 pushbuttons in a row, except the 3-row group mentioned, will cause the pushbutton to glow brightly, indicating a selection has been made. Depressing the *enter* button will finalize the change and cause the lamps to glow at a reduced level. The circuit is disconnected by using the *release* pushbutton in the same sequential manner as the *enter* button.

The panel is functionally divided into an outgoing section, incoming section, and a teletype monitor section. The arrangement of both the incoming and outgoing sections is similar. The traffic indicator modules are associated with a specific incoming (outgoing) line and will glow to indicate when a message is being received (sent) on that particular line.

The distortion indicator modules are also associated with a particular line. When the circuit distortion exceeds a preset level, a control signal from a distortion sensing circuit will cause the selected light to glow, indicating high distortion on that line.

Line status modules generate signals for remote display of line status. Upon determination by operating personnel of the line status for a particular line, the appropriate pushbutton is depressed, causing that indicator pushbutton and other such indicating devices in the SFOF communications system to glow.

The incoming line assignment module controls the orientation of incoming (outgoing) external teletype circuits with incoming internal SFOF teletype circuits. The need for this arrangement derives from the fact that distribution techniques employed require that circuit selectors at users' stations be permanently labeled. Thus, to effect this distribution so that users can be uniquely aware of the origin or destination of traffic, it is necessary to connect the external circuits onto appropriate incoming circuits before they are directed to users' areas. Orientation is accomplished by use of the two rows of indicator pushbuttons, and the *enter* and *release* pushbuttons. The top row of 36 pushbuttons is uniquely associated with the 36 incoming lines and the bottom

ALL DIMENSIONS IN INCHES

			OUTGOING TTY LINES
A			
B	EXTERNAL	RA 54 □□□	
C	INTERNAL	J A	
D	DL/DL	5 6	
E	INTERNAL	JOBG F □□□	
F	COMP A	1 2	
G	COMP B	1 2	
I	SEND POS	1 2	
J	TTY/TV	6	

			INCOMING TTY LINES
K			
L	EXTERNAL	RA 30 □□□	
M	INTERNAL	J A	
N			
O	INTERNAL	JOBG E □□□	
P	LINE DENY	□	
Q	TRAFFIC/DSIF	T K □	
R	TRAFFIC/COMM	T K	
S	COMP A	1 2	
T	COMP B	1 2	
U	TTY/TV	1 2	
V			

W: COMPUTER LOOP A — START TEST STOP □ □ □ — RCV / SEND ; COMPUTER LOOP B — START TEST STOP □ □ □ — RCV / SEND

Dimensions: 29, 33, 78, 2, 14, 18, 18, 56, 12, 236

row with 36 internal teletype circuits. Thus, by depressing the appropriate external and internal keys and the *enter* pushbutton, interconnection is effected.

The teletype monitor modules, *mon #1* and *mon #2*, are used for selecting desired nonoriented teletype circuits available for television monitoring. The two-position switch at the right of the rows of indicator pushbuttons enables the monitoring of both incoming and outgoing teletype circuits, using a single indicator pushbutton for each geographical location.

Distant lines to distant lines (DL/DL) modules effect connections between the external teletype circuits. This module is used with the external row of indicator pushbuttons on the line assignment modules of both the incoming and outgoing sections of the panel, the conference indicator pushbuttons (HDX) 1, 2, and 3, and the DL/DL *enter* pushbutton. The module allows a single incoming circuit to be connected to a single outgoing circuit in a full duplex arrangement or groups of circuits can be formed for a maximum of three conferences. Connection of a single incoming circuit to a single outgoing circuit is accomplished by momentarily depressing the appropriate indicator pushbutton on the desired external incoming and outgoing lines. Three half duplex conference nets may be formed by using the HDX pushbuttons (1, 2, or 3), the appropriate line selector indicator pushbuttons, and the *enter* pushbutton.

c. Communications data distributor's panel. The communications distributor's panel is used to control the distribution of all incoming and outgoing teletype circuits. The panel, shown in Fig. 14, consists of two similar sections associated with incoming and outgoing circuits. The incoming section provides the means for controlling
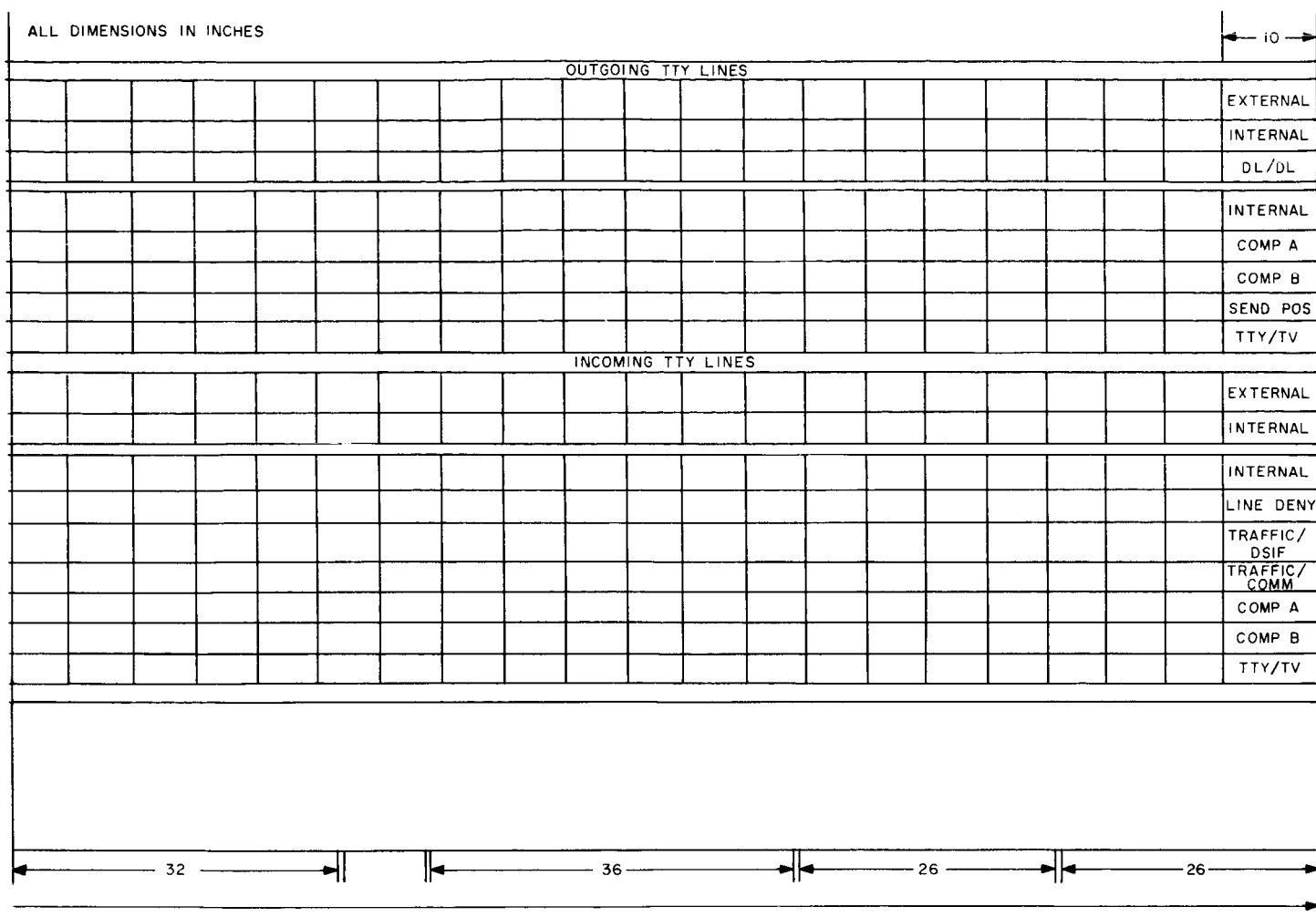
ALL DIMENSIONS IN INCHES

OUTGOING TTY LINES

EXTERNAL
INTERNAL
DL/DL

INTERNAL
COMP A
COMP B
SEND POS
TTY/TV

INCOMING TTY LINES

EXTERNAL
INTERNAL

INTERNAL
LINE DENY
TRAFFIC/DSIF
TRAFFIC/COMM
COMP A
COMP B
TTY/TV

|← 32 →| |← 36 →| |← 26 →| |← 26 →|

Fig. 12. Communications status board

the distribution of internal incoming teletype circuits to the indicated users, contains the facilities for entry of traffic identification into the teletype display portion of the SFOF communications system, and enables the denial of all incoming teletype circuits. The functions are performed through five modules designated on the panel as:

(1) Traffic indicator module.

(2) Traffic designation module.

(3) Line inhibit module.

(4) Internal line assignment module.

(5) Teletype monitor module 3.

The traffic indicator module is identical in use and operation to those used on the communications technical

coordinator's panel. It serves as a visual means for observing that messages are being received on the various incoming lines.

The traffic designation module is the means for entering traffic identification information (pertaining to the 36 incoming lines) into the SFOF communications status display and television channel selectors.

The line inhibit module is used to inhibit reception of incoming messages at the various operational areas, television/teletype interfaces, and the computers. Any one or all of the incoming lines may be inhibited by depressing the appropriate indicator pushbutton. The circuit is released from the inhibit condition by depressing the associated button a second time. When a line is inhibited (or released) control signals are sent to the
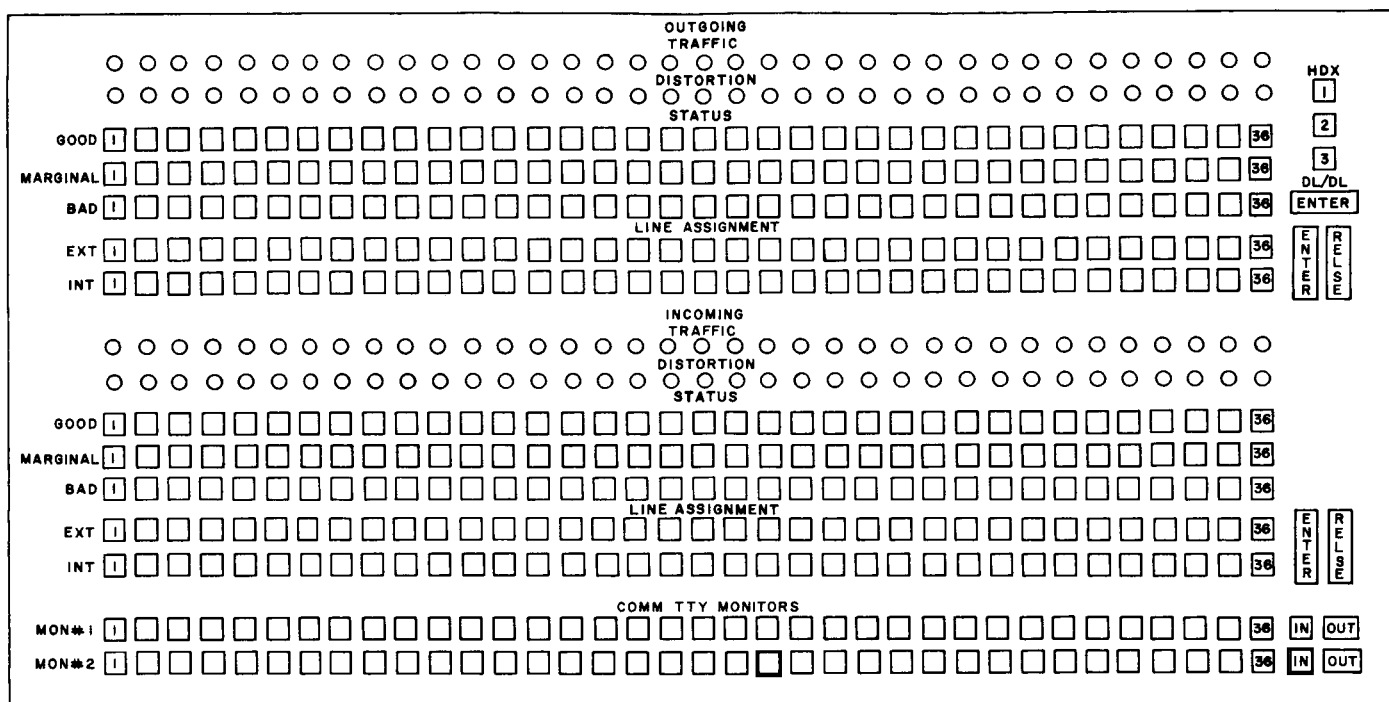
Fig. 13. Communications technical coordinator's panel layout
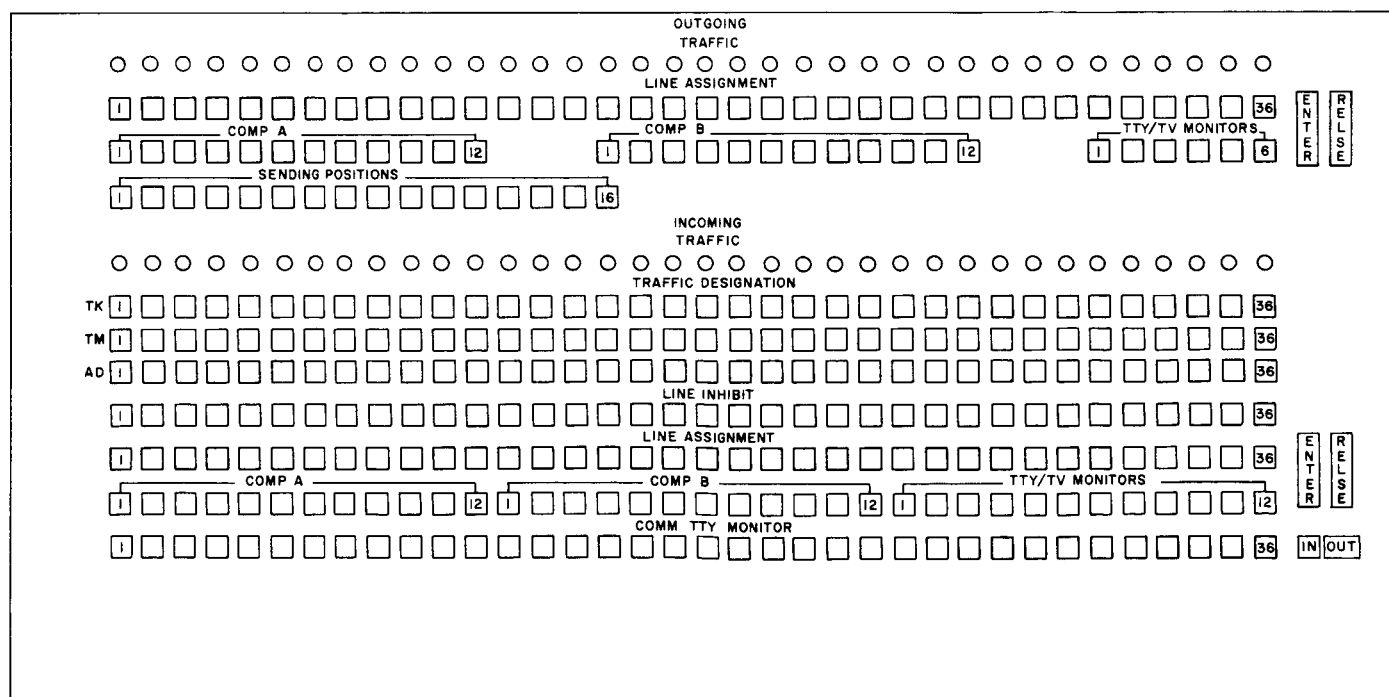
Fig. 14. Communications data distribution panel layout

communications status board and the Deep Space Instrumentation Facility control room to effect display of the status of the line deny indicator pushbuttons.

The internal line assignment modules in both the incoming and outgoing sections are identical in function and use to the line assignment module in the communi-

cations technical coordinator's panel. These modules are used to effect connection between any one of the incoming (outgoing) lines to any of the areas indicated on the panel.

d. Selector box. Selector boxes in operational and technical areas give users the means for selecting incoming teletype circuits. The selector box consists of 36 indicator pushbuttons, each one individually and uniquely associated with each of the 36 incoming oriented teletype circuits. Each indicator pushbutton is permanently marked with the circuit identification that designates the message origin. Selection of a particular incoming circuit is made by momentarily depressing the appropriate indicator pushbutton. The associated page printer will immediately start printout of the incoming data from the selected line and the associated indicator pushbutton will glow. The selected line is disconnected either by depressing the same button a second time or by depressing another indicator pushbutton.

e. Television channel selector. The television channel selector is associated with the closed circuit television subsystem. The selector allows the user to select for viewing on his TV monitor any of several remotely televised page printers.

Reference

1. "Communications System," *SPS 37-20,* Vol. VI, pp. 53–56, Jet Propulsion Laboratory, Pasadena, California, April 30, 1963.

VII. Test and Support Equipment

A. Environmental Test Laboratory

1. Thermal-Vacuum Testing

Modifications of the 7- × 14-ft vacuum chamber in JPL Building 144 have been completed. The modifications included the replacement of a 6-ft-long cylindrical copper cold wall by a two-shroud cold wall system and changes in the liquid-nitrogen piping arrangement.

The new cold wall consists of a stainless-steel embossed-plate cylinder shroud and back wall shroud (B and C, respectively, in Fig. 1). The shroud surfaces facing the chamber wall are electropolished to reduce the radiative heat transfer between the shroud and the chamber walls. The inside surfaces are finished with black Cat-A-Lac epoxy paint.

The new shrouds have increased the effective working length of the chamber from 72 to 122.75 in. (Fig. 2). The 74.5-in. ID of the working volume is slightly greater than that before the modification.

B. Operational Support Equipment

1. Ranger Gamma-Ray Decoder

As a part of the proposed Ranger Block V scientific operational support equipment, decoding equipment was developed to provide real-time monitoring of the gamma-ray spectrometer. Since the gamma-ray readout rate to the data automation system was faster than could be normally handled by standard display equipment, the mechanization of the decoder included the use of a magnetostrictive delay line memory to allow data-rate conversion. With the cancellation of the Ranger Block V program, the final phase of the development was completed to demonstrate this technique for application to future high-data-rate scientific instruments.

The gamma-ray decoder (Fig. 3) is comprised of logical elements which accept coded data from the gamma-ray instrument aboard the spacecraft (via hard line),

convert this information into channelized decimal data, and apply it to an output mechanism for quick-look evaluation. The decoder consists of three basically separate functional elements: the control logic and memory, a binary–to–binary-coded-decimal (BCD) converter, and a BCD digital recorder.

a. Functional description. The decoder serves as a data processing, storage, and display unit between the gamma-ray instrument and an operator. In addition to data-rate conversion capabilities, the delay line memory is able to accumulate and sum sequential readouts, allowing larger samples to be displayed, to determine the gamma-ray "signature" of various source materials. Fig. 4 illustrates the functional operation of the decoder. Data flow is represented by the heavy lines and control functions by the dashed lines. The basic parts of the control logic and memory subunit are: (1) an input register, (2) a parallel comparator and address control logic, (3) a serial memory, (4) a serial adder, (5) an output register, and (6) a timing system.

Input register. Data are applied to the input register, the least-significant bit first, through a control *nand* gate. The input register is a 16-bit shift register. Data shifting pulses (bit sync) are obtained from the spacecraft at a 2.4-kc rate. When the complete 16-bit word is present in

Fig. 1. New shrouds installed in 7- × 14-ft vacuum chamber
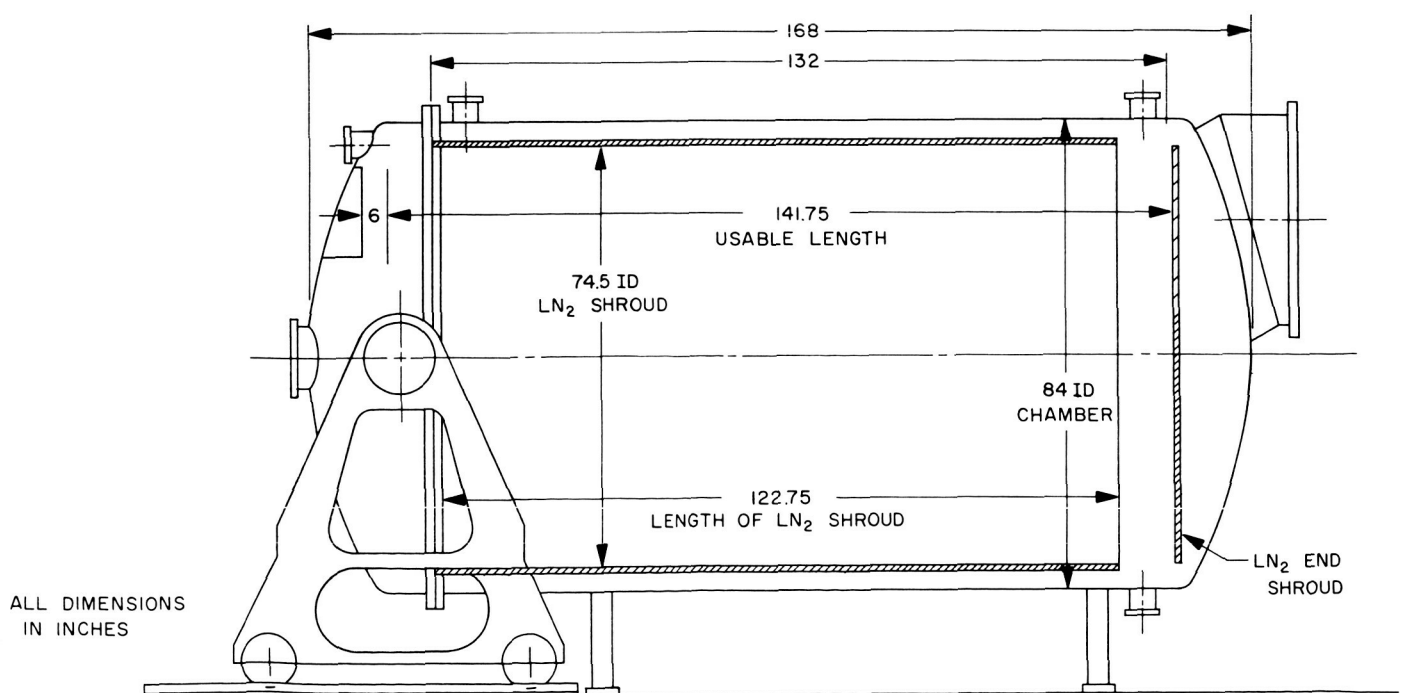
Fig. 2. 7- × 14-ft vacuum chamber, showing dimensions of working volume

the register, the action of the input bit counter indicates to the control logic that transfer to the memory can then be accomplished. During this transfer, the input control *nand* gate is inhibited to prevent any incoming data from

interfering with this transfer. Because the maximum elapsed time required for this transfer operation could be as much as 2064 μsec, it was necessary to provide a buffer to the input register to accept incoming data during the transfer time. This buffer is a 5-bit shift register which is enabled during the transfer process. The five stages provide 2080 μsec of storage, which is adequate under "worst case" operation. The transfer-complete function disables the buffer input, parallel dumps the data into the input register, and re-enables the input control gate. Throughout all input operations, the input bit counter maintains a continuous count to accurately control the transfer operation, regardless of whether the buffer or the input register is being used.

Parallel comparator and address logic. Memory position identification is accomplished by three binary counters, which are set to count 16 bits, 32 words, and 4 subframes. These subdivisions were chosen to correspond to the makeup of the gamma-ray data block, which is made up of 32 gamma-ray energy channels of 16 bits each. There are four unique data blocks (all possible combinations of two parameters: high/low gain and reject/non-reject circuits) which are considered subframes of the memory
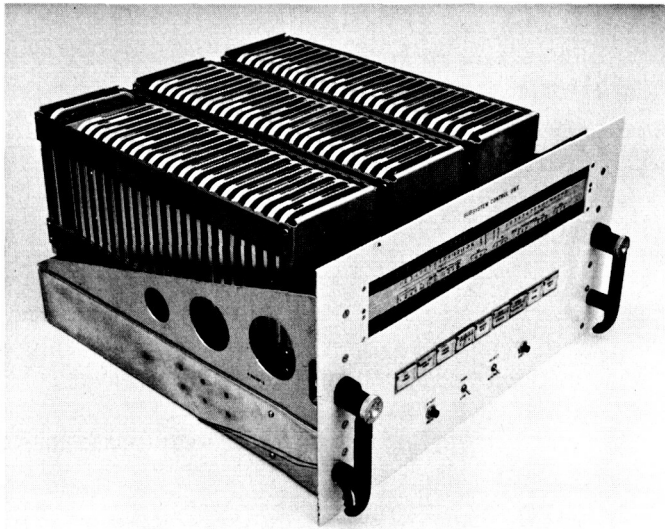
Fig. 3. Gamma-ray decoder chassis
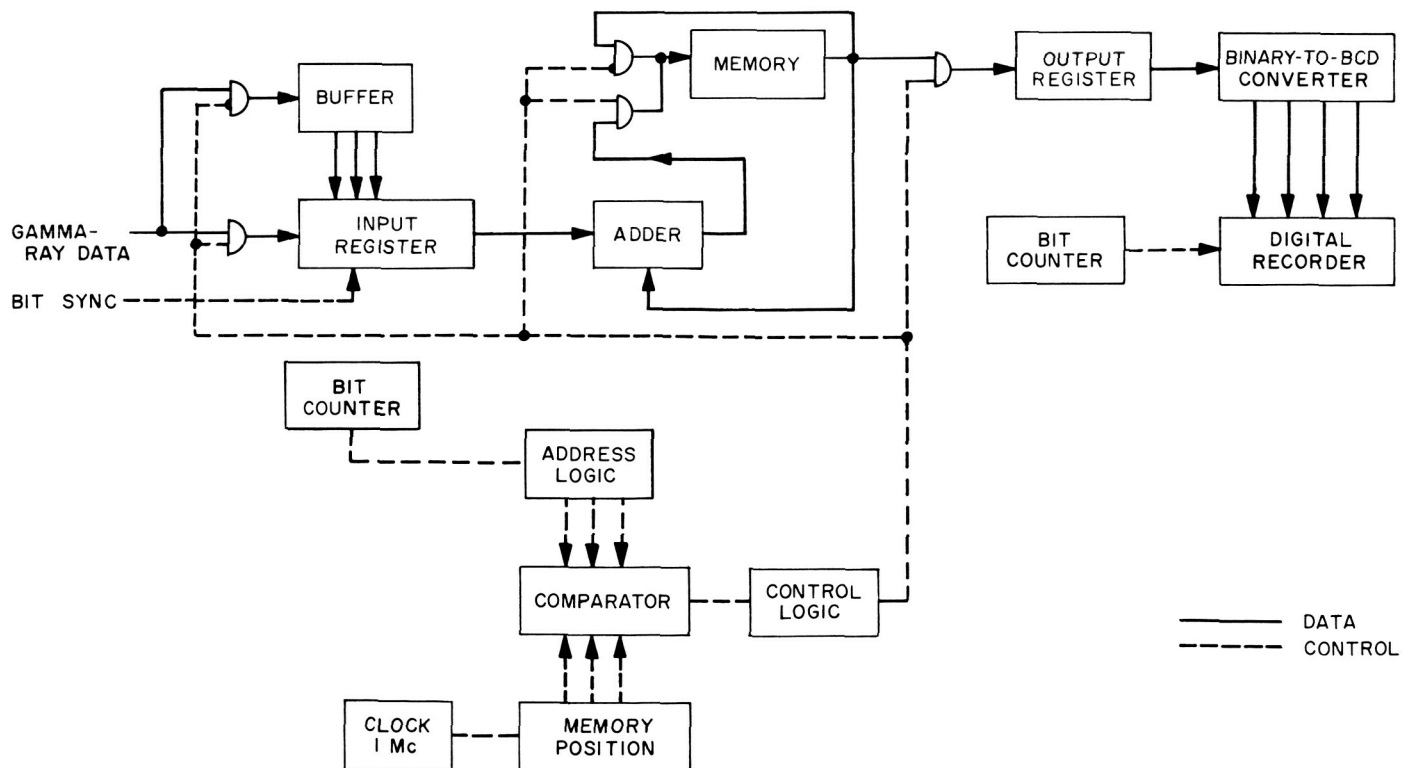
Fig. 4. Gamma-ray decoder block diagram

frame (2048 bits). A corresponding grouping of counters was set up to act as addressing logic. These counters are the word and subframe address units. This address mechanism sets up a given address, e.g., word 05, subframe 3. By means of a parallel comparator, the address logic and memory position logic are compared. When the correct position in the memory is reached, the memory input circuits are enabled for the period of time (16 bits) required to insert the addressed word. At the end of 16-bit times, the memory word counter advances one count, address sync is lost, and the memory is allowed to return to its circulating mode. This operation is continued until the memory is filled or a readout command is initiated. The action of the addressing logic and comparator during the readout cycle is identical to that during the storage cycle, except that output circuits are enabled during address sync rather than input circuits.

Serial memory. To accomplish the rate conversion and accumulation of consecutive readouts, the use of a storage, or memory, device was required. Storage capability (2048 bits) eliminated such storage devices as shift registers and ring counters, and physical size eliminated such devices as magnetic drums or discs. Of the remaining two types of simple storage mechanisms, the magnetostrictive delay line (Fig. 5) was selected as the most suitable. The delay line chosen was a wire acoustical type, which will, in effect, reduce the velocity of an electrical wave by converting it into a sound wave and then reconverting it back into its electrical form. The acoustical

Fig. 5. Magnetostrictive delay line

properties of the delay line require that it be continuously in motion; hence, the memory position logic described previously is necessary. The operation of the decoder therefore utilizes dynamic logic, as opposed to the less-complex static logic used with register storage. Storage is accomplished by recirculation. During the storage portion of the memory cycle, the output is connected to the input and data are permitted to circulate through the delay line.

To maintain small physical size and at the same time provide a large storage capability, a memory clock rate of 1 Mc was chosen. It was then possible to store 2048 bits of data in a delay line whose delay was only 2.048 msec. The access time to a given memory address was therefore fixed to a "worst case" figure of 2.048 msec. This access time plus 16-μsec transfer time defined the required buffer register length.

Serial adder. The timing of the gamma-ray instrument is such (10-sec samples) that only a small number of counts result from the test stimuli. To obtain a sufficient number of counts to accurately determine the gamma-ray "signature" of the various sources, it is necessary to somehow accumulate and sum consecutive like readouts. To accomplish this function, a serial adder was incorporated in the decoder. The equations for the adder are:

$$S = (A \cdot \bar{B} \cdot \bar{C}) \vee (\bar{A} \cdot B \cdot \bar{C}) \vee (\bar{A} \cdot \bar{B} \cdot C) \vee (A \cdot B \cdot C)$$
$$C = (A \cdot B) \vee (B \cdot C) \vee (C \cdot A)$$

The sum equation is implemented directly with *nand* gates, and the output is applied to the input of the serial memory. Each shift pulse transfers the sum into the serial memory, advances the addend and augend registers, and generates a new sum. The carry equation is implemented directly with *nand* gates, and the output is applied to a shift register stage which effectively delays the carry–1-bit time. The output of this stage is the carry from the previous bit addition. In operation, the data from the serial memory are applied (the least significant bit first) to the augend inputs, and the data from the input register are applied to the addend inputs. The addition is accomplished in the adder, and the sum is inserted into the memory in place of the augend. This accumulation and summing is continued for 10 operations, after which readout is accomplished.

Output register. The output register is a 16-stage shift register which may be shifted either left or right. During the readout cycle, data are shifted from the serial memory into the output register at the 1-Mc clock rate. The data
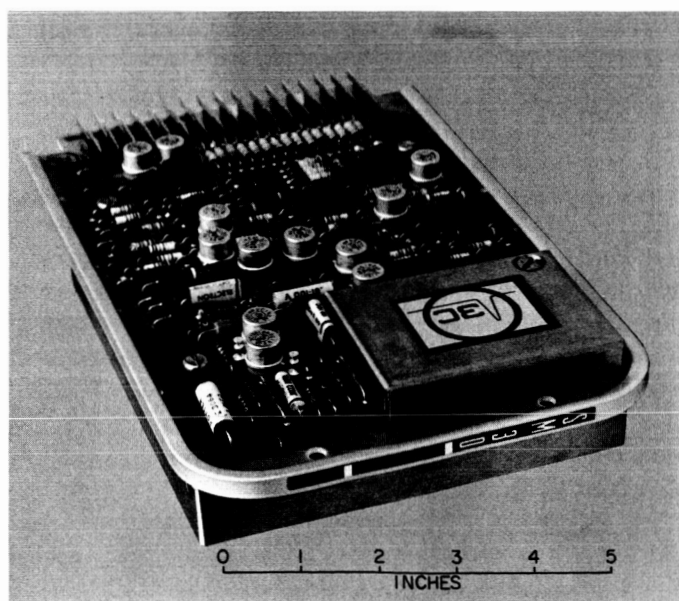
from the memory were entered into the register with the least-significant bit first. Since the binary-to-BCD converter operates on the most-significant bit first, it was necessary to provide the output register with shift-left and -right capability to prepare the data for the converter. The converter need only operate fast enough to be compatible with the speed constraint of the digital recorder; therefore, for reliability considerations the conversion rate chosen was 400 bits/sec.

Timing system. The timing system is the heart of the decoder. A precision crystal-controlled 1-Mc clock was used to generate the data pulses which operate the serial memory. A multivibrator was used to generate internal bit sync of 400 bits/sec, which is used to self-test the decoder and to operate the binary-to-BCD converter.

b. Binary-to-BCD converter. The converter provides an interface between the decoder and the digital recorder. By converting the serial binary to parallel BCD, this unit makes the decoder output and recorder input compatible. The conversion is accomplished by the so-called "double-dabble" method. Given an N-bit pure binary number, the conversion method is as follows:

(1) Begin with the most-significant bit.

(2) If the next bit is a *zero*, double the accumulated sum.

(3) If the next bit is a *one*, double the accumulated sum and add 1.

(4) Continue this process for all succeeding bits, carrying along the accumulated sum.

The properties of binary numbers are such that a number may be halved or doubled simply by shifting one place right or left. A BCD number has the same property, but numbers which are doubled must be adjusted because a radix of 10 is imposed. Thus, the doubling of any 4-bit digit which is 5 or greater results in a digit (10 or greater) that is outside the limits of constraint. By adding 6 to any number greater than 9 (which results from doubling), a 2-digit number is created within the constrained radix of 10.

A convenient method of implementing the "add 6 correction" is to detect 4-bit digits that are 5 or greater and add 3 to them before doubling. This, in effect, is equivalent to adding 6 to the doubled number, but it eliminates

the need for carry generation between decades. Doubling and doubling-and-adding-3 are accomplished automatically by shifting.

The data from the output register are shifted into the code converter. At the end of 16 shift pulses, the action of the output bit counter causes the contents of the converter to be parallel-dumped into the digital recorder. The information available as an output from the recorder is 32 decimal numbers properly identified as to which channel and which subframe each number represents. In this manner a table of numbers is presented for each of the four conditions under which the spectrometer operates. These numbers, when plotted against the channel number (or gamma-ray energy level it represents), indicate the so-called gamma-ray "signature" of the test stimuli.

c. Performance. Using Computer Control Company's 1-Mc logic, a decoder and converter were constructed to demonstrate the feasibility and performance of this data-processing technique. The number of cards required to mechanize both units fit into one standard logic chassis. Except for initial timing difficulties caused by accumulative logic delays, the equipment checkout phase was accomplished in an orderly fashion. Certain remechanization of logic functions was accomplished to solve the timing problems and improve the margin required for card interchangeability.

2. Mariner C Magnetometer Mapping Fixture

A fixture has been designed and built by Sperry Company to allow rotation of the Mariner spacecraft about the x, y, and z axes of the magnetometer and to allow the spacecraft 50 ft of linear translation. Since the magnetometer is remote from the main body of the spacecraft, and since the spacecraft must be complete with the attitude control gas jets near their flight positions, the fixture required is quite large. The fixture consists of four major assemblies: the magnetometer test probe support, the horizontal test fixture, 70 ft of track for linear travel, and solar panel fixtures.

The complete setup is shown in Fig. 6. The spacecraft is eccentrically mounted on a worm gear driven vertical turntable so that the centerline of the table passes through the center of the magnetometer. Permanently attached counterweights are used to bring the combined cg back to the table centerline to reduce the loads on the gears.
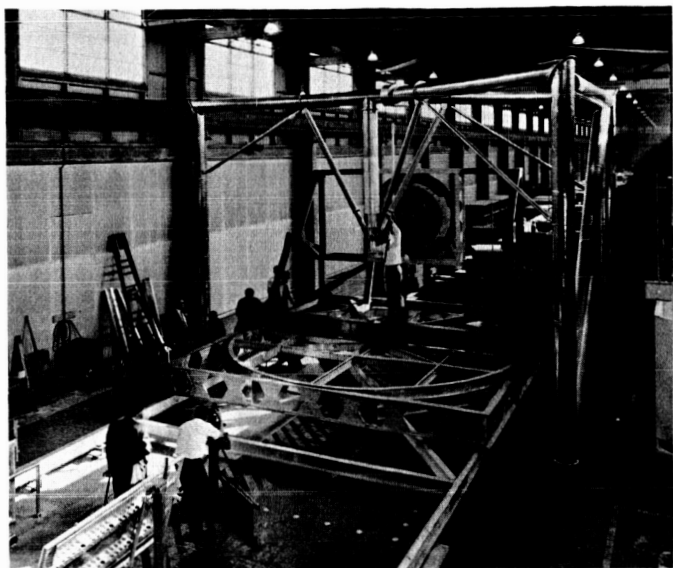
Fig. 6. *Mariner C magnetometer mapping fixture*

Turning the table provides rotation about the z axis. Rotation about either the x or y axis is obtained by rotating the top part of the fixture around with respect to the carriage. The weight of the fixture and spacecraft is carried on rollers on an 18-ft-D track, and guiding is accomplished by a center pin in a bearing. The solar panel fixtures can be placed on the rotating portion of the fixture for mapping, or they can be used on the floor with separate dollies.

To provide for accurate linear motion of the spacecraft for a distance of 50 ft, the entire fixture described above is placed on 70 ft of track. The carriage is manually pushed along the track and a scale on the track is read for a distance versus field strength plot.

The test magnetometer is supported by the large tubular structure spanning the rails and structure. With the spacecraft mounted on the horizontal test fixture and the flight magnetometer removed, the spacecraft can be moved up under the probe support. Adjustments are provided on the mounting head of the probe support to allow exact positioning of the test probe to where the flight probe would ordinarily be mounted. The spacecraft magnetic field is then mapped by rotating the spacecraft on the fixture about the stationary probe. All parts of the fixtures which move with the spacecraft are nonmagnetic, and to reduce local fields, the fixtures are also nonmagnetic. The structural elements and all nuts and bolts are aluminum and all bearings are fiberglass/Teflon compounds.

All of the fixtures can be disassembled for storage and shipment. The entire test setup can be packed in two 26-ft trailers. A trained crew can assemble the fixtures for use in approximately 12 hr.

3. Voltage Monitoring of Mariner C AC Power

Because of the complex waveforms of the spacecraft ac power and the various test cabling configurations of operational support equipment (OSE), transmission problems are encountered that make direct monitoring of the pertinent ac voltages unsatisfactory. To reduce transmission problems in the *Mariner C* power OSE, signal conversion or conditioning is employed as close to the spacecraft power system as is permissible. The ac conditioner, located within the umbilical tower junction box, monitors the spacecraft ac power system voltages and produces dc output voltages that are directly proportional to the rms value of the monitored ac voltages. These dc voltages are sent to the power OSE monitoring assemblies where they are continuously monitored by the tolerance detectors and periodically sampled by the automatic data monitoring system.

Since the conditioners are used between the spacecraft and OSE monitors, the power OSE self-test and transfer functions must be extended to the conditioner circuits, and power must be supplied to operate the conditioners. A block diagram of one of the six conditioner channels is represented in Fig. 7. The ac signal from the spacecraft is connected through a low-capacitance, low-thermal-coefficient cable to the monitor input of the conditioner assembly and is then connected through the *Operate* position of the transfer relay to the input of the signal conditioner. The dc output of the conditioner is connected through the power OSE/umbilical J-Box cable run to the power OSE monitor circuits. This cable also carries the *Test* and *Operate* transfer commands to the conditioner circuits and the *Test* and *Operate* verifying indications back to the OSE. The dc power to operate the signal conditioner is provided by the transformer-rectifier (TR) supply contained within the conditioner assembly. The TR supply is powered from the regulated 400-cps source within the power OSE through a separate cable. Another cable from the power OSE brings self-test inputs to the conditioner by way of the *Test* position of the conditioner transfer relay. The *Function* command from the transfer relay is used to program the conditioners, as required, to accept a clipped sine wave as a test voltage.

The conditioner self-test is initiated by the power OSE *Monitor-Test* function and is integrated with that func-
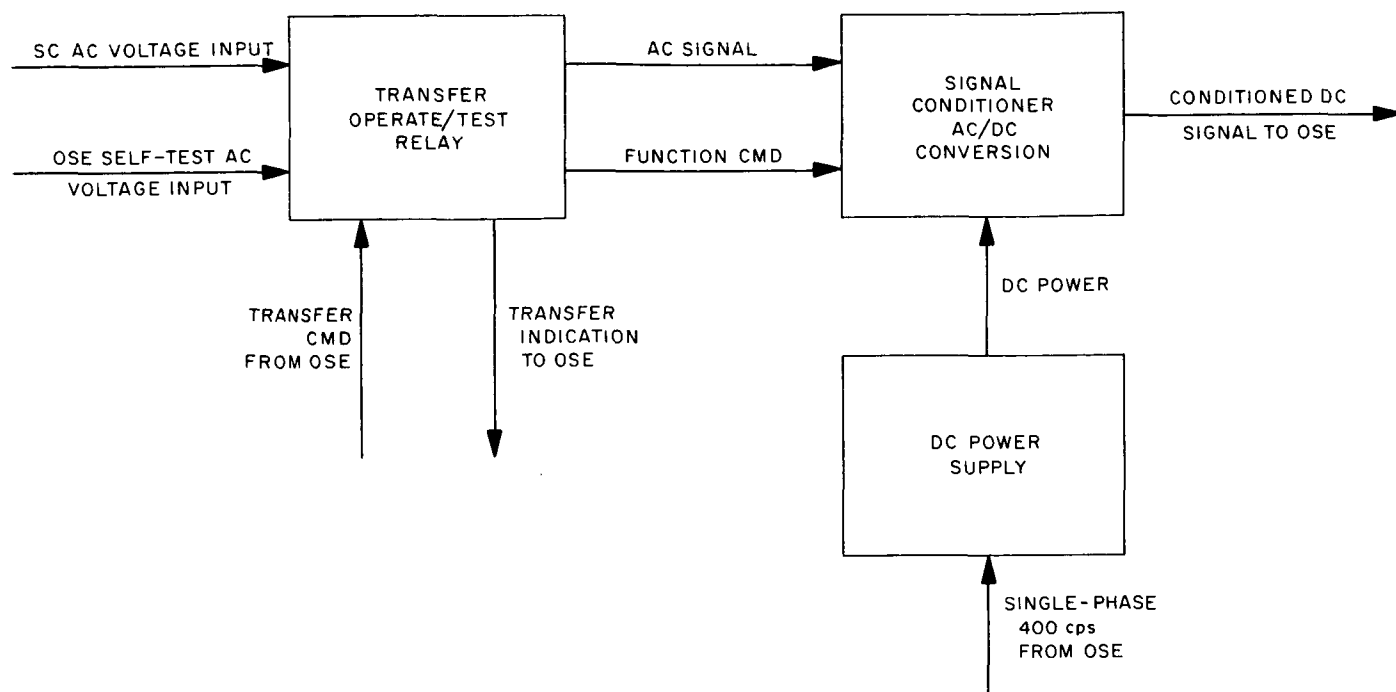
Fig. 7. Block diagram of ac conditioner

tion to transfer ac conditioners inputs from spacecraft voltages to test voltages that originate in the power OSE self-test assembly. The high, low and normal test voltages applied to the conditioners substitute for the spacecraft voltage waveforms and in conjunction with the tolerance detector test logic circuits provide a check on the performance of the conditioner circuits. In addition, the automatic data monitoring system can be used to display and compare the self-test voltages.

The conditioner assembly housing, shown in Figs. 8 (a) and (b), is a cast-aluminum box with removable top and bottom cover plates and gasket seals. Within the housing, all active circuit components are mounted on ten plug-in printed circuit cards of which there are six ac conditioners, two dc power supplies, and two transfer relay assemblies. These cards are held in the sockets by retainer brackets fastened to the top cover plate. A plate recessed in the top face of the housing holds twenty-two test points that permit monitoring the internal input and output voltages of the conditioner cards. The conditioner assembly is 9 in. long, 9 in. wide, and 7 in. deep, and weighs approximately 7 lb.

4. Mariner C Laboratory Test Set

In order to define properly the function of the laboratory test set (Fig. 9), three stages of secondary power

subsystem testing will be described in chronological order. First, all power subassemblies, or modules, at completion of fabrication are tested in a bench test set. This is a self-contained test set which can exercise any module individually and independently of the remainder of the power subsystem. In addition, the test set has the ability to test the whole subsystem while electrically connected but not physically located in the flight configuration.

In the second stage of the test program, which is the subject of this discussion, the power subsystem is assembled into its electronic cases and tested by the laboratory test set. Type approval and flight acceptance tests are also conducted at this stage.

Finally, the power subsystem is installed in the spacecraft, and a system test set [part of the spacecraft operational support equipment (OSE)] is used to operate the power subsystem as a part of the spacecraft at the Spacecraft Assembly Facility (SAF) and at the Atlantic Missile Range.

The laboratory test set was designed primarily for type approval and flight acceptance testing, with either of the spacecraft power assemblies Case I or Case VIII under test. Previously, it has been customary to adapt a bench test set (or subassembly test set) to this purpose by
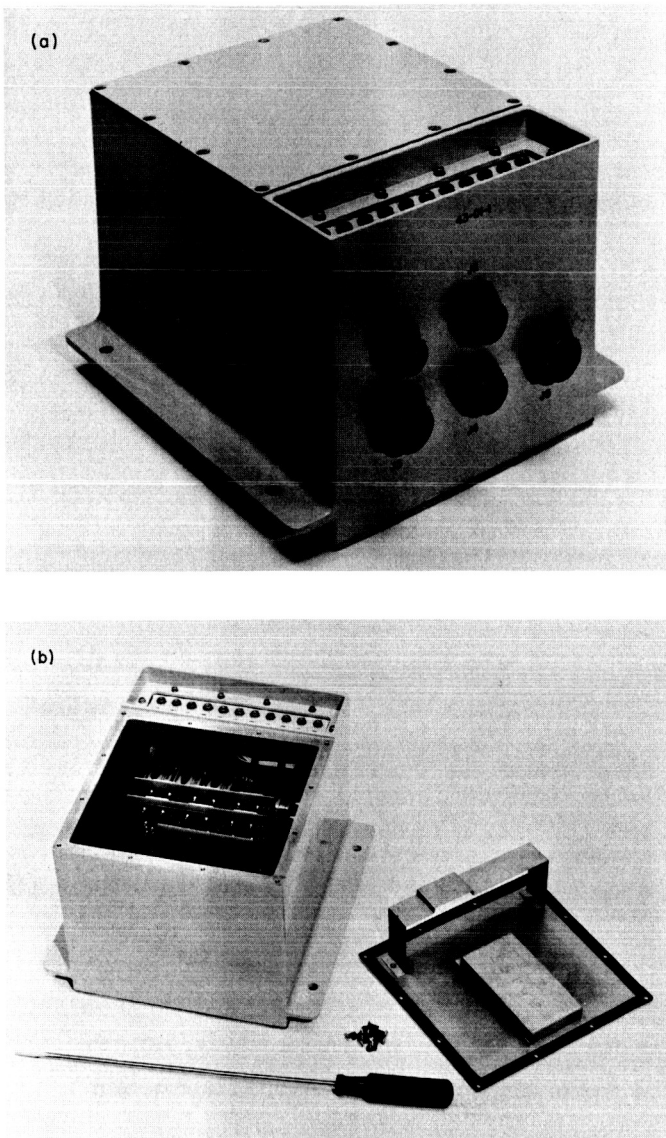
(a)

(b)

Fig. 8. Views of conditioner assembly: (a) exterior;
(b) interior, top cover removed

Fig. 9. *Mariner* C secondary power laboratory
test set

means of an adapter cable. In the case of the *Mariner C* program, a new approach has been taken, and the requirement for a case-level test set was met by combining a system test set (OSE) with a third console called the "laboratory test adapter." Fig. 9 shows a front view of the laboratory test set. The adapter rack routes all functions from the system test set/system test complex cables directly to Cases I and VIII, thus permitting the system test set to monitor, control, and power the power subsystem independently of a complete spacecraft. A secondary function is to make available directly at the adapter rack some 40 functions not available at the system test set.

The versatility of the test set is increased by providing switching capability to enable both cases to be tested together. This permits performance testing and design evaluation of the complete power subsystem prior to delivery to the SAF along with compatibility verification between OSE and flight hardware.

All the normal features of the OSE system test set apply in the laboratory test set configuration: a digital recording system with manual or automatic operational capability, tolerance detectors, controls for applying internal, external, or simulated solar panel power, and self-test of both monitors and controls. Power supplies provide for external or simulated solar panel power, as well as dummy loads for all subassemblies and command inputs to the power distribution subassembly.

Type approval and flight acceptance testing of the power subsystem utilizes the full capabilities of the laboratory test set. Cases I and VIII are subjected to the vibration program independently. Both cases are then tested simultaneously in the thermal vacuum chamber, making use of the test set capability to operate the cases together and thus effecting a considerable saving of test time and facilities.

5. Automatic System for Acquisition and Processing of Mariner C Systems Test Data

A real-time on-line automatic data system is presently being used as an aid in the checkout of the *Mariner C* spacecraft (Ref. 1). Major objective of the data system is to provide printout of only the significant data which is acquired or processed during spacecraft systems tests. By suppressing the printout of redundant data, it is believed that the performance of the spacecraft can be effectively monitored in real time, and that later examinations of the printed record will be sufficiently easy so that all test records obtained actually will be used and interpreted.

The input data to the computer data system consists of:

(1) Spacecraft pulse-code modulated (PCM) telemetry.

(2) Analog voltages which are scanned by a multiplexer and then digitized.

(3) Pulses or contact closures which represent significant events in the spacecraft or operational support equipment (OSE).

(4) Pulse trains or groups, or periodic waveforms for cycle-counting.

All data is recorded on digital magnetic tape without processing or editing to permit subsequent nonreal-time analysis using the data system or other computer systems.

The data system contains a Univac 1218 computer system with 16384-word memory and four digital magnetic tape units. A photograph of the computer main frame, control console, and magnetic tape unit is shown in Fig. 10. The computer room also contains a card reader, keypunch, incremental-type plotter, and an equipment rack housing clocks, displays, and line drivers–terminators which communicate with the equipment located at the spacecraft test complex. Input signals from the spacecraft and output signals to the on-line printers enter the three Astrodata racks (Fig. 11) located in the OSE complex near the spacecraft. Control signals from the test director's console also enter the data system at this point. The three-rack Data Input Subsystem may be located up to 4000 ft from the computer room.

The main data printer is a Series 5 ANelex which operates at a maximum speed of 5 lines/sec with 120 columns/line. This printer displays all messages or data generated by the data system. Four Series 29 teleprinters are used to display messages and data selected to be of

Fig. 10. Univac computer system
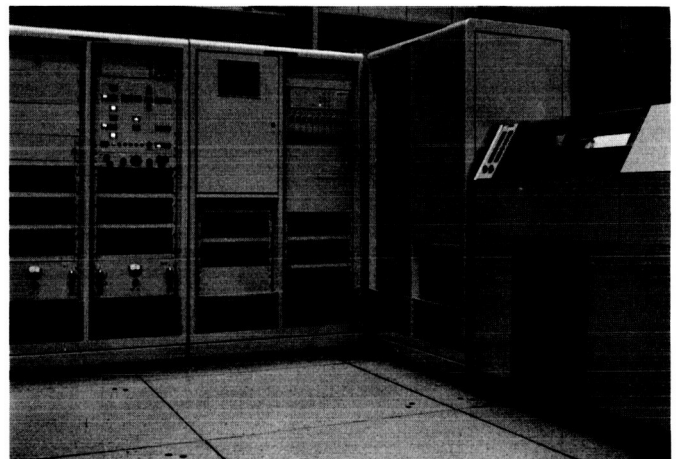
Fig. 11. Data-input subsystem and output data printer

interest to representatives of specific spacecraft subsystems.

In addition to processing the data from a complete *Mariner C* spacecraft system test, the data system can simultaneously process the telemetry data from another *Mariner* system test; however, the printout of the second real-time telemetry data is solely on teleprinters.

The real-time program flow chart (Fig. 12) outlines the main software features of the system which include telemetry decommutation, limit checking, data suppression, engineering-units conversion, events and counters processing, multiplexer scan control, message formatting, and routines for processing spacecraft clock reading, real-time clock reading, and control information.
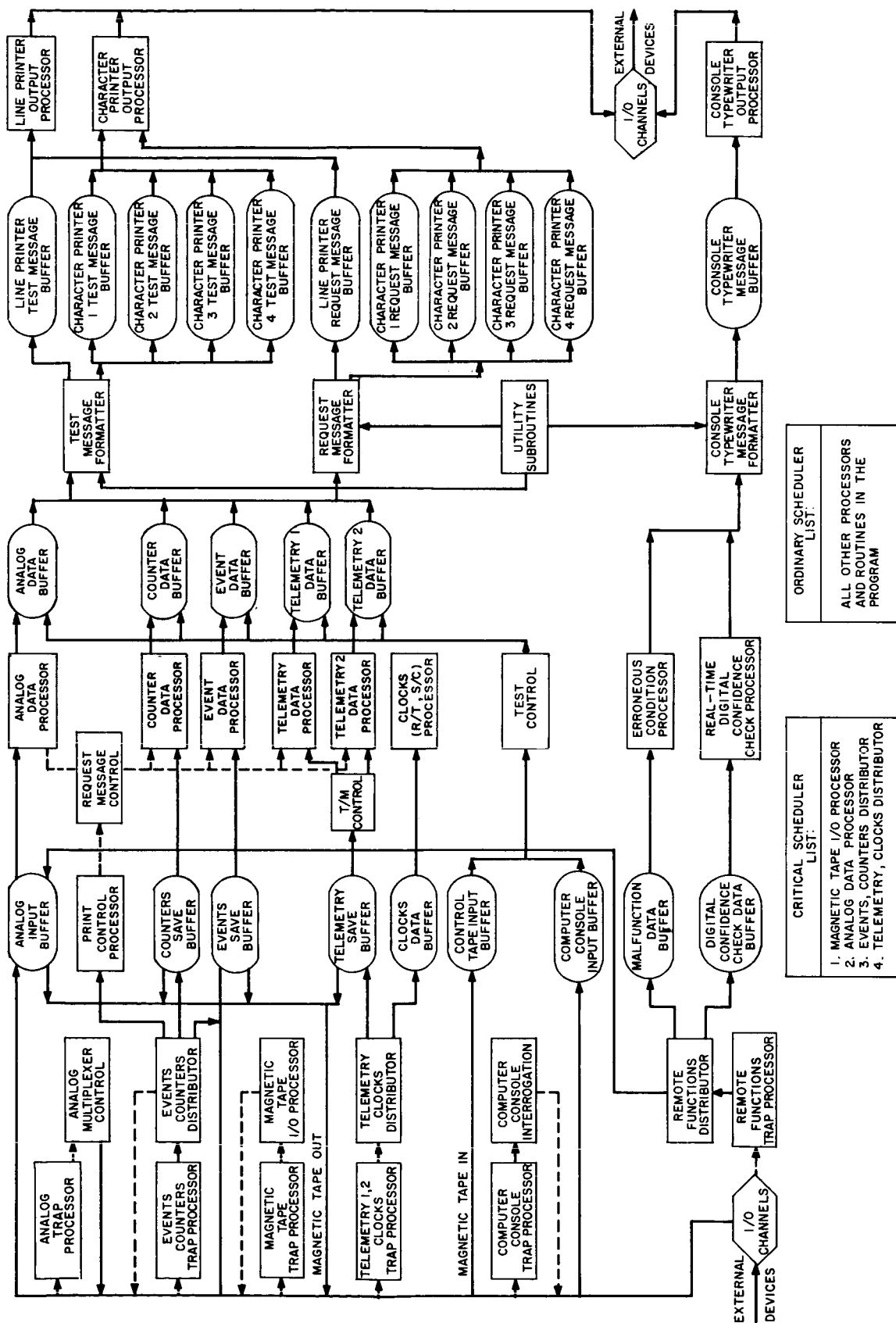
Fig. 12. Real-time program for processing data from spacecraft system tests

Reference

1. "Automatic Data Systems for Systems Test Application," *SPS 37-20, Vol. VI*, pp. 68–70, Jet Propulsion Laboratory, Pasadena, California, April 30, 1963.

SPACE SCIENCES

VIII. Space Instruments Development

A. *Mariner C Magnetometer*

The *Mariner C* magnetometer is being fabricated by the Apparatus Division of Texas Instruments under contract to JPL. In the period from March through September 1963, a series of design and method reviews were held both at JPL and at Texas Instruments. Extensive testing was performed on the magnetometer breadboard by JPL personnel to determine the capability of the instrument to meet the operational design performance requirements. The packaging design was reviewed to determine whether or not the hardware would comply with the reliability requirements for the *Mariner C* project set forth in JPL Engineering Planning Document 150. Evaluation of the design analysis and breadboard testing of the instrument resulted in a number of JPL-originated design changes in circuit, optical, thermal, electronic packaging, and mechanical design.

System concept. Figs. 1 and 2 show schematically the magnetometer sensor and a system block diagram. The physical principle underlying the operation of the helium magnetometer involves the transparency of a plasma of metastable helium atoms to a beam of resonant

radiation of 1.083-μ wavelength and the dependency of this transparency on magnetic fields. A set of Helmholtz coils are used to produce a rotating magnetic field vector in the plasma contained in the absorption cell, and the lead sulfide detector senses the modulation of the light beam. Any asymmetry in the resultant magnetic field (vector sum of the sweep vector plus ambient field) causes
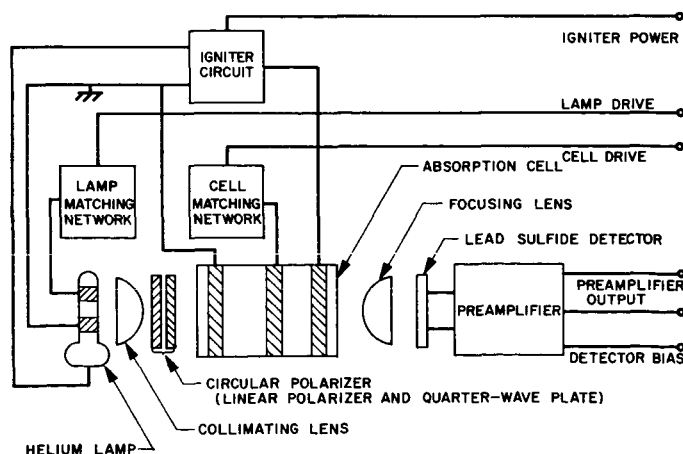
Fig. 1. *Mariner C* magnetometer sensor schematic
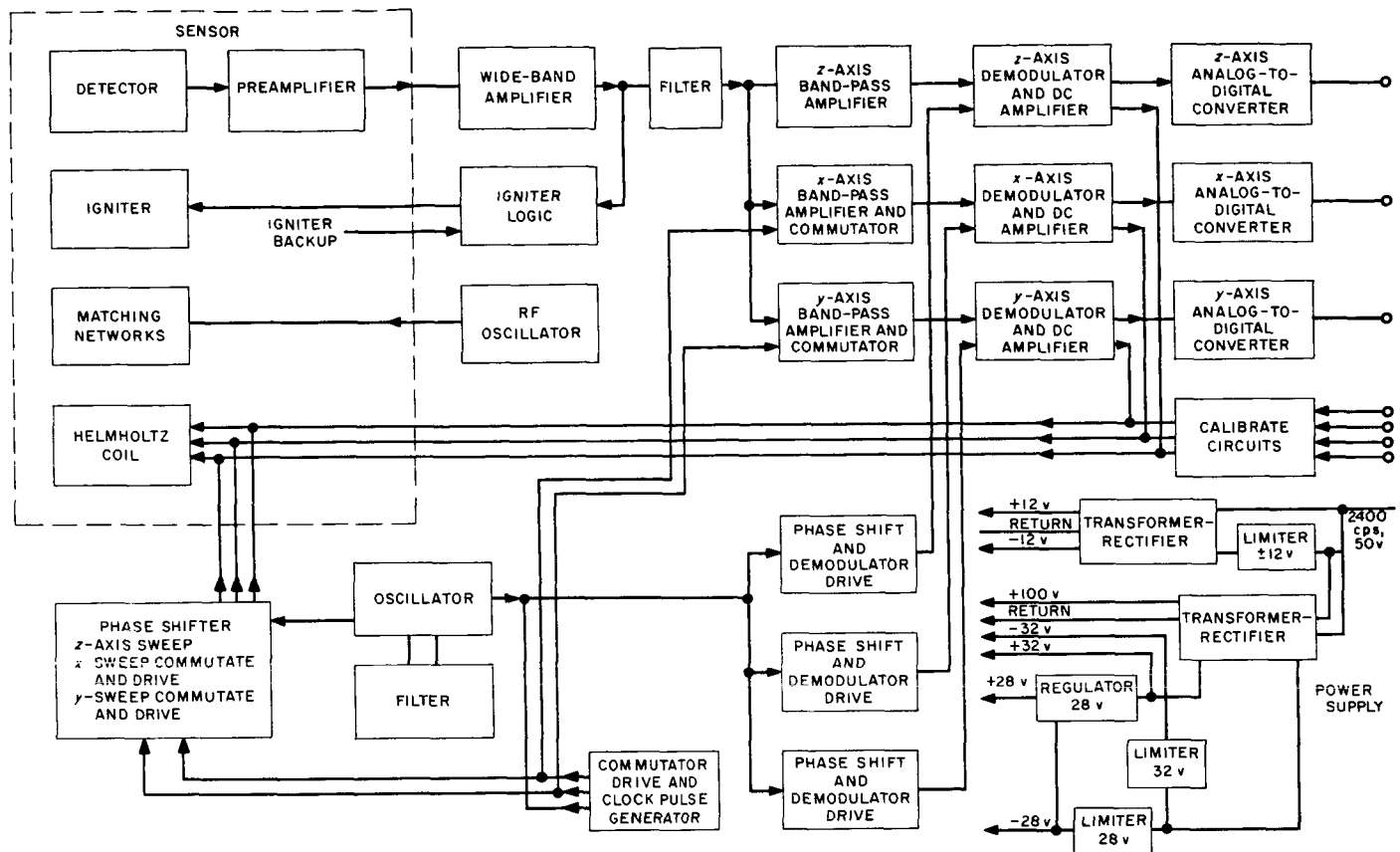
Fig. 2. *Mariner C helium magnetometer block diagram*

an asymmetry in the light modulation. With a sweep vector of constant amplitude and angular frequency, external dc fields cause a component in the modulation at the frequency of the sweep vector which is phase dependent on the direction of the field with respect to the light axis. In the absence of external fields, the modulation of the light beam is at twice the frequency of the sweep vector. Any fundamental component caused by an ambient field is amplified by the system electronics and synchronously demodulated. The demodulated signal is integrated, amplified, and fed back as current to the sensor coil system to null out the external field. The voltage output of the system is directly proportional to magnetic field component being nulled out.

The sweep vector is commutated between the x-z plane (z being the light axis) and the y-z plane to accomplish three-axis operation.

The RF power is used to maintain a discharge in the lamp to provide a source of the resonant radiation and to maintain a glow discharge in the cell to generate the

metastable helium atoms. The igniter system is used only to initiate the discharge.

Sensor design—optics. The original sensor design done by Texas Instruments utilized plastics throughout the optical system. Because of the deleterious effect of high vacuum on plastic materials, it was necessary to replace such unsuitable materials with materials of proven reliability.

The collimating and imaging lenses were originally $f/0.8$ Fresnel lenses made of Lucite. There is some evidence that Lucite will craze in vacuum environment, and hence the lenses would become opaque. The Fresnel lenses were replaced by $f/0.5$ plano-convex, aspherical, crown glass lenses. The increased speed and transparency of the glass lenses resulted in an increase in the optical efficiency of greater than two.

The polarizer initially employed was a standard Polaroid HR polarizer, which is basically a thin sheet of iodine-stained polyvinyl alcohol sandwiched between two sheets

of cellulose acetate butyrate. The cellulose acetate is butyrated to make it more flexible, but plasticizers such as butyrate are known to outgas in high vacuum; the result of such outgassing could cause degradation in the transparency of the polarizer. A study was made of crystal polarizers such as the Glan-type calcite prism, but two factors inhibited application of such devices. The crystal polarizers of large aperture-to-thickness ratios require a collimated light beam of very small angular divergence. The helium lamp is sufficiently large and in close enough proximity with the polarizer as to rule out near-perfect collimation. Tests conducted with a Glan-Foucault polarizer also established that the light beam could not be adequately collimated. Crystal polarizers with sufficiently large acceptance angles have a small aperture-to-thickness ratio, and the size and weight of polarizers of the Glan-Thomson type for the aperture size required were prohibitive. The unsupported sheets of polyvinyl alcohol were obtained from the Polaroid Corporation and were bonded between plates of glass for support and to minimize exposure to vacuum.

The quarter-wave plate used in the original design was made by adjusting two sheets of stressed cellulose acetate with respect to each other to achieve one-quarter-wave retardation. The birefringence in plastics is generally due to stresses in the material. Such stresses are not necessarily stable with time, especially at elevated temperatures, and measurements made on quarter-wave plates which were approximately six months old indicated a degradation of as high as 40%, although the measurements are suspect because of the unknown history of the quarter-wave plates under test. Attempts were made to obtain quartz quarter-wave plates, but all commercially supplied quartz quarter-wave plates tested failed to meet the design requirement of less than 2% linearly polarized light. Unsupported mica sheets were obtained and adjusted with respect to each other to achieve less than 1% linear polarized light when properly adjusted with a linear polarizer. The mica sheets are encapsulated between plates of glass to reduce any possible degradation in vacuum.

The polarizers and quarter-wave plates are fabricated at JPL and are built into an integral circular polarizer and supplied under contractual commitment to Texas Instruments for inclusion in the final magnetometer assembly.

The behavior of the lead sulfide detector used in the breadboard design indicated it as the limiting factor in maximizing system signal-to-noise ratio at the operating temperature extremes. Initial attempts to find a replacement detector were futile. The only competitive detector at 1.08 μ found in available literature was the silicon photovoltaic cell, but testing indicated that although the signal-to-noise ratio was competitive with the lead sulfide, the actual signal from the best silicon detector tested was two orders of magnitude lower than the lead sulfide detector. The decision was made to concentrate effort on optimizing the application of the lead sulfide detector. The only variable parameters were the detector biasing and the preamplifier input impedance. Testing indicated that the breadboard detector was biased close to optimum, but at low temperatures the detector impedance goes above 10 MΩ. The breadboard preamplifier which had an input impedance of ¼ MΩ severely loaded the detector output, and so, in the redesign of the preamplifier at JPL, the input impedance was increased to 20 MΩ to reduce detector loading. Texas Instruments designers also included automatic gain control (AGC) amplifier stage in the wide-band amplifier to control the signal level over the operating temperature range so that the effect of the detector responsivity variation on loop gain would be minimized. This was accomplished by controlling the gain of the wideband amplifier so as to maintain the second harmonic component at a constant level.

Sensor design—packaging. The initial sensor design utilized phenolic and fiberglass as basic structural materials. This design was reviewed and several major problems were uncovered which led to a redesign of the sensor. With nonconductive base materials, the local heating due to the power dissipated in the helium lamp caused the temperature gradient to be as high or higher than 15°C per inch. Since there was no provision for cooling the lamp, thermal control could have been achieved only by using Sun energy. Under these conditions the sensor would have experienced large temperature excursions over the flight from Earth to Mars. RF shielding was extremely difficult with nonconductive base materials because of problems encountered in maintaining integrity of the plated surfaces during fabrication. Another factor leading to sensor redesign was the concern of JPL packaging engineers as to the mechanical integrity of the original design in light of the anticipated high shake level on the omni-antenna waveguide where the sensor is to be mounted.

The basic mechanical features of the redesigned sensor are shown in Fig. 3. The igniter and preamplifier housing are 0.030-in. wall aluminum boxes, and the optics housing is a cylinder with 0.010-in. wall thickness. The mounting rings on the Helmholtz coils are used as part of
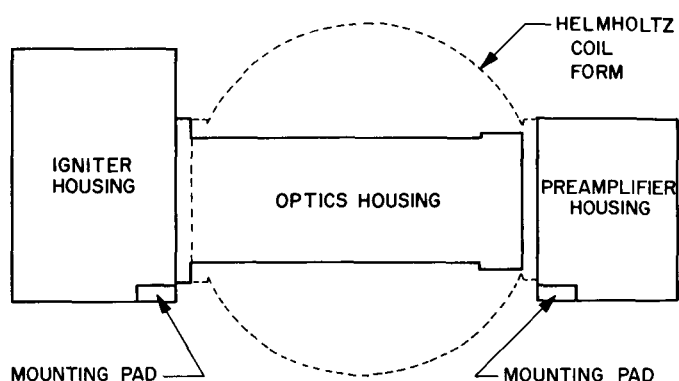
Fig. 3. Magnetometer sensor mechanical structure

the mechanical structure, and all mating surfaces are joined through Indium foil washers to increase the thermal conduction at the interfaces. The ground electrode on the helium lamp is an aluminum yoke and is bolted directly to the igniter housing to provide maximum heat transfer away from the lamp. Thermal control is accomplished by heat from the lamp which is conducted uniformly through the metal structure. The sensor is now essentially Sun independent and will have an estimated change of 40°C between Earth and Mars.

The spherical Helmholtz coil form was developed at Texas Instruments and consists of bonded fiberglass string which is formed on a sphere of cerrobend. Once the coils have been wound and bonded in grooves in the cerrobend and the epoxy fiberglass spherical surface is formed over the cerrobend ball, the cerrobend is melted away in boiling water, and the spherical shell containing the Helmholtz coils is left as an integral unit.

System and electronics design. Review of system design, circuit design, and operational testing of the magnetometer breadboard uncovered the following problems:

(1) Low sensor preamplifier input impedance.

(2) Inadequate system thermal null stability and offsets.

(3) Excessive decoupling networks throughout the system.

(4) Questionable reliability of igniter operation.

(5) Sweep vector asymmetry.

(6) RF oscillator instability.

(7) RF power matching crosstalk.

(8) Inadequate recurrent surge, turn on transient, and short circuit protection in the power supply.

Sensor preamplifier. The function of the preamplifier is to provide a buffer between the detector used in the sensor and the signal cables connecting the sensor to the magnetometer electronics in the bus.

The basic requirements for the amplifier are shown in Table 1. The noise contribution of the amplifier is difficult to specify, since the detectors used vary considerably in source impedance and noise characteristics. A further requirement is that the parts must be nonmagnetic.

Original preamplifier. A schematic of the original preamplifier is shown in Fig. 4. The elaborate input network was intended to provide protection from bias drift of the input stage due to capacitor leakage. Operation of the amplifier is straightforward. The first two stages are voltage inverting. The third stage is a phase splitter (to provide complementary outputs) and the output stages are emitter followers. Feedback around the amplifier is coupled from the in-phase output back to the emitter of the first stage. The amplifier has a gain of about 10.5 at 50 cps.

Aside from the large number of parts used in the amplifier, the major disadvantage of the amplifier is its low input impedance and the dependence of the input impedance on the first stage transistor parameters. Looking directly into the base of this stage one sees an impedance of about 450,000 Ω at $-55°C$ for a "typical" transistor and one third to one half of that for a worst-case unit. The large thermal variation of the input resistance in combination with the large detector source impedance variation resulted in objectionable system loop gain variations. The large number of components, especially tantalum capacitors, is also a source of concern.

JPL preamplifier. The preamplifier of Fig. 5 was designed to replace the original preamplifier. The philosophy underlying the design of this preamplifier is that an

Table 1. Basic requirements for the preamplifier

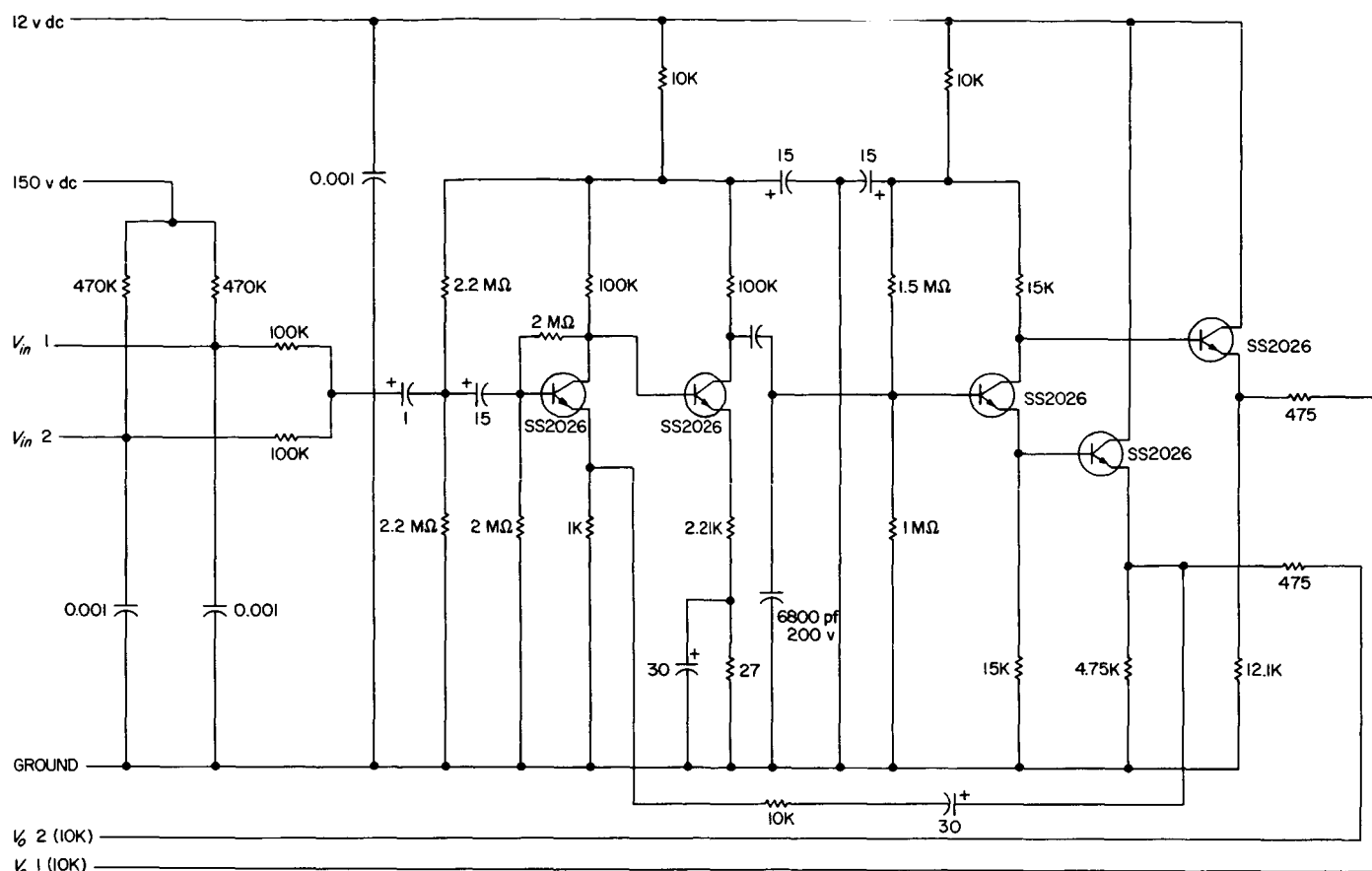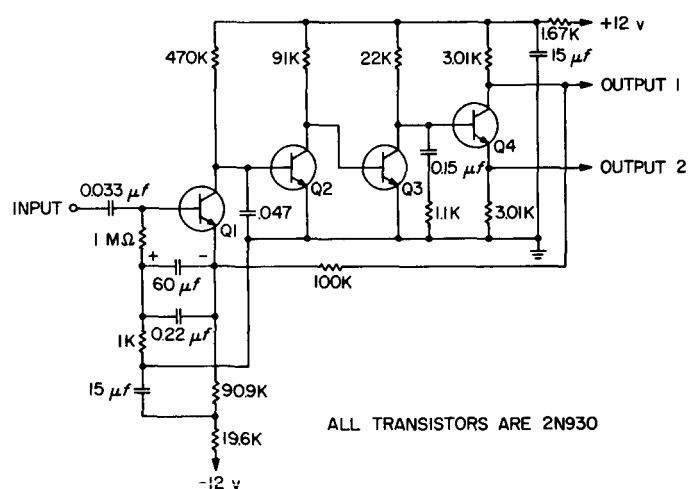| Parameter	Specification
Voltage gain (at 25 and 50 cps)	Variable 10 to 100
Gain stability	±10%
Input impedance	≥10 MΩ
Output impedance	10 kΩ
Output	Differential
Noise	See text
Phase stability	±3 deg
Relative phase (25 to 50 cps)	±6 deg
Temperature range	−55 to +55°C

Fig. 4. Original preamplifier

Fig. 5. JPL preamplifier schematic

over-all feedback loop should be incorporated which stabilizes the dc and ac characteristics of the amplifier. Through this design approach large coupling and bypassing resistors are avoided and bias networks are minimized, yet excellent operating point stability is obtained.

The preamplifier consists of three inverting stages followed by a phase splitter. Gain and operating point stability is obtained by feedback from the output stage collector to the input stage emitter. Input impedance of the amplifier is greater than 20 MΩ over the specified temperature range. The high input impedance was obtained by bootstrapping the input stage base return resistor as well as its emitter. Loop gain of the amplifier was about 100 at 25 cps and 90 at 50 cps. The amplifier met the specifications of Table 1.

System null stability. The primary sources of electronically caused offsets were ground loops, pickup, equivalent dc amplifier input drift, offset caused by the demodulator driver, and insufficient loop gain preceding the dc amplifiers.

An estimate was made that the loop gain preceding the dc amplifiers would have to be at least 4 to reduce the effect of their equivalent input drift on the system null stability. Although the design specification was modified to include this carrier section requirement, evaluation of

the breadboard magnetometer revealed a problem. A periodic waveform which was several gammas in peak-to-peak magnitude was observed in the system output, and it was determined to be the residual second harmonic component. This was to be expected since the second harmonic component is several orders of magnitude larger than the frequency of interest (first harmonic) and the integrating network offers only 6 db per octave attenuation. Increasing the carrier section gain would increase this component still more and, in addition, would have caused saturation of the bandpass amplifiers due to limited dynamic range. A twin-tee feedback element was then added to the bandpass amplifier which provided increased reduction of the second harmonic component, reduced the output ripple, and subsequently allowed the carrier section gain to be increased.

The shielding and grounding philosophy was reviewed and modifications were recommended by JPL. These modifications were incorporated in the breadboard, and comparison of the demodulator waveforms before and after the modifications were incorporated showed an appreciable reduction in noise. Offset measurements made by flipping the sensor in zero magnetic field showed a decrease in zero offset by an order of magnitude.

DC amplifier. The dc amplifier provides the filtering necessary to extract passband signals from the various frequencies generated at the synchronous demodulator. The original amplifier and its block diagram are shown in Figs. 6 and 7, respectively (the demodulator is included on the schematic).

An undesirable feature of the amplifier in Fig. 6 is its balancing control, R1 and R2. The amplifier input differential stage is balanced with these resistors by unbalancing the emitter currents of the differential stage. In order to reduce the equivalent input drift of the amplifier as temperature varies, the emitter currents
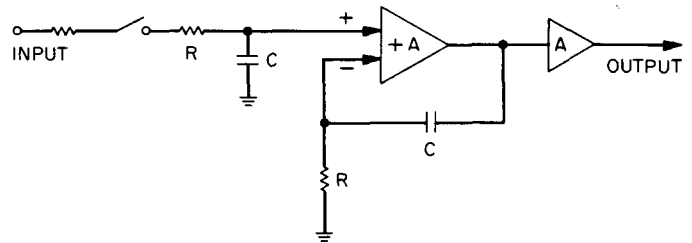
Fig. 7. Original dc amplifier block diagram
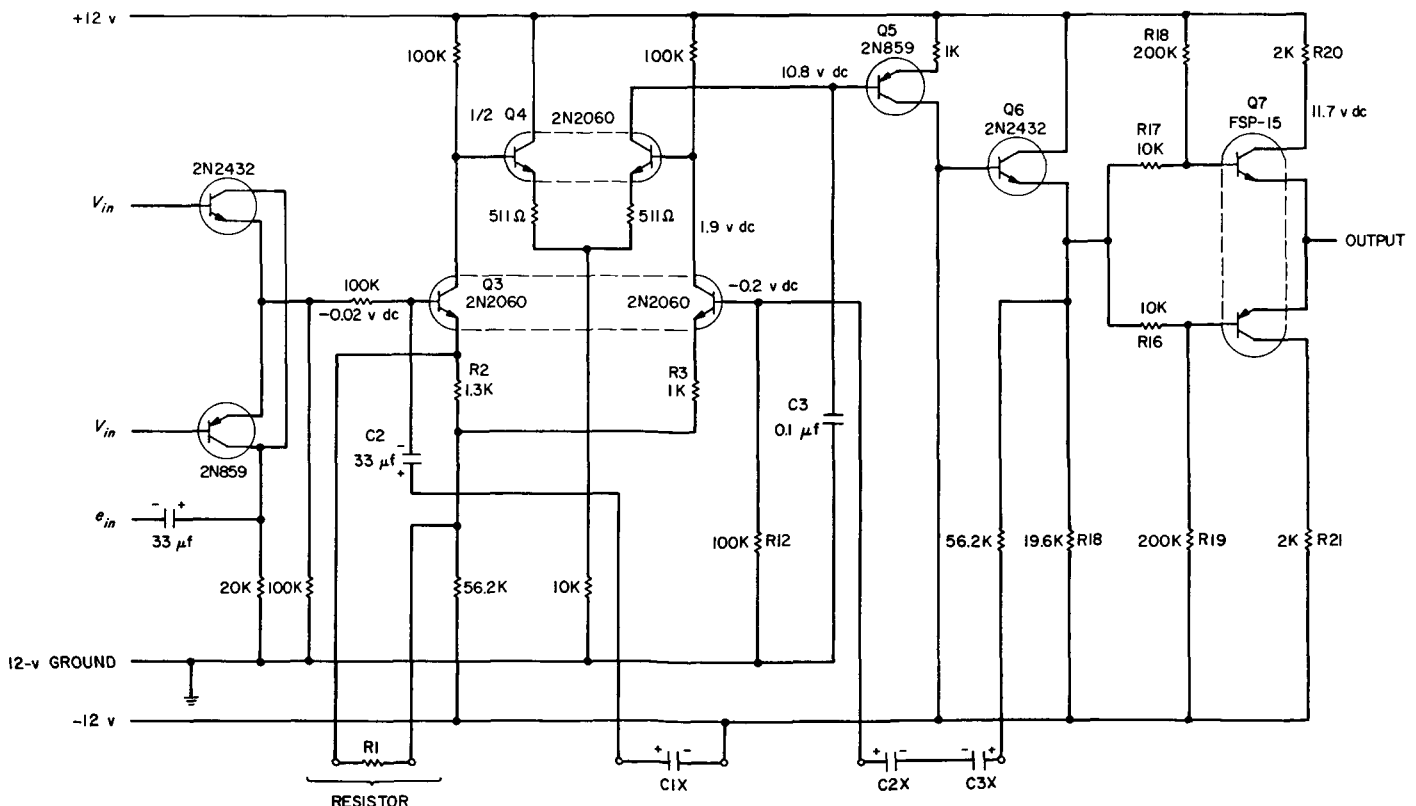
Fig. 6. Original dc amplifier and demodulator

should be balanced. This is particularly important for the subject amplifier since it is operating from high source resistances. Therefore, it was recommended that the reference base return resistor (R12 of Fig. 6) be voltage referenced to balance the amplifier. Fig. 8 shows how this was accomplished.

The second differential stage, Q4 in Fig. 6, is operating in a rather unconventional manner. The side which feeds Q5 is directly connected to the base of Q5 and is allowed no other return path. There are three problems which are encountered in this sort of connection:

(1) The collector current of the driving half of Q4 must vary greatly with temperature and the amplifier output voltage. Therefore, the differential tracking and the transfer parameters of Q4 vary greatly.

(2) At the higher temperatures the sum of the leakages of Q5 and the driver in Q4 constitute the minimum base drive of Q5 and therefore limit the negative swing at the collector of Q5.

(3) The pole in the amplifier loop gain expression is poorly defined and greatly temperature sensitive.

The pole is caused by C3 and the resistance seen at its positive side—namely, the output resistance of the driver in Q4 in parallel with the input resistance of Q5.

The existence of these three problems was considered sufficient reason to justify modification to the amplifier to improve these conditions. The modifications are shown in Fig. 8. A load resistor has been added to the collector of the driving half of the differential stage.

Another problem encountered in the dc amplifier was the presence of excessive 2400-cps ripple on its output. This was traced to Q5 in Fig. 6. Observe that the capacitor C3 grounds the base of Q5 for high-frequency signals. Consider then the effect of 2400-cps ripple on the +12-v supply. To the ripple Q5 acts as a grounded base amplifier with a voltage gain of about 50. This amplified ripple is then fed directly to the dc amplifier output through Q6 and Q7, a complementary symmetry emitter follower. A practical solution is to return the capacitor to +12 v. The ripple then becomes common mode (equal at emitter and base) and is no longer amplified. A later change resulted in a pole and zero at this point, and the placement of a higher frequency at the base of Q5 (Fig. 8).
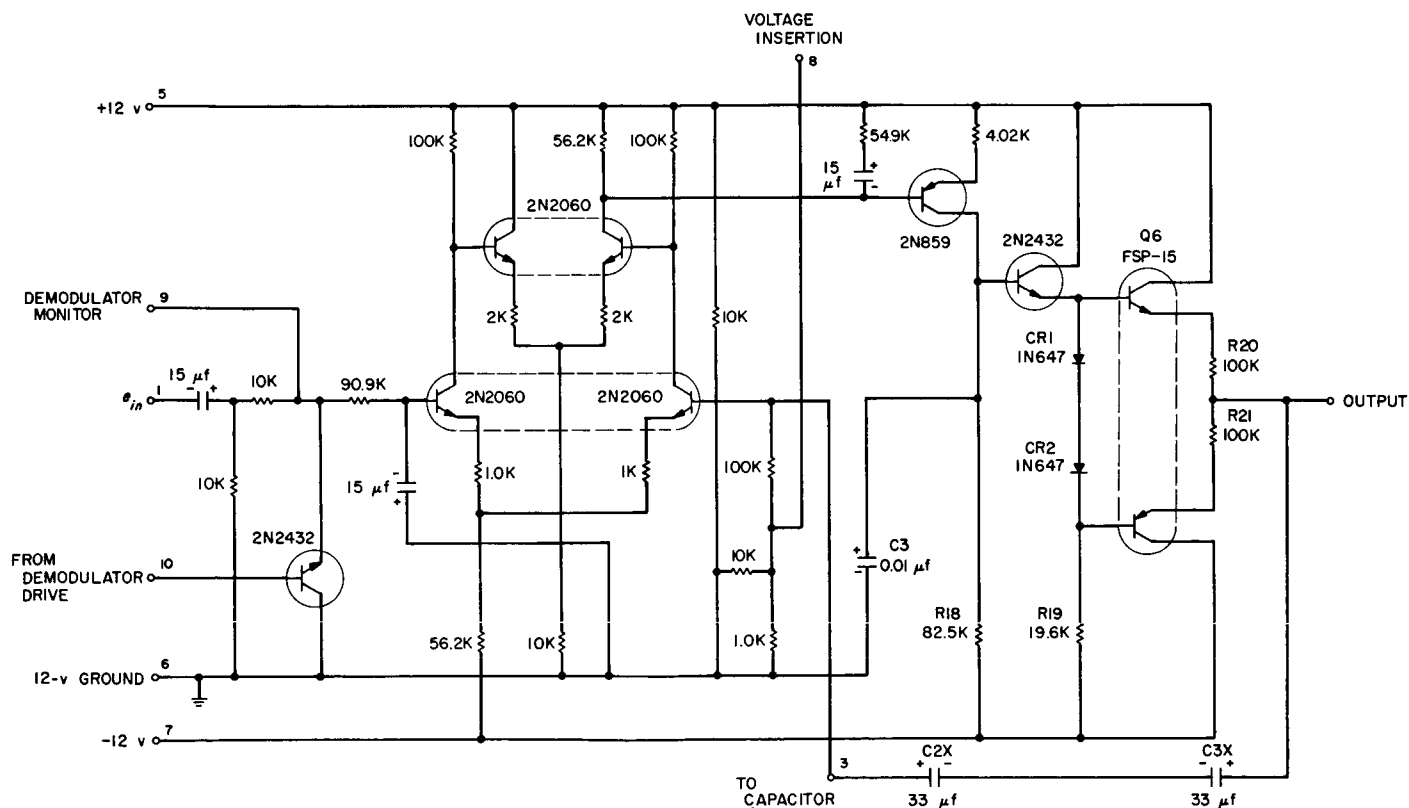

Fig. 8. Demodulator and dc amplifier, as modified

C3 of Fig. 8 also attenuates output ripple that might be picked up from the negative supply through R18 and R19 (Fig. 8).

The input capacitor pair C1X and C2 (Fig. 6) were replaced with a single device since the polarity at this point does not reverse. Note that capacitors C2X and C3X (Fig. 6) are connected to the emitter of Q6. In Fig. 8 they are connected to the output so that an ac feedback loop encloses the entire amplifier.

The final modification made to this amplifier consisted of replacement of the output stage consisting of R16, R17, R18, R19, R21, and Q7 in Fig. 6. The replacing configuration consists of CR1, CR2, R20, R21, and Q6 (Fig. 8). This change was made when it become evident that the original final stage output impedance rose greatly (to about 1000 Ω) near null. The increased output impedance caused an error in the output voltage sampled by the analog-to-pulse width converter. This circuit modification yielded approximately an order of magnitude reduction in output impedance over the original circuit.

Demodulator and driver. The magnetometer uses synchronous demodulators to translate the carrier-centered information back to its original low-frequency bandwidth. Transistor switches are used for this function.

The basic requirement for the transistor demodulator circuitry is that it be capable of switching a signal of about 6 v peak-to-peak without introducing offset signals (at the input of the dc amplifier) of more than about 10 mv over the operating temperature range.

The original circuit proposed is that shown in Fig. 9. The circuit connects the carrier input signal to the dc amplifier input for one half of a carrier period, then isolates it for the remaining half period. The resultant waveform is then low-pass filtered by the dc amplifier to obtain the passband signal components. The major problem in this circuit is that large offset voltages (50 mv or more) can be expected, due to the tolerances accumulated in the demodulator driver components. The driver will also be subject to differential variations in the absolute magnitude of the +12 and −12 v supplies.

It was recommended that a shunt demodulator and suitable driver replace the series device. The design of Fig. 10 was subsequently generated. This demodulator has an offset voltage of about 0.3 mv at room temperature and varies less than ±0.2 mv from −20°C to +55°C. Use of the shunt demodulator greatly simplified the driver, as can be seen by comparing Fig. 10 with Fig. 9.

Excessive decoupling. The original design philosophy used by Texas Instruments designers included decoupling
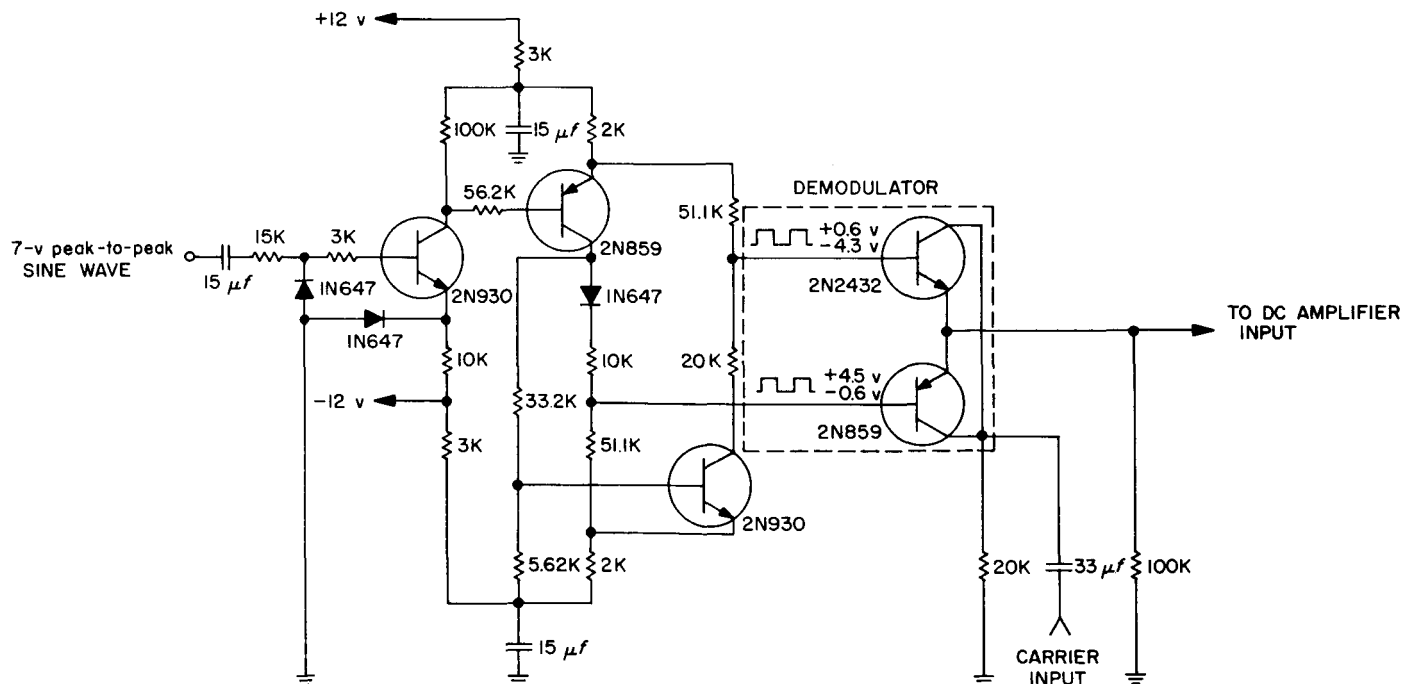

Fig. 9. Original demodulator and driver

Fig. 10. Shunt demodulator and driver

of every stage of every amplifier with an R-C network on both the ±12 v supply. Because of the low reliability of tantalum capacitors and the severe packaging density, JPL requested that Texas Instruments change their decoupling scheme to block-by-block zener diode decoupling. The result was the elimination of 80 capacitors and 80 resistors with no degradation in system performance.

Igniter reliability. The circuit in Fig. 11 was originally intended for lamp and cell ignition. The theory of operation for Fig. 11 is the same as the JPL circuit in Fig. 12, with two notable exceptions. There is no form of active current limiting for Q1. The maximum collector current, at any instant, is dependent upon base current and beta of Q1. The operating point of the circuit in Fig. 11 is
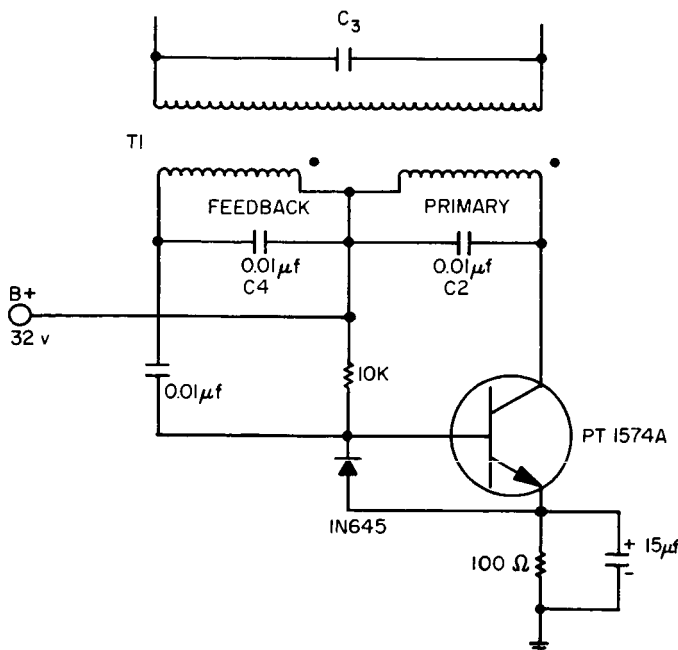
Fig. 11. Igniter oscillator

Fig. 12. Igniter oscillator, JPL modified circuit

unstable because beta is subject to change with temperature and age. The operating frequency is dependent upon C2 and C4.

The igniter circuit is a transistor version of the familiar tuned plate oscillator as shown in Fig. 12. When V_{in} is applied, a current will flow through the parallel combination of R1 and C1. This current will initially flow through the base emitter of Q1 and R2. A resultant collector current will flow through the parallel combination of C2 and the primary of T1 and the series combination of Q1 and R2. The combination of D1, D2, D3, Q1, and
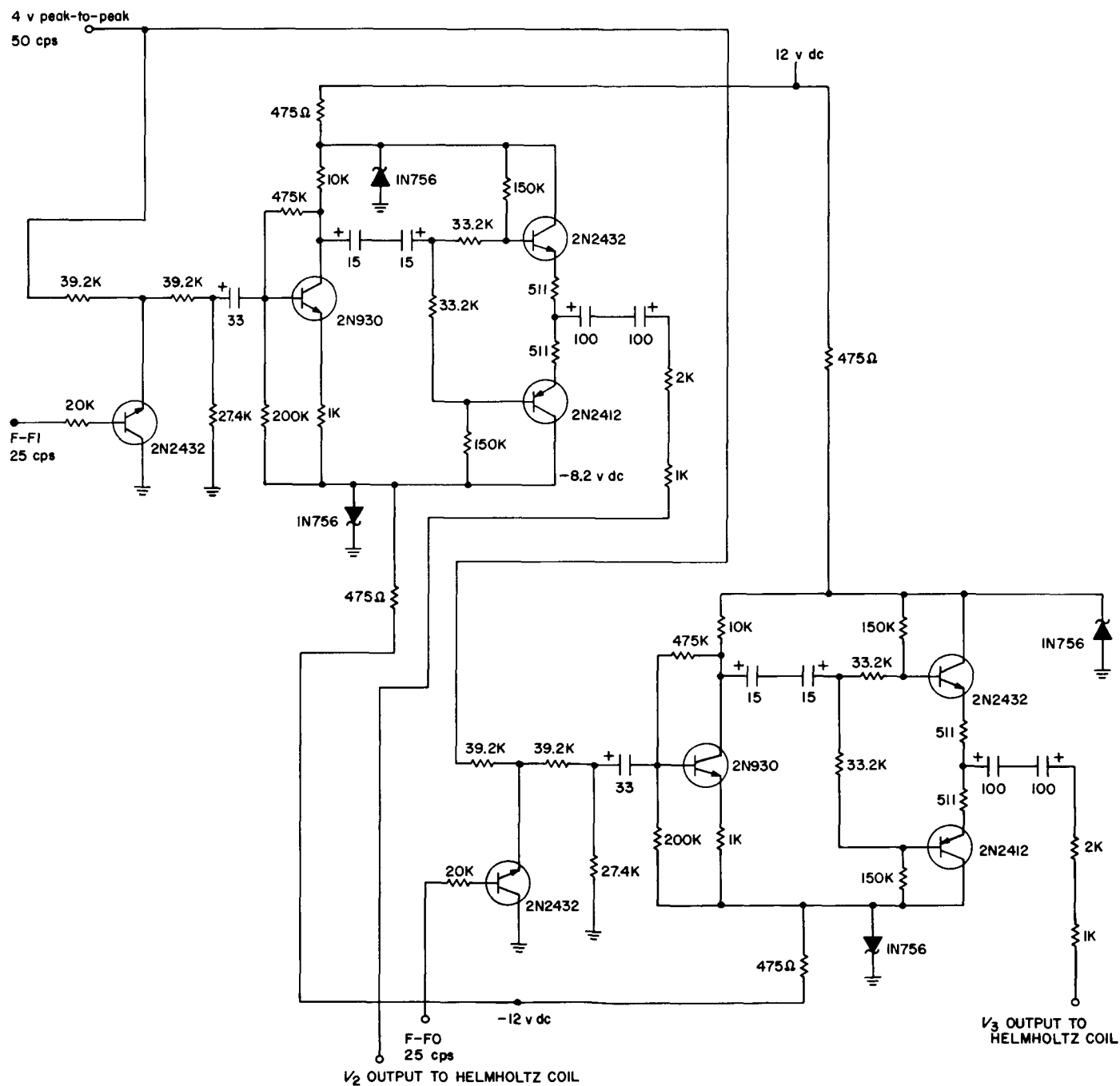
Fig. 13. Original x and y sweep drivers

R2 forms a circuit which limits the collector current of Q1. When the base-emitter voltage of Q1 and the voltage drop of R2, due to collector current, equals the forward conduction voltage of D1, D2, and D3, the base current is limited. Therefore, collector current is limited. As a result, C2 will charge at a slow rate compared to C1. When C2 is fully charged the voltage across the primary of T1 will stop increasing. The magnetic flux in T1 will then collapse and the coupling between the primary and feedback winding of T1 will turn off the base drive to Q1 and thereby remove charging current from C2. C2 will discharge then into the primary of T1 and when current from C2 stops flowing in the primary of T1 the field of T1 will collapse. Q1 will turn on and the cycle will repeat again. The frequency of oscillation is mainly dependent on the primary inductance of T1 and the value of C2.

For the component values in Fig. 12 the frequency of operation is 100 kc.

Sweep vector symmetry. If the sweep vector amplitude does not remain constant as it rotates (e.g., magnitude of x component larger than the z component) then the input to the system electronics contains even harmonics of order higher than 2. The filtering in the electronics is designed primarily to remove the large second harmonic component, and, as a consequence, the higher harmonics can be large enough that the integrator will not attenuate them sufficiently; they then appear as ripple on the output which appears as noise to the data system. This problem was observed on the breadboard system and was corrected on the breadboard by reducing the sweep vector asymmetry to below 1% by balancing the amplitudes of the x, y, and z sweep drivers to better than 1%.

To reduce the sweep symmetry problem and simplify the sweep circuits, the separate commutated x and y sweep drivers were replaced, at the request of JPL, by a single sweep driver with commutated outputs. This change removed the necessity for balancing the x and y amplifiers.

The original x and y axis sweep drivers are shown in Fig. 13. The purpose of these circuits is to commutate the 50-cps sweep signals and drive the x and y axes of the Helmholtz coils. The ideal waveforms are shown with the block diagram in Fig. 14. Notice that the amplifiers are allowed to pass alternate cycles of the oscillator output.

The basic requirements imposed on the sweep circuits by the Helmholtz coils and the magnetometer system are:
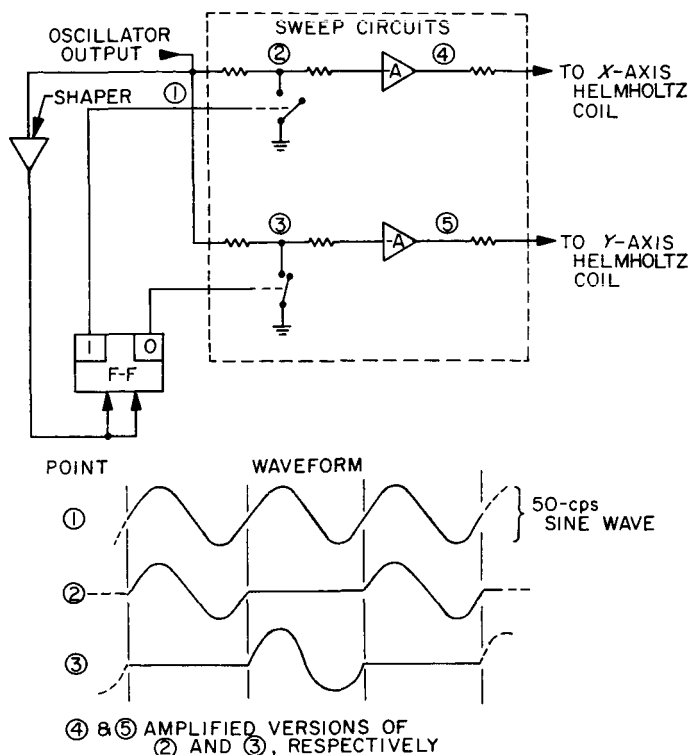

Fig. 14. Sweep driver block diagram and waveforms

(1) DC output voltage (due to capacitor leakage into 3000 Ω) must be less than 4 mv.

(2) Voltage output of the x and y system should be identical within several percent to avoid system saturation problems (absolute value can vary by perhaps 20%).

These requirements place severe constraints on the performance of the amplifiers following the commutators of Fig. 14. The amplifier gain must be very tightly controlled. Since the waveform contains 25 cps and its harmonics, the bandwidth must be fairly wide. In particular, its low-frequency cutoff must be well below 1 cps to avoid tilt (phase distortion) in the flat portion of the waveform.

Perhaps the most obvious solution to these problems is to use a single amplifier and perform the commutation after amplification as blocked in Fig. 15. The waveforms are shown with the block diagram. In this configuration the amplifier is required to pass only a single frequency (50 cps). Gain stability is no longer a problem since the x and y sweeps are taken from the same point so that the sweep currents will be equal within the tolerances of the sweep resistors CR1 through R4. It should be noted that the method eliminates one-sweep amplifier.
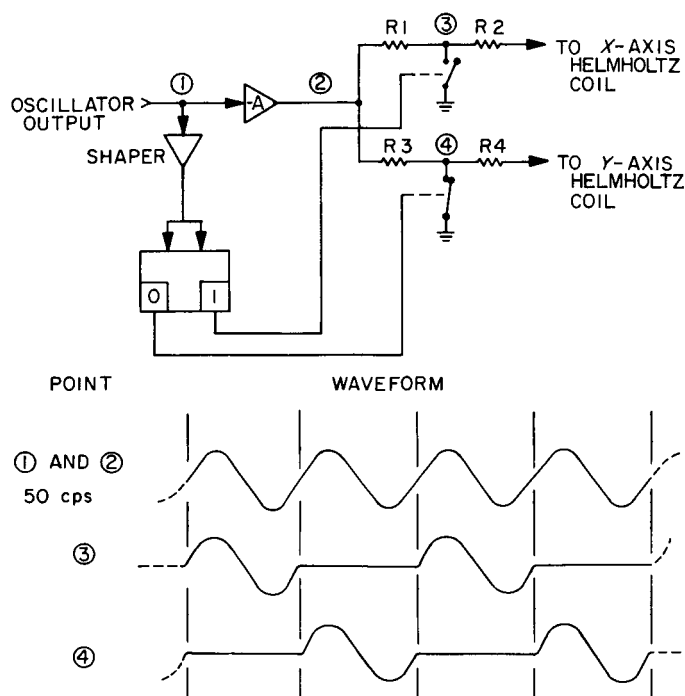
Fig. 15. Modified sweep driver block diagram and waveforms

Fig. 16 shows the circuit presently incorporated in the magnetometer. One amplifier (Q2, Q4, and Q5) of the original circuit has been retained. Q6 and Q7 perform the switching function. The use of transistors results in about 0.5-mv offset voltage at the switching point. Since the sweep coils are only about 30-Ω resistance (to ground), this is equivalent to 1.5 mv at the amplifier output and is well within the 4-mv requirement. When one switch is on, its resistance is about 6 Ω. The off-axis sweep current caused by this resistance is thus about 1/3000 of the full sweep. This effect is negligible.

RF oscillator stability. The original RF power supply was designed using a free running power oscillator. The output of the oscillator was fed to a step-up auto transformer whose output was capacitively divided to drive the lamp and the cell. Two features rendered this design undesirable. The starting transients when reflected back into the oscillator would occasionally cause the oscillator to go into a nonsinusoidal oscillating mode, and hence no power was delivered to the lamp and cell. The adjustment of the lamp and cell matching networks was subject to severe crosstalk which made it quite difficult to adjust the lamp and cell to their nominal levels of 1 and 100 mw, respectively.

A crystal-controlled RF oscillator design was supplied by JPL (Fig. 17) which offered greater power efficiency than the proposed unit, and, in addition, allowed either output to go from a short to an open circuit condition with a negligible change in the other output.

RF power matching crosstalk. Measurements were made at JPL to determine the operating impedance of the lamp and cell, and these values were used to design π matching networks to match power from the 50-Ω coaxial cable termination into the lamp and cell from their respective power supplies.

Power supply design. Evaluation of the Texas Instruments breadboard power supply at JPL revealed the following problems:

(1) The current limiter functioned only on a total short-circuit condition; it did not limit recurrent waveform transient current spikes.

(2) The power transformers had resonant frequencies below 100 kc, and, as a result, appeared as a capacitive reactance to the incoming power waveform. This resulted in excessive current spikes in the input current waveform.

(3) The infrared detector bias supply reflected an undamped, oscillatory current into the primary power distribution system.

(4) The output impedance of the ± 12 v dc supply was excessive.

(5) The regulation of the $+28$ v dc supply to the RF oscillator was inadequate. This is an extremely important design constraint since any 50 cps appearing on the 28 v dc will appear as 50-cps modulation on the helium plasma, and, dependent on its phase, the system would not be able to distinguish it from an induced magnetic field component. A further complication was caused by the fact that only one current limiter was used for the entire power supply system, and, as a result, a common mode condition was created which resulted in a large amount of 50 cps on the unregulated 28 v dc.

To solve these problems a breadboard power supply (Fig. 18) was designed and constructed at JPL. This unit along with complete transformer and choke design information were supplied to the instrument vendor. The
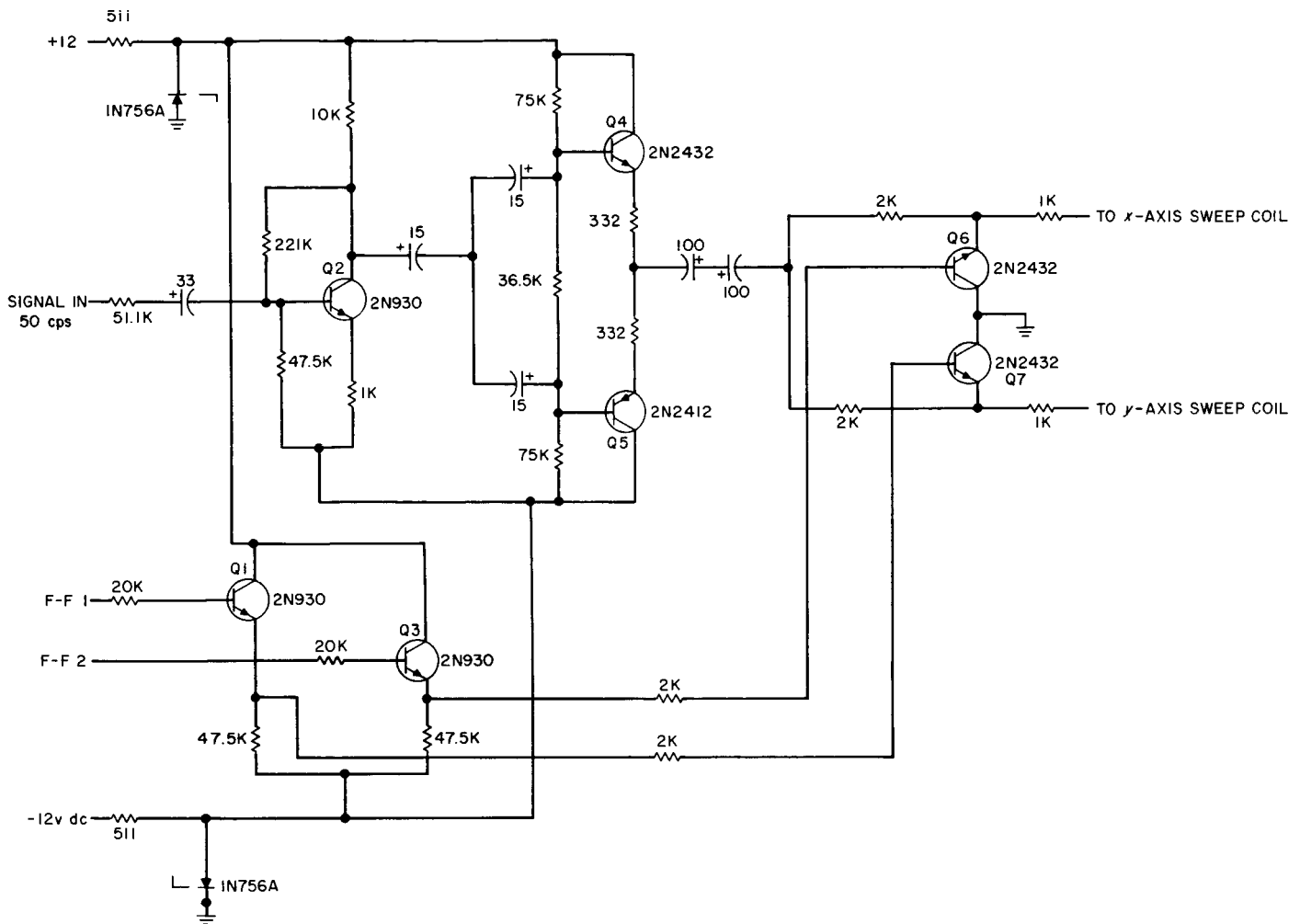
Fig. 16. Modified sweep driver

power supply has an operating conversion efficiency of 80%, meets all JPL current limiting requirements (e.g., short circuit, turn-on, and recurrent waveform transients), and offers a 50-cps rejection factor on the RF B+ supply of greater than 100,000 to 1.

Electronics packaging design. Because of the high packaging density anticipated for the magnetometer at the outset of the *Mariner C* project, the packaging philosophy for the electronics modules was centered around welded cordwood construction. When the JPL Welding Specification 30995 was released in March 1963, it was incorporated as an applicable specification under a contract modification. The initial effects of the welding specification on packaging design were extensive modifications of the module layouts to ensure adequate electrode

clearances and to maintain a minimum tolerance on ribbon bending and separation. The second phase of the welding problem was in actual fabrication of modules. It was necessary to develop a complete new set of weld schedules to meet the JPL quality standards for welds. The welding of modules has been closely monitored by JPL quality assurance representatives, and continuous iterations were made in weld schedules prior to flight-unit fabrication.

Measured parameters on PTM unit. The final acceptance tests on the first unit delivered by Texas Instruments were performed at Addison, Texas, using bench checkout equipment designed and built at JPL. The test set up consisted of a cylindrical fluxtank for shielding against the geomagnetic field, the *Mariner C* magnetom-
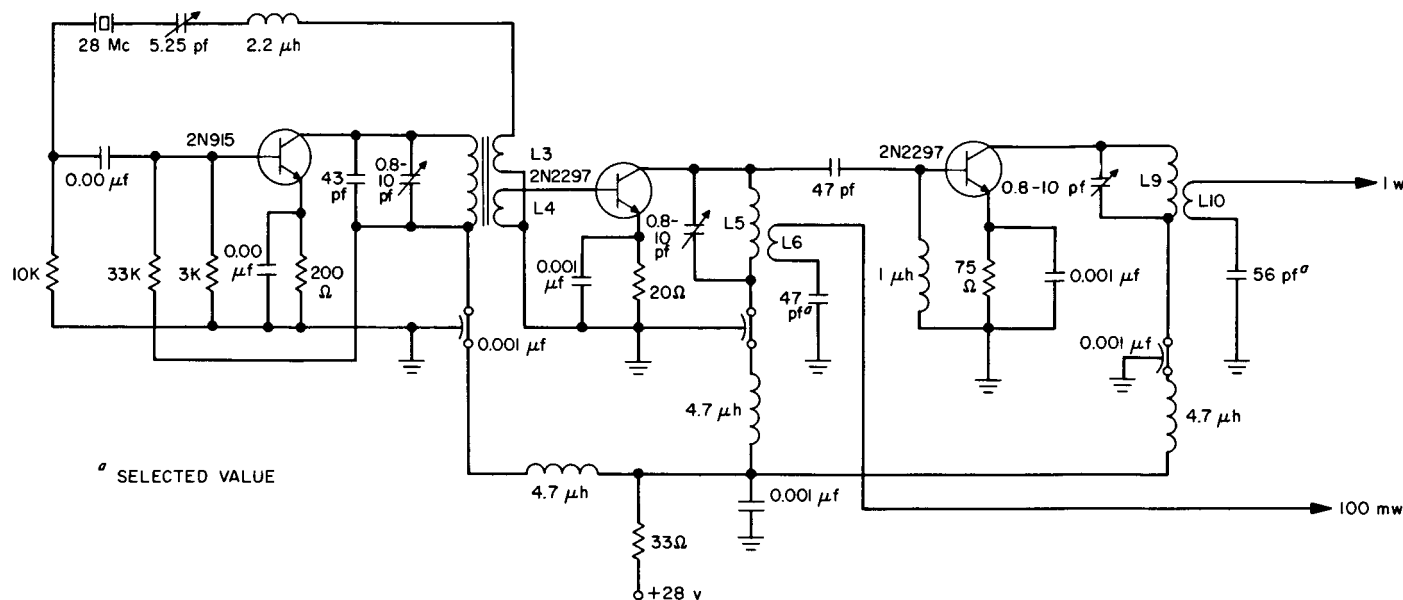
Fig. 17. RF oscillator

eter test console, and a Delta oven used to temperature cycle the electronics. The entire system was evaluated at the temperature extremes measured, and it was determined that both the sensor and the electronics performed over the specified temperature limits (sensor from -55 to $+55°C$ and electronics from -20 to $+65°C$).

The system noise was nominally 1.5 γ peak-to-peak on all three axes, and, in the worst case, with both the sensor and the electronics at the upper temperature limits, the noise was approximately 2 γ peak-to-peak on all three axes.

The system offset was measured by adjusting all three outputs of the system to a null, using the coil system inside the fluxtank and then rotating the sensor 180 deg in two planes. The offsets were nominally ⅔ γ on the x axes, 3 γ on the y axis, and ½ γ of the z axis. The variation in measured offsets over the temperature range were less than system noise. Further thermal tests will be run in the shielded room at JPL to determine whether these offsets are in the magnetometer or are due, as is suspected, to inadequate shielding.

The system bandwidth was measured by finding the frequency of field excitation for which the system output was down to 6 db. The 6-db point was nominally 0.8 cps, and under worst-case temperature conditions, the 6-db point was at 0.6 cps.

The crosstalk between the three axes was measured by injecting fields of $+400$ γ and -400 γ on two axes and observing the shift in output of the third axis. No measurable crosstalk was observed on any axis at any temperature. The system linearity was better than 1% when measured with both the electronics and sensor at room temperature. The carrier section gain, with the sensor and electronics at room temperature, was 4.5 on the x axis, 4.8 on the y axis, and 5.8 on the z axis. With the electronics and the sensor at the upper temperature extremes the carrier section gain was 3.0 on the x axis, 3.3 on the y axis, and 5.5 on the z axis.

Two factors that could have affected the noise and offset performance on the PTM unit were the infrared detector noise and the linear polarized component passing through the circular polarizer. During installation of the first infrared detector, the detector was damaged and was replaced with a detector which had not been screened, so nothing was known of its noise characteristics. The fabrication of the circular polarizer was done without an interference filter in the path of the light chopper. Subsequent measurements have indicated that only 94% of the light passing through the HR polarized filters used with the light chopper was caused by the 1.083-μ line from the helium lamp. Light of wavelengths other than 1.083 μ introduce an erroneous null when the polarizer and quarter-wave plate are aligned. For these two reasons, there is hope that the performance of the flight units may be better than the PTM unit.
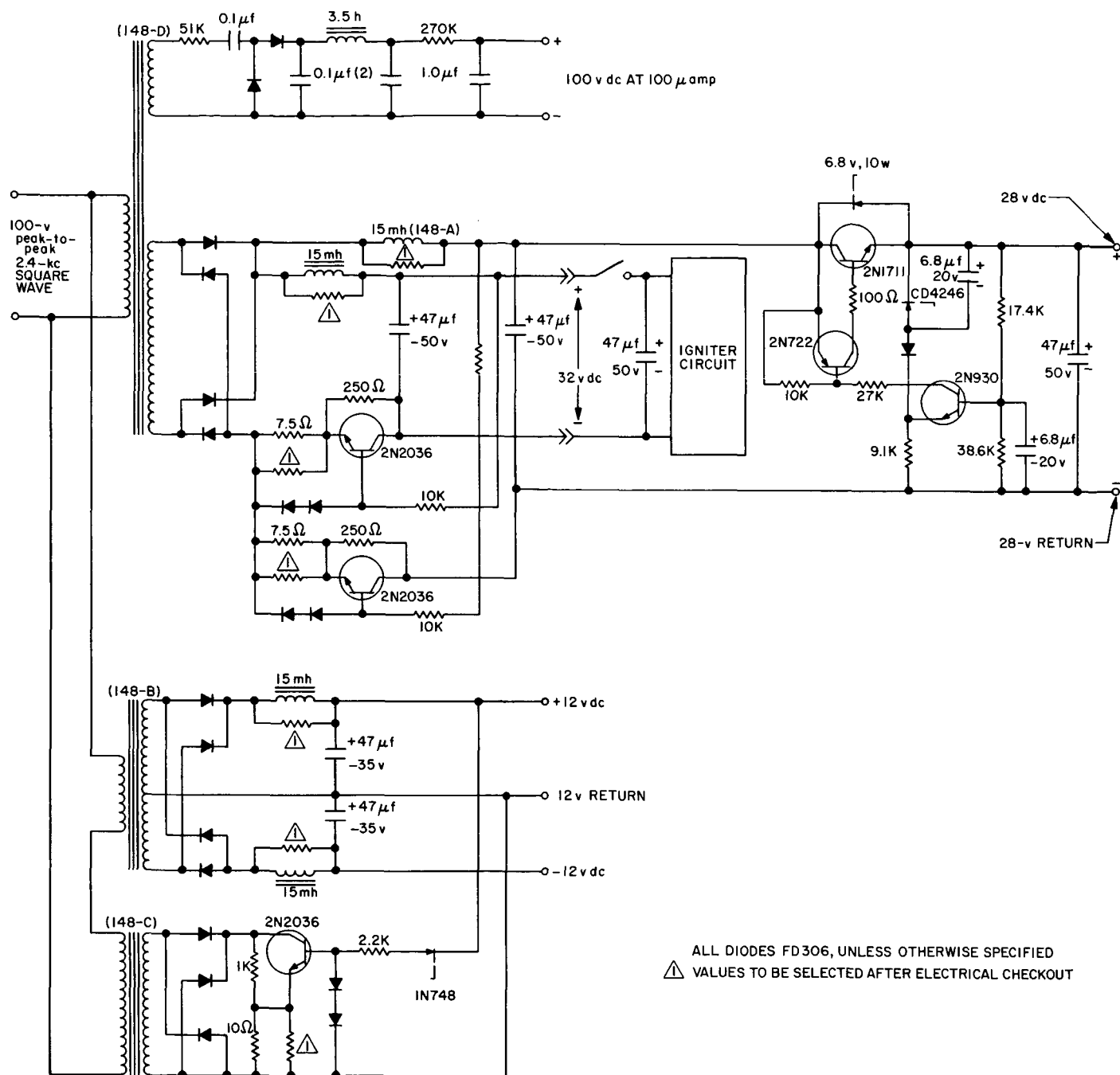
Fig. 18. JPL power supply

f. System and subsystem testing. Because the full scale of the magnetometer is approximately 0.01 that of the Earth's field, the testing of the instrument must be performed using either magnetic shielding or using a coil system to buck out the geomagnetic field. For testing of the instrument on the spacecraft, magnetic shielding is not practical, so coils must be employed. Fig. 19 is a photograph of the Helmholtz coils which will be used for system and subsystem testing. The basic coil form is a mahogany sphere with grooves into which the coils are wound. The coil constant of the triaxial coil array is 1 oe/amp. The coil will be placed over the omni-antenna waveguide and will be centered on the magnetometer sensor.

the second phase a number of experimental vidicons were supplied to determine the range of variations of the vidicon characteristics. The electronic circuits during this phase were then arranged to accommodate in a logical manner the widest expected variations in camera-tube parameters. The third phase which is now proceeding is to obtain consistent high quality camera tubes that will fit the present design and meet the program requirements.

The manufacturer chosen was General Electrodynamics Company (GEC), Garland, Texas, a successful producer of the slow-scan vidicon. This was necessitated because of the complex nature of the problem and the limited facilities both at JPL and at the manufacturing plant for handling a program of this magnitude.

The vidicon is in the peculiar position of embodying two of the more vigorous pace-setters in the technological fields: semiconductors and electron tubes. In the vidicon both technologies are contained within the same envelope, and highly sophisticated industrial processing is required to achieve acceptable performance standards.

Characteristic differences between the quantity produced broadcast-type vidicon and the highly specialized space photographic vidicon are confined almost entirely to the semiconductor photosensitive region. The beam-control section that forms part of the vacuum-tube electronics is almost identical for the two types. Hence, the space vidicon vacuum-tube electronics can take advantage of the many years of vidicon production. The electrode construction must of course be ruggedized for space applications, and heater power minimized with the introduction of the newer, more efficient cathode assemblies. In addition, more effective shielding of the electron beam is required to ensure stability when the spacecraft emerges from the Earth's magnetic field.

Semiconductor photosurfaces developed for space applications, however, are in a more vulnerable position. Fiducial marks and an optically black mask must be inserted adjacent to the transparent target contact-electrode. This poses problems in quality control. Semiconductors are sensitive to an atomic impurity of the order of 1 part in 10^8. But transistors, for example, are manufactured in 100,000 lots; slow-scan vidicons are only manufactured a few at a time. Quality assurance both with vacuum-tubes and transistors becomes increasingly difficult as production quantities are reduced. In the vidicon the problem is aggravated because the semiconductor photoperformance cannot be assessed until the optical target blank is sealed to the glass envelope. The vidicon

Fig. 19. Magnetometer test console and Helmholtz coils

B. Improved Slow-Scan Vidicon Camera Tubes (Mariner C)

During the past year a continuous development effort has been directed toward improving the performance of vidicons for use in the *Mariner C* spacecraft TV system. This has resulted in a camera tube that has superior performance characteristics for space photographic applications.

The work has proceeded in three phases. In the first phase a slow-scan vidicon was developed that would most nearly meet the needs of Mars TV camera exploration in the terms outlined by the cognizant scientist. The camera electronics during this phase was directed at optimizing circuit parameters for best picture quality. In

may, in fact, be viewed at this stage as a scanning device that permits surface examination of the physical characteristics of the semiconductor.

Once the electronic parameters associated with the scanning-beam are established for a given mode of slow-scan operation, the quality of the reproduced image becomes determined almost entirely by the homogeneity of the characteristics of the semiconductor. These characteristics must be established with a beam current of a few nanoamperes as compared, for example, to a broadcast vidicon that may operate with a few microamperes.

Some of the more important criteria for establishing space camera-tube performance that are directly associated with the semiconductor surface and its characteristics are:

(1) Sensitivity

(2) Dynamic range

(3) Erasure of preceding images

(4) Shading

(5) Freedom from blemishes

(6) Low background granularity

(7) Low dark current

(8) Spectral response

(9) Linearity of transfer characteristics

(10) Quality of fiducial marks

(11) Face-plate alignment with beam control section

(12) Operation over a wide temperature range

(13) Ability to survive temperature extremes

(14) Temperature stability of the optically black signal

In an attempt to more closely meet the requirements enumerated above with the GEC Type 1351B vidicon, a selenium-compound semiconductor was developed. The more outstanding characteristics of this compound are its highly effective erase capability and the improved sensitivity, 20-db S/N ratio for 0.003 ft-c-sec target illumination. However, tests of the first tubes delivered for evaluation at JPL revealed that saturation became evident at illumination levels greater than 0.045 ft-c-sec. As applied to the *Mariner C* TV camera this would necessitate a reduction in the illumination supplied by the optical system. Any reduction in illumination would, of

course, nullify any advantages gained by improvement in sensitivity.

Steps were thus taken to combine the feature of improved sensitivity with a wide dynamic range. This was accomplished by an alteration in the processing of the photosensitive faceplate. The result was an increase in the saturation level to 0.25 ft-c-sec, with a possible further increase in sensitivity. The process requires additional intermediate steps in the treatment of the vacuum-deposited photosensitive layer during application to the transparent stannic-oxide substrate. While this altered process does add more steps to the preparation of the photosensitive faceplate with a possible decrease in the yield of acceptable vidicons, it is felt that the improved performance, especially in relation to *Mariner C* TV, justifies the change.

The difference in vidicon performance for the two processes is shown in Fig. 20, where the processes are defined as Group I and Group II. As can be seen, the abrupt saturation experienced with the Group I vidicon has been modified with the Group II process. The increase in the dynamic range presents a valuable increment for space photography as the illumination of small planetary areas viewed by the space camera is not accurately known. The problem of setting up the camera prior to spacecraft launch for the expected illumination is thereby greatly reduced and improved performance can be expected from terminator region photography where maximum sensitivity is desired. To ensure compatibility in the
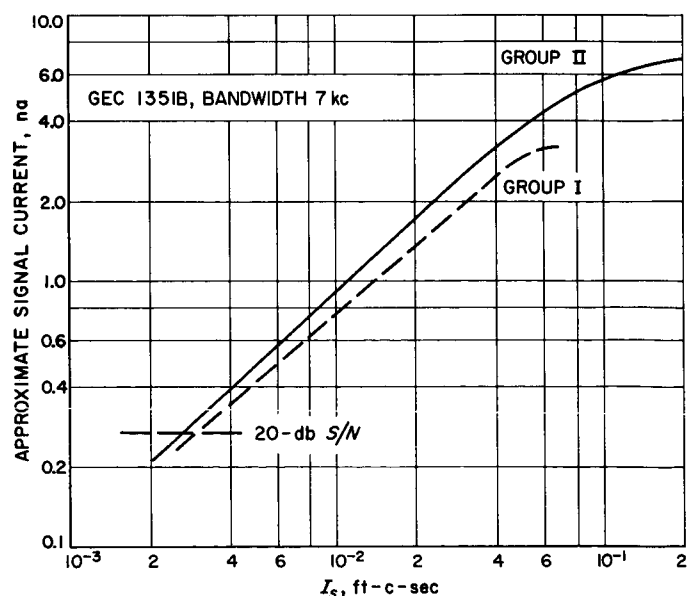

Fig. 20. Improved dynamic range, Group II vidicon

space environment, picture quality has been checked with the Group II vidicon over a temperature ranging from −40 to +70°C. Only a perceptible decrease in quality has been noted at the temperature extremes. Processing facilities have now been set up at GEC to produce a small quantity of these Group II vidicons. The tubes will be finally evaluated at JPL in a *Mariner C* TV subsystem.

C. Effects of Bit Errors on Pulse-Code Modulated (PCM) Television Picture Data *(Mariner C)*

In the analysis of a television picture, quality is generally stated in terms of analog signal-to-noise ratio. The ratio found to be useful is a peak-to-peak signal to rms

noise. In a digital picture such as the *Mariner C* system, noise is produced as a result of quantization and bit errors, and becomes important in the determination of picture quality.

The work described deals with the bit error. To obtain picture data on the effects of various bit error rates, equipment was assembled using the basic *Mariner C* television system parameters. The bit errors were inserted in picture data maintaining high quality sync information. The study of the effects of bit errors on sync information would be a separate investigation.

The block diagram in Fig. 21 illustrates the test setup assembled for this study.

The following commercial equipment was used:

(1) General Radio random noise generator, Model #1390A.
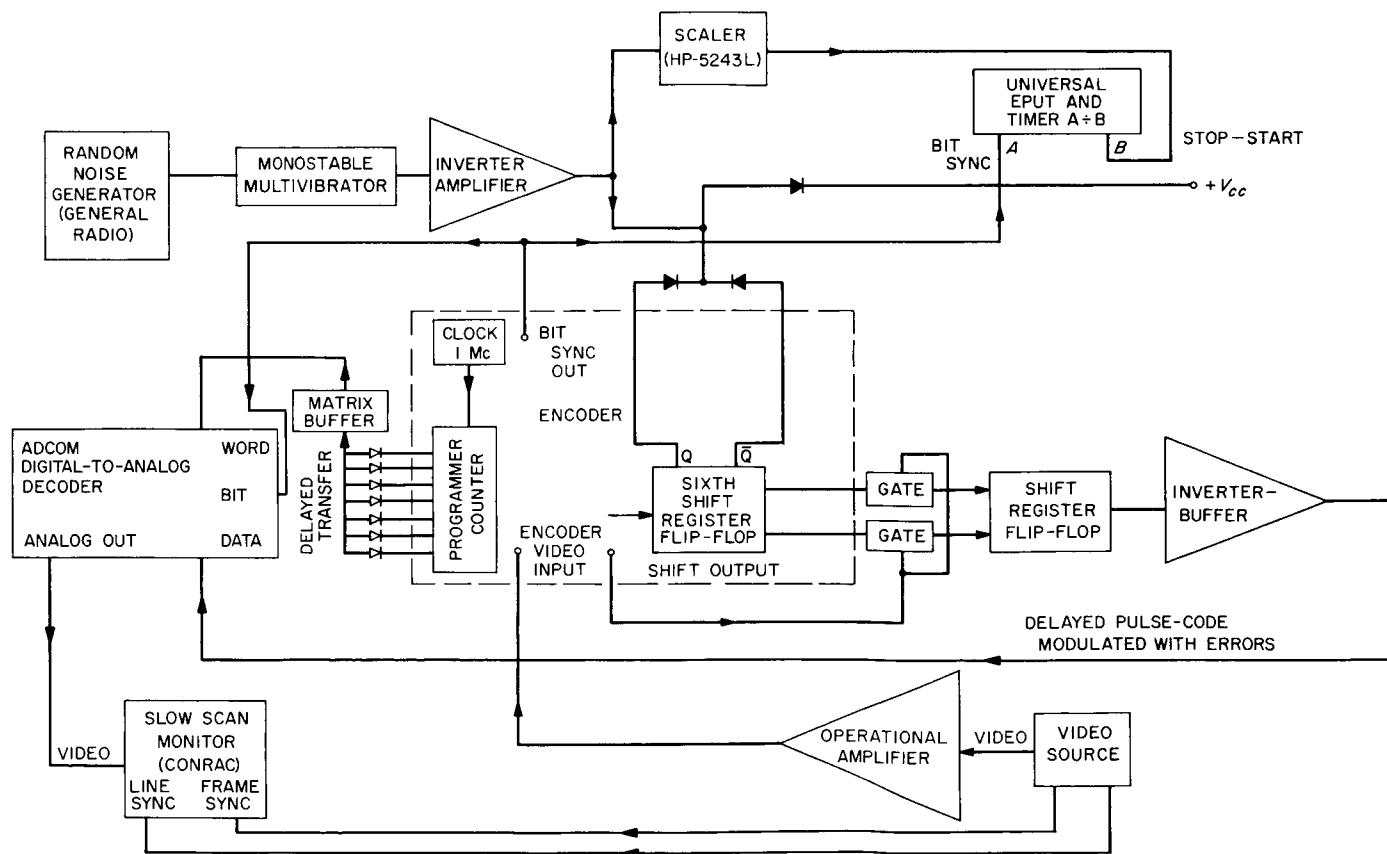
(2) Berkeley universal timer, Model #7360.

Fig. 21. Bit error analysis system

(3) Hewlett-Packard electronic counter, Model #5243L.

(4) Adcom digital-to-analog converter.

(5) Two Conrac CSS5 slow-scan monitors (modified).

(6) C-12 Tektronics oscilloscope camera.

In addition, multivibrators, amplifiers, inverters, buffers and matrix circuits were fabricated for the tests. The encoder and television camera are *Mariner C* developmental breadboards.

White noise from the General Radio generator is shaped by a monostable multivibrator, then amplified, inverted, and injected into the sixth and last stage of the encoder shift register.

The introduction of the random-spaced noise pulses changes the state of the last stage of the shift register and thus causes bit errors. Errors occur in any bit of the six-bit PCM word with equal probability.

An extra flip-flop, a seventh, was added to the encoder shift register to restore any changed bits to a full 12-μsec duration. The introduction of noise changes the bit pulse duration so it was necessary to restore the bit sync to the full 12 μsec.

The seventh flip-flop also delays the data by one bit. A correction is achieved by providing a matrix connection to the encoder programmer. Diode logic provides a new word sync pulse delayed 12 μsec.

The bit errors are counted by scaling 10^3 noise pulses to produce one integrated noise pulse which is then coupled to input B of a Berkeley Universal counter. Bit sync from the encoder is inserted into Input A. The counter function was set at

$$\frac{A}{B} \text{ or } \frac{\text{Number of bit sync pulses}}{\text{Number of integrated noise pulses}}$$

The first integrated noise pulse to appear at the B input opens the gate, and the counter counts bit sync pulses until the next integrated noise pulse closes the gate and stops the count. The readout is a ratio of total bits per bit error averaged over 1000 bit errors. The error rate depends on the gain setting of the random noise generator. As a result of scaling 10^3:1, all noise pulse readings are an average of 10^3 individual gated intervals.

Three separate scenes were used as a source of video, two of which were 2½ × 3½ in. lunar slides. Selection of these two slides were made on the basis of their variation of contrast. An 8 × 10 in. positive transparency of a RETMA test pattern was selected, but due to its large size and the length limitations of the optical bench only a portion of the pattern could be utilized. The transparency was placed in an illuminated light box, and together with the *Mariner C* camera head was mounted on an optical bench. The object distance was 2 ft 8 in. Optimum focus and adjustments were achieved in a semidarkened room with the aid of a Conrac slow-scan storage monitor and an oscilloscope A presentation. Fig. 22 shows three photographs of the scenes used in the test.

The display was photographed with a Tektronics C-12 oscilloscope camera attached to a modified Conrac monitor. The kinescope was a special long persistence orange phosphor. This phosphor peaks near 5900 Å. The relative brightness percent of maximum is 2% in 1 min. The storage varies as a function of the monitor's contrast and brightness settings. For the time of exposure the shutter was open for a full 24-sec frame with the lens stopped down to $f/4$. The film was Eastman Plus X with an ASA rating of 160. Test photos were made with Polaroid 400 with an ASA rating of 350. The lens was stopped down to $f/8$ when Polaroid 400 was used to compensate for the difference in ASA ratings between Plus X and Polaroid. The development process used was Polydal developer at 68°F for 6 min.

By averaging 10^4 consecutive bit errors, it can be shown that the counting errors fall within ±5%. The noise pulses as they appear at the last stage of the encoder shift register have a pulse duration of 0.3 μsec. The shift pulses are 1 μsec wide and spaced 12 μsec apart.

Figs. 23 and 24 show the timing and interference relationship of the shift event and noise pulse.

$$\frac{A_i}{A_t} = \frac{\text{area of interference}}{\text{total area}} = \frac{1.6 \,\mu\text{sec}}{12 \,\mu\text{sec}}$$

Assuming half of the noise pulse-shift pulse interferences will cause no errors to be introduced in the data stream and half of the interferences will produce the desired errors, this ratio A_i/A_t is divided by two to give $A_i/2A_t = 1.6/24 = 6.7\%$.

From this expression it can be seen that for N noise pulses, there will be 0.933 N errors introduced into the data stream.
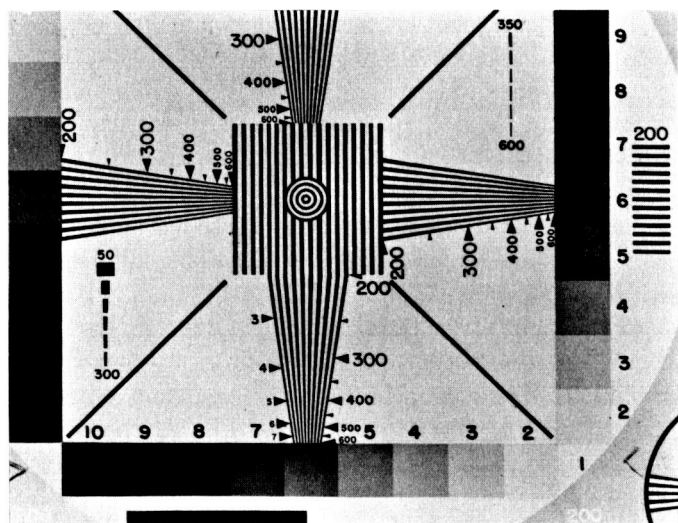
Fig. 22. Photographs of three scenes used as a source of video

NO. 1 EARLIEST POSITION OF NOISE PULSE FOR INTERFERENCE
NO. 2 INTERMEDIATE POSITION OF NOISE PULSE FOR INTERFERENCE
NO. 3 LATEST POSITION OF NOISE PULSE FOR INTERFERENCE
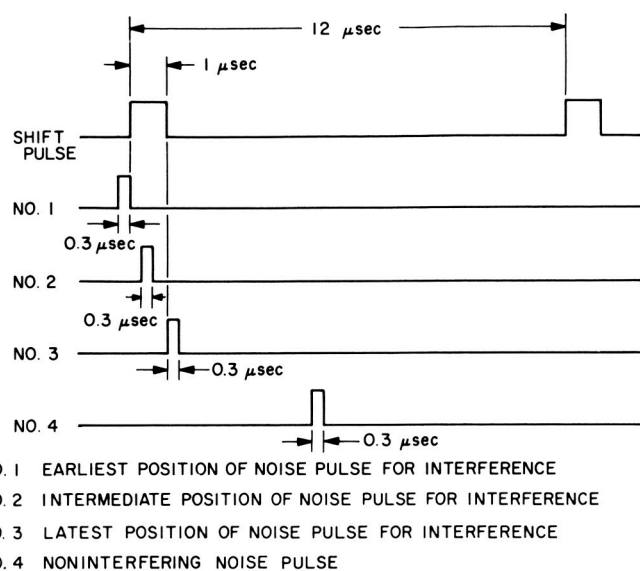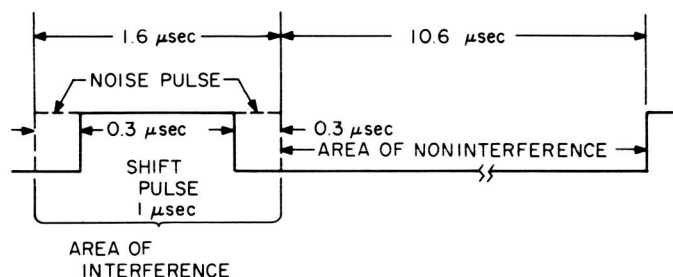NO. 4 NONINTERFERING NOISE PULSE

Fig. 23. Shift pulse–noise pulse interference

Fig. 24. Detail of interference area

This factor was taken into account in all noise measurements made during the test. For unrelated errors, the total system error

$$E = (e_1^2 + e_2^2)^{1/2}$$

$$E = [(0.067)^2 + (0.05)^2]^{1/2}$$

$$E = 8.4 \times 10^{-2} = \pm 8.4\%$$

The video characteristics were those of the *Mariner C* television system. The data stream for the encoder is 83.3 kbits/sec, 6 bits per picture element, 200 elements per line, and 200 lines per frame. The horizontal sweep time is 14.4 msec active line time with a 105.6 msec dead time. The frame is scanned in 24 sec with a 24-sec wait for the next frame.
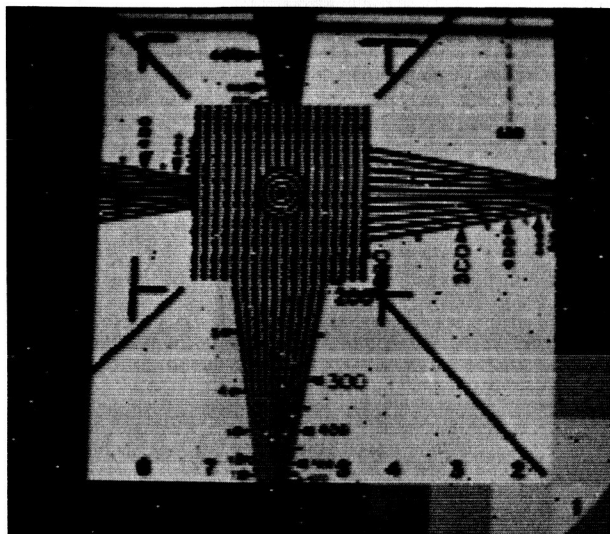
The photographs shown in Fig. 25 are three different scenes at various bit error rates. The bit error rate is given as the ratio of correct bits to error bits. No attempt
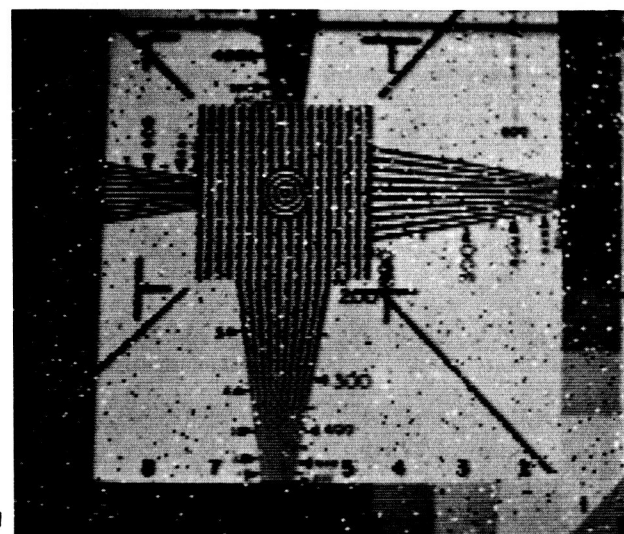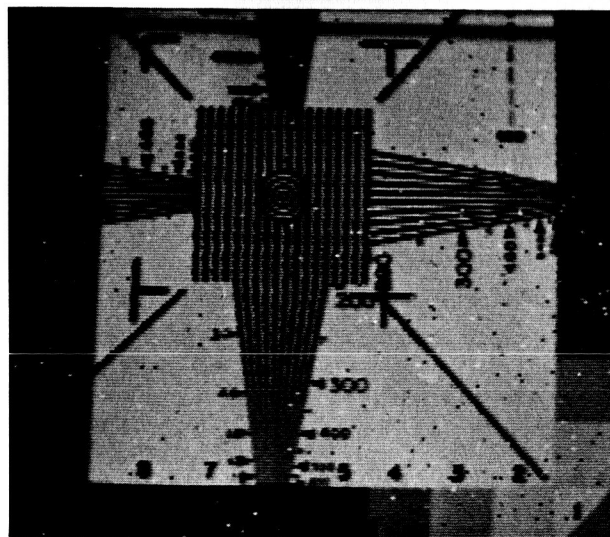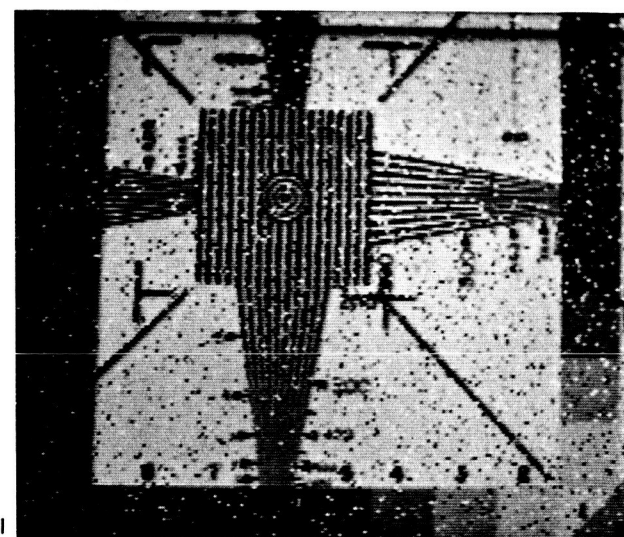
Fig. 25. Three different scenes at various bit error rates

Fig. 25. Three different scenes at various bit error rates (cont'd)

NO
NOISE

104:1
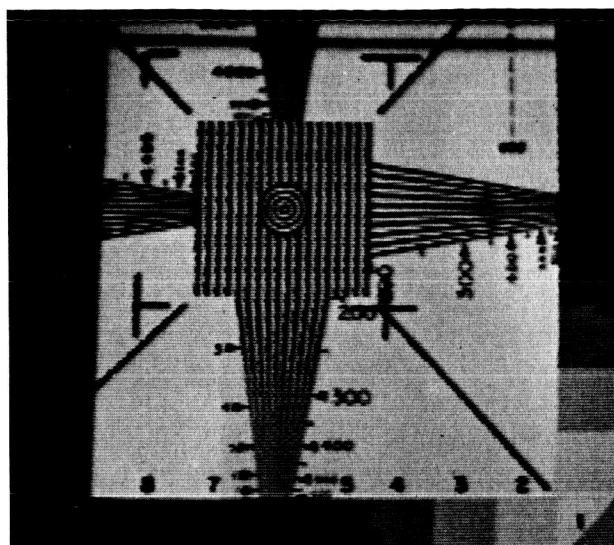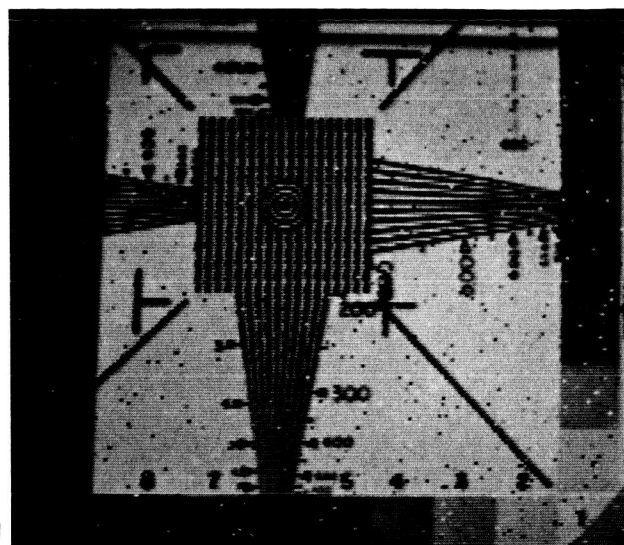
290:1

50:1

200:1

25:1

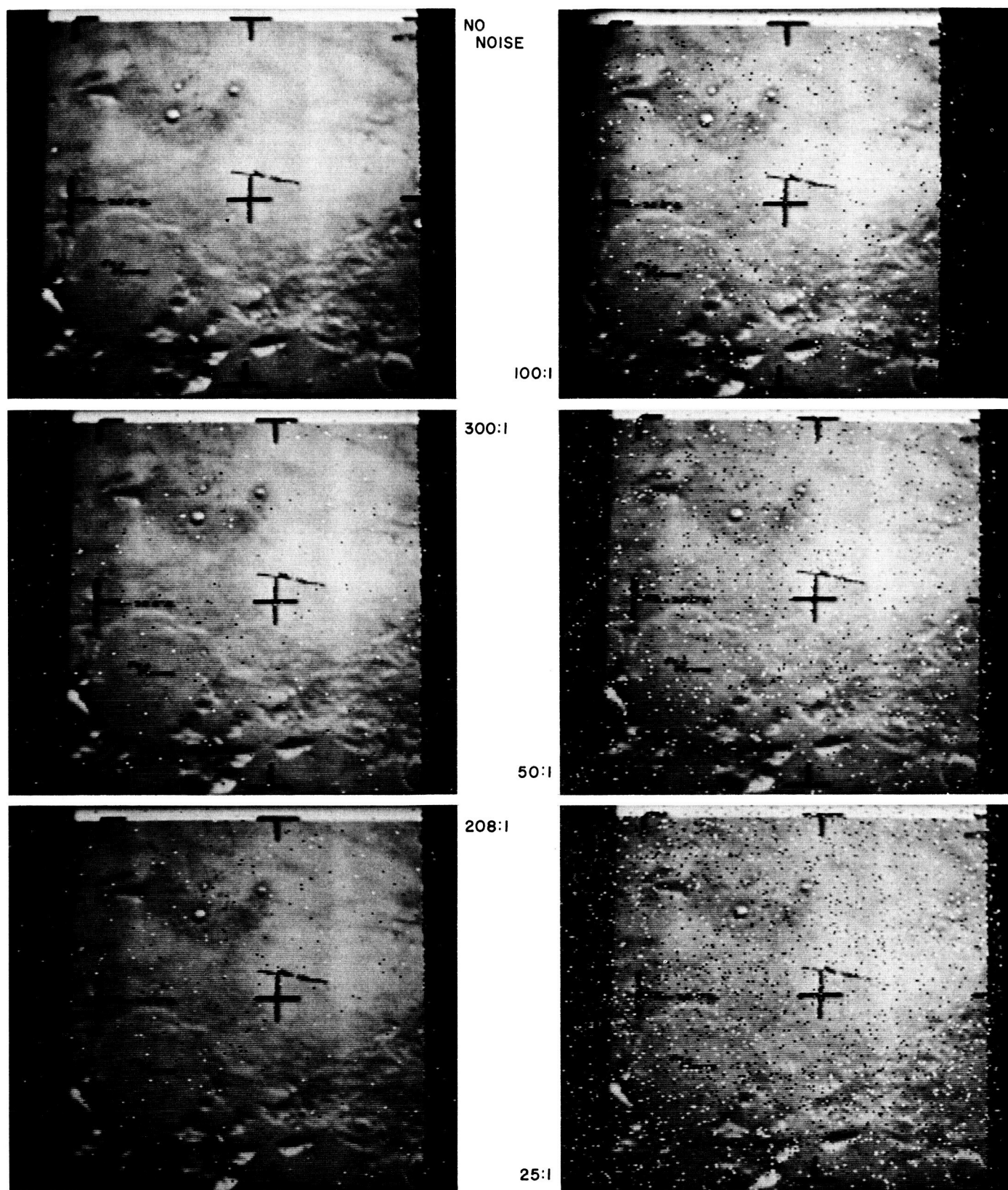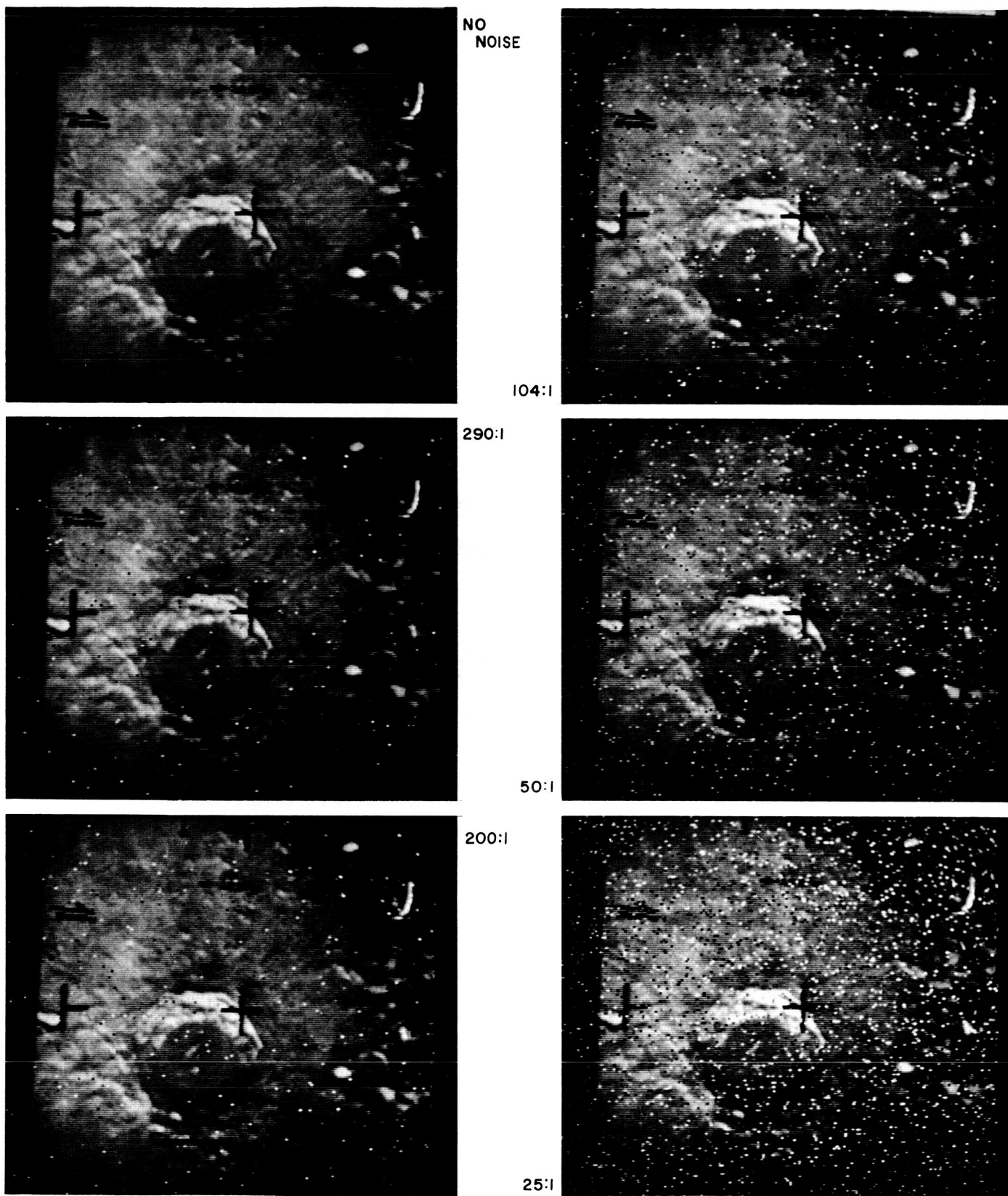**Fig. 25. Three different scenes at various bit error rates (cont'd)**

has been made at this time to draw any specific conclusion from the data. Picture evaluation plus additional subject information is planned for a continuation of the work described. Future plans also include the use of sine wave test charts as a video source, performance of qualitative and quantitative picture analysis, and investigation of methods of picture enhancement using computer techniques.

Erratum

The following correction should be noted for *SPS 37-25*, Vol. VI, p. 42:

For

$$\frac{1}{R_{over-all}} = \sum_{i=1}^{n}\left(\frac{1}{R_i}\right)^2$$

read

$$\left(\frac{1}{R_{over-all}}\right)^2 = \sum_{i=1}^{n}\left(\frac{1}{R_i}\right)^2$$